

NOTE TO USERS

This reproduction is the best copy available.

UMI[®]

Realization of Current Mode Filters Using the Concepts of Transposed Networks and Nullors

Nong Tian

A Thesis

in

The Department

of

Electrical and Computer Engineering

Presented in Partial Fulfilment of the Requirements
for the Degree of Master of Applied Science at
Concordia University
Montreal, Quebec, Canada

August 2005

©Nong Tian, 2005



Library and
Archives Canada

Bibliothèque et
Archives Canada

Published Heritage
Branch

Direction du
Patrimoine de l'édition

395 Wellington Street
Ottawa ON K1A 0N4
Canada

395, rue Wellington
Ottawa ON K1A 0N4
Canada

Your file *Votre référence*

ISBN: 0-494-10252-7

Our file *Notre référence*

ISBN: 0-494-10252-7

NOTICE:

The author has granted a non-exclusive license allowing Library and Archives Canada to reproduce, publish, archive, preserve, conserve, communicate to the public by telecommunication or on the Internet, loan, distribute and sell theses worldwide, for commercial or non-commercial purposes, in microform, paper, electronic and/or any other formats.

The author retains copyright ownership and moral rights in this thesis. Neither the thesis nor substantial extracts from it may be printed or otherwise reproduced without the author's permission.

AVIS:

L'auteur a accordé une licence non exclusive permettant à la Bibliothèque et Archives Canada de reproduire, publier, archiver, sauvegarder, conserver, transmettre au public par télécommunication ou par l'Internet, prêter, distribuer et vendre des thèses partout dans le monde, à des fins commerciales ou autres, sur support microforme, papier, électronique et/ou autres formats.

L'auteur conserve la propriété du droit d'auteur et des droits moraux qui protègent cette thèse. Ni la thèse ni des extraits substantiels de celle-ci ne doivent être imprimés ou autrement reproduits sans son autorisation.

In compliance with the Canadian Privacy Act some supporting forms may have been removed from this thesis.

Conformément à la loi canadienne sur la protection de la vie privée, quelques formulaires secondaires ont été enlevés de cette thèse.

While these forms may be included in the document page count, their removal does not represent any loss of content from the thesis.

Bien que ces formulaires aient inclus dans la pagination, il n'y aura aucun contenu manquant.


Canada

Abstract

Realization of Current Mode Filters Using the Concepts of Transposed Networks and Nullors

Nong Tian

Current-mode circuits have become very important in the design of high-speed analog integrated circuits that are highly linear and possess a wide dynamic-range. Efficient design of current-mode (CM) filters is still a major challenge to the designer. Considerable researcher efforts have been made for the realization of current-mode filters from the existing voltage-mode (VM) filters. In 1971, Bhattacharyya and Swamy introduced the principle of network transposition, which has led to a very efficient way to convert a voltage-mode circuit to a current-mode circuit with the same transfer function, and with a one-to-one correspondence between the elements of the two circuits.

In this thesis, using the concepts of the transposed networks, and the nullator-norator representation for active devices, it is shown that a voltage-mode filter implemented using an operational amplifier (OA) can be very easily converted to a current-mode filter using the same OA, when the OA is configured as a three-terminal element. The effects of the finite gain bandwidth of the OA on the CM and VM filters are studied. If the OA is configured as a four-terminal device in a voltage-mode filter, it is shown that the corresponding current-mode filter can be implemented using an operational floating amplifier (OFA), which is a practical realization of a four-terminal nullor. The theoretical analysis about the proposed method is verified by using simulation

results as well as by practical experiment using discrete components, such as resistors, capacitors and LM741 (OA) devices. Finally, an OFA is designed and laid out using 0.18 μm CMOS technology to validate the design of a current-mode filter using the OFA as the four-terminal nullor. Simulations as well as the experimental results show very good agreement with the theoretical analysis.

Acknowledgements

I would like first to express my sincerest gratitude to my supervisors Dr. M.N.S Swamy and Dr. R. Raut, who originally suggested the idea for this thesis, for their never failing support and encouragement, for all the insightful comments they gave me at different stages of my research, as well as for challenging and criticizing my ideas and for making me think harder than I thought I could.

Special thanks are given to Dave Chun for his help in lab experiment and Ted for his support in the computer software. I also would like to thank my classmates for all their valuable helps and suggestions.

I would like to dedicate this work to my wife Hui Zhao and lovely daughter Tiffany, who always give me their love, support and encouragement through all my study.

Table of Contents

List of Figures	ix
List of Tables	xii
List of Symbols and Abbreviations	xiii
Chapter 1 Introduction and Motivation	1
1.1 Introduction	1
1.2 History of Synthesizing Current-Mode Filters.....	2
1.2.1 Direct Generation of Current-Mode filters.....	2
1.2.2 Derivation From Voltage-Mode Filters.....	2
1.3 Motivation	7
1.4 Thesis Organization.....	9
Chapter 2 The Nullor Principle and Network Analysis	11
2.1 Review the Concept of Nullors	11
2.1.1 Definition of Nullors	11
2.1.2 Simplification of Nullor Networks.....	13
2.1.3 The Nullor Models of the Four Controlled Sources.....	15
2.2 Network Analysis Methods.....	17
2.2.1 Review of the Nodal Analysis of a Passive RLC Network.....	17
2.2.2 The Nodal Analysis of a RLC-Nullor Network	18
2.3 RLC-Nullor Network Transformation	19
2.3.1 Three-Terminal Nullor — Three-Terminal OA	20
2.3.2 Four-Terminal Nullor — Operational Floating Amplifier	22
2.4 Summary	25

Chapter 3 Four-Terminal OA-Based VM and CM Filters	26
3.1 Fundamentals of Active VM Filters.....	27
3.1.1 Operational Amplifiers.....	27
3.1.2 Mathematical Model of General Filters	28
3.1.3 Mathematical Model of Second-Order (Biquadratic) Filters	30
3.1.4 Realization of the Second-Order Filters.....	30
3.2 Realizing CM Filter with Three-Terminal Operational Amplifier.....	31
3.2.1 Single Amplifier Biquadratic Filter Using Ideal VCVS	31
3.2.2 Multiple Amplifier Filter Using Ideal VCVS	33
3.3 Effect of GainBandwidth of OA on the Pole Frequency and Pole Q	36
3.3.1 The Voltage-Mode A & M Filter	37
3.3.2 The Current-Mode A & M Filter.....	39
3.3.3 Simulation Results for Pole- ω and Pole-Q.....	41
3.4 Summary	48
Chapter 4 Experiment and Simulation Results	49
4.1 Simulation of the Current-Mode and the Voltage-Mode Filters.....	49
4.1.1 Single-OA Biquadratic Filter	49
4.1.2 Multi-OA Biquadratic Filter.....	53
4.2 Lab-bench Experiment	56
4.2.1 Characteristics of the Discrete Components	56
4.2.2 Experimental Test Set Up	58
4.2.3 Experimental Results.....	59
4.3 Summary	63
Chapter 5 Four-Terminal OA-Based VM Filters and OFA-Based CM Filters	64
5.1 Operational Floating Amplifier (OFA)	64
5.2 Realizing CM Filter Using OFA	66
5.2.1 Single-OA Biquadratic Filter	66
5.2.2 Multi-OA Biquadratic Filter.....	68
5.3 Simulations of the Four-Terminal OA Configuration.....	70

5.3.1	Single-OA Biquadratic Filter	70
5.3.2	Multiple-OA Biquadratic Filter.....	73
5.4	Summary	75
Chapter 6 Realizing Operational Floating Amplifier in CMOS		
Technique	76
6.1	Realizations of OFAs	77
6.1.1	OA-Based OFA	77
6.1.2	CCII-Based OFA.....	79
6.2	System Structure and Basic Building Blocks.....	80
6.2.1	Bias Stage.....	81
6.2.2	Differential Amplifier Stage.....	82
6.2.3	Output Stage.....	83
6.2.4	Current Amplifier Stage.....	84
6.2.5	The Performance of the OFA	85
6.3	Basic Building Blocks Implemented by Layout	86
6.3.1	Transistor.....	86
6.3.2	MiM Capacitor	88
6.3.3	Resistor.....	89
6.3.4	ESD Protection Structure	89
6.4	System Layout.....	90
6.5	The Performance of the OFA	92
6.5.1	Corner Analysis of the OFA.....	93
6.5.2	Deliyannis-Friend Biquadratic Filter	95
6.6	Summary	96
Chapter 7 Conclusion and Future Work		
7.1.	Conclusion	98
7.2.	Future Work	100
References	101

List of Figures

Figure 1-1	Two-port network model	3
Figure 1-2	Nullator and norator network transform	7
Figure 2-1	(a) Symbol of a nullor (b) Symbol of a nullator. (c) Symbol of a orator	12
Figure 2-2	Series connection with a nullator	13
Figure 2-3	Series connection with a norator	13
Figure 2-4	Parallel connection with a nullator.....	13
Figure 2-5	Parallel connection with a norator.....	14
Figure 2-6	Series connection with a nullator and a norator	14
Figure 2-7	Parallel connection with a nullator and a norator.....	14
Figure 2-8	Star connection of two three-terminal nullors.....	15
Figure 2-9	(a) VM network. (b) VM network using nullor.(c) VM network using CCCS-nullor. (d) CM network using VCVS-nullor	21
Figure 2-10	The corresponding CM network of Figure 2-9(a).....	22
Figure 2-11	(a) VM network. (b) VM network using nullor.(c) VM network using CCCS-nullor. (d) CM network using VCVS-nullor.....	23
Figure 2-12	The corresponding CM network of Figure 2-11(a).....	24
Figure 3-1	(a) Circuit symbol and (b) small signal equivalent circuit of an OA	27
Figure 3-2	One-pole model frequency response of an OA	28
Figure 3-3	A filter on the system level	29
Figure 3-4	Voltage-mode SAB filter	32
Figure 3-5	Voltage-mode SAB filter using a CCCS.....	32
Figure 3-6	Current-mode SAB filter.....	33
Figure 3-7	Voltage-mode Tow-Thomas biquadratic filter.....	34
Figure 3-8	Current-mode Tow-Thomas biquadratic filter	34
Figure 3-9	Voltage-mode A & M biquadratic filter.....	36
Figure 3-10	Current-mode A & M biquadratic filter	36
Figure 4-1	Voltage-mode low-pass SAB filter using an ideal VCVS	50
Figure 4-2	Current-mode low-pass filter SAB using an ideal VCVS.....	50

Figure 4-3	Frequency responses of the VM and the CM low-pass SAB filters using an ideal VCVS	51
Figure 4-4	Voltage-mode low-pass SAB filter using a non-ideal OA	51
Figure 4-5	Voltage-mode low-pass SAB filter using a non-ideal OA	52
Figure 4-6	Frequency responses of the VM and the CM low-pass SAB filters using a non-ideal OA	52
Figure 4-7	Voltage-mode A & M filter using non-ideal OAs.....	53
Figure 4-8	Current-mode A & M filter using non-ideal OAs	53
Figure 4-9	Frequency responses of the VM and the CM band-pass A & M filters using non-ideal OAs	54
Figure 4-10	Frequency responses of the VM and the CM low-pass A & M filters using non-ideal OAs	54
Figure 4-11	LM741 package order diagram	57
Figure 4-12	LM13700 package order diagram	58
Figure 4-13	Lab-bench experiment set up	59
Figure 4-14	Voltage-mode A & M filter for the lab-bench experiment	59
Figure 4-15	Current-mode A & M filter for the lab-bench experiment.....	60
Figure 4-16	The output signals of the VM and CM filters at frequency 724Hz	61
Figure 4-17	The output signals of the VM and CM filters at frequency 1559Hz.....	61
Figure 4-18	The output signals of the VM and CM filters at frequency 7238Hz.....	62
Figure 4-19	Magnitude-frequency responses of the VM and CM band-pass A & M filters	62
Figure 5-1	(a) Nullor model and (b) Symbol of an OFA	65
Figure 5-2	Implementation circuit of an OFA adapted from	65
Figure 5-3	VM SAB filter using a finite gain amplifier	66
Figure 5-4	VM SAB using an ideal OA with four-terminal configuration	67
Figure 5-5	CM SAB filter using an ideal OFA	67
Figure 5-6	VM M & B biquadratic filter using ideal OAs with	69
Figure 5-7	CM M & B biquadratic filter using ideal OFAs	69
Figure 5-8	VM band-pass SAB filter using a non-ideal OA.....	71
Figure 5-9	CM band-pass SAB filter using a non-ideal OFA	71

Figure 5-10	Frequency responses of the VM and CM band-pass SAB filter	72
Figure 5-11	VM band-pass M & B filter using non-ideal OAs	73
Figure 5-12	CM band-pass M & B filter using non-ideal OFAs	73
Figure 5-13	Frequency responses of the VM and CM band-pass M & B filter.....	74
Figure 6-1	Implementation model of an OFA	77
Figure 6-2	OA-Based implementation of an OFA.....	78
Figure 6-3	CCII-Based implementation of an OFA.....	79
Figure 6-4	The schematic of the OFA	80
Figure 6-5	Enhanced output-impedance current mirror	85
Figure 6-6	Fingered structure to reduce parasitic drain capacitances	87
Figure 6-7	Common-centroid structure to minimize the matching errors	87
Figure 6-8	The cross-section of MiM capacitor.....	88
Figure 6-9	Capacitor layout diagram	88
Figure 6-10	Transistor version of resistor.....	89
Figure 6-11	ESD protection layout	90
Figure 6-12	The OFA system layout	91
Figure 6-13	Corner analysis for the gain of the OFA	94
Figure 6-14	Voltage-mode band-pass Deliyannis-Friend biquadratic filter	95
Figure 6-15	Current-mode band-pass Deliyannis-Friend biquadratic filter	96
Figure 6-16	Frequency responses of the VM and the CM Deliyannis-Friend biquadratic band-pass filter	97

List of Tables

Table 1.1	Active devices and their corresponding transposes	4
Table 2-1	Controlled sources and corresponding nullor models	16
Table 3-1	Some Special Cases of Second-order Transfer Functions	30
Table 3-2	Voltage-mode band-pass A & M filters	42
Table 3-3	Current-mode band-pass A & M filters.....	43
Table 3-4	Voltage-mode low-pass A & M filters.....	44
Table 3-5	Current-mode low-pass A & M filters	45
Table 3-6	Current-mode band-pass filters with non-ideal input and output	46
Table 3-7	Current-mode low-pass filters with non-ideal input and output	47
Table 6-1	Specification of the OFA.....	86
Table 6-2	The specification of the OFA after layout.....	92

List of Symbols and Abbreviations

C	Capacitor
R	Resistor
Q	Quality Factor
ω	Frequency in Radians
H(s)	Frequency Domain Transfer Function
h(t)	Time Domain Transfer Function
CTF	Current Transfer Function
VTF	Voltage Transfer Function
V _{th}	Threshold Voltage of the Transistor
IC	Integrated Circuit
W	Channel Width of the MOS Transistor
L	Channel Length of the MOS Transistor
g _m	AC Transconductance
CMOS	Complementary Metal Oxide Semiconductor
PMOS	Positive-channel Metal Oxide Semiconductor
NMOS	Negative-channel Metal Oxide Semiconductor
MOSFET	MOS Field Effect Transistor
VLSI	Very Large Scale Integration
BSIM	Berkeley Short-Channel IGFET Model
OA	Operational Amplifier
OFA	Operational Floating Amplifier
CCII	Second-Generation Current Convey
FTFN	Four Terminal Floating Nullor
VCVS	Voltage Control Voltage Source
CCCS	Current Control Current Source
CCVS	Current Control Voltage Source
VCCS	Voltage Control Current Source

Chapter 1

Introduction and Motivation

1.1 Introduction

Analog filters are widely used in signal processing systems, such as telecommunication, consumer electronic devices, and industrial control systems. Traditionally, the transfer function of a filter has been considered as a ratio of two voltage signals. With the advent of integrated circuit (IC) technology and the requirement of low power and portability, electronic filters are now vastly implemented as a sub system in a typical very large scale integrated (VLSI) system using, for example, complementary metal oxide semiconductor (CMOS) IC technology.

With the shrinkage of feature dimensions in a modern CMOS technological process, operation under low DC power supply is becoming imminent now-a-days. With very low values for the overall voltage supply, the processing of voltage signals is becoming more and more difficult. Since early 90s, current-mode filters based on the current signals have been receiving a lot of attention [1-9]. Since a current flowing through a circuit component necessarily causes a voltage drop, we can choose proper impedance levels, achieving sufficiently small voltages compatible with reduced DC supply voltages in a modern VLSI electronic system. Since substantial current can flow only through a very low resistance, current-mode operation naturally leads to higher frequency of operation (low resistance \rightarrow low value of time constant, leading to high

value of associated pole frequency), than a similar voltage-mode signal processing system.

Voltage-mode filters based on operational amplifiers and operational transconductance amplifiers have been well developed and widely used. Implementing a current-mode filter efficiently is still an important challenge to a designer. Two main techniques have been followed to realize a desired current-mode filter function; (i) direct realization in the current domain, (ii) derivation from existing voltage-mode filters. These are discussed below.

1.2 History of Synthesizing Current-Mode Filters

1.2.1 Direct Generation of Current-Mode Filters

Methods that directly generate current-mode filters are almost the same as those directly synthesize the voltage-mode filters [1][2]. The main difference is that the signals at the building block level are treated as electrical currents for the current-mode filters. We need to have current summing and differencing operation, current feedback, current integrators/differentiators, and current amplifiers. Many researchers have taken this route [6-9]. Substantial efforts are needed for this method of implementation.

1.2.2 Derivation from Voltage-Mode Filters

Network Transposition

As early as 70's, Bhattacharyya and Swamy proposed the concept of "network transposition" [10], and showed how to convert a voltage-mode (VM) network to a

current-mode (CM) network. The principle is: given a linear time-invariant two-port network N , another network N_T , called the transpose of network N , can be formed such that

$$[Y]_{N_T} = [Y]_N^T$$

where $[Y]_N$ and $[Y]_{N_T}$ correspond to the admittance matrices of the network N and N_T , respectively. Such a two-port network is shown in Figure 1-1.

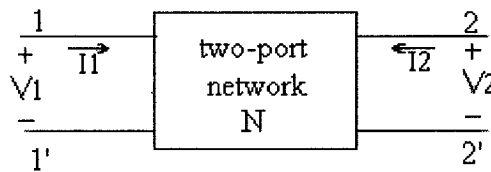


Figure 1-1 Two-port network model

These two networks have the following properties [1],[10], and [13]

- The voltage transfer function in the forward direction for network N is the same as the current transfer function in the reverse direction of N_T , and vice-versa.
- The transfer function corresponding to the voltage-input current-output in the forward direction for network N is the same as that of the current-input voltage-output in the reverse direction of N_T , and vice-versa.
- The driving point functions of N and N_T remain unchanged.

It is obvious that the transpose of a reciprocal network is itself. The transposes of the basic four controlled sources are listed in Table 1.1. The sensitivity of the voltage-mode transfer function of network N with respecting to a particular parameter is same as

that of the corresponding current-mode transfer function of N_T [10]. They have further extended the transposition concept to networks with n-input and m-output nodes.

Table 1.1 Active devices and their corresponding transposes.

Active devices	Corresponding transpose

Recently, the application of transposed network in converting VM filters using operational transconductance amplifiers (OTAs) to OTA-based CM filters, as well as in obtaining new OTA-based CM oscillator circuits has been considered [14][15].

Dual Network Transformation [11]

Swamy, Bhattacharyya and Bhusan also introduced the concepts of duals and dual transposition of existing VM networks [11][12]. They defined the generalized dual of a network N consisting of one-port elements and controlled sources to be a network N^* for

which the topology is dual of that of N and each element is the generalized inverse of the corresponding element of N. To obtain the dual network N*, first generate the graph G of N. Then, we obtain the dual graph G* of the graph G in the conventional way. Last, replace the internal one-ports and two-ports by their generalized inverses to obtain the dual network N*[11]. The generalized inverses of the different active as well as distributed elements are listed below:

Controlled Sources: CCCS \leftrightarrow VCVS, CCVS \leftrightarrow VCCS

Negative Impedance Converter: VNIC \leftrightarrow CNIC

Generalized Impedance Converter: VGIC \leftrightarrow CGIC

The [z] of N is related to the [y] of N*: $[y] = \frac{1}{f(s)}[z]$.

Finally, the voltage transfer function of N becomes the current transfer function of N* and vice-versa. The sensitivities of these two functions are the same with respect to the corresponding parameters. These results have been further extended to the dual transposed networks [12].

Recently, Wang Guo-hua, Kenzo Watanabe, and Yutaka Fukui described a method using the concept of dual networks [11] and nullors to convert a VM network to a CM network [20][21]. The dual network generation

$$[V] = [Z][I] \quad (1.1)$$

where [V],[Z] and [I] are the voltages of independent or dependent sources, impedances, and currents in the loops respectively. Introducing a scaling factor α ($\neq 0$), where the dimension and the value of α are chosen depending on the application, we can rewrite

$$(1.1) \text{ as } [V/\alpha] = [Z/\alpha^2][I\alpha] \quad (1.2)$$

If $\alpha = 1$ ohm, then (1.2) represents a conventional dual transformation of (1.1), and $[V/\alpha]$, $[\alpha I]$, and $[Z/\alpha^2]$ in (1.2) represent the currents, voltages, and admittances $[Y_\alpha]$ in the transformed network N_α . For $\alpha = \sqrt{R/SC}$, the proposed transformation includes RC-CR transformation. The nullator and norator are dual themselves and invariant to the transformation. Therefore, if active elements, such as transistors and OA, are modeled in-terms of the nullator and norator, an active RC voltage-mode circuit can be transformed by (1.2) to its dual current-mode circuit.

In the late 80's and early 90's, Sedra and Roberts used the concept of adjoint [16] and interreciprocal networks to derive CM filters from VM filters using VCVS [17-19]. This operation is the same as the network transposition defined early by Bhattacharyya and Swamy [10] and discussed in the earlier part of this section.

Nullor Networks

In 1993, A. Carlosena and G. S. Moschytz pointed out some known properties of RC-nullor networks and shown how current-mode circuits could be easily derived from voltage-based circuits by simply interchanging nullators and norators [22][23]. They considered a network N formed by a passive reciprocal network and pairs of nullators and norators connected to its nodes as shown in Figure 1-2(a). Consider another network N', shown in Figure 1-2(b), resulting from interchanging of all nullators and norators in network N by describing the reciprocal network by its definite admittance matrix and applying the well-known reduction rules [24], it can be shown that the admittance matrices Y and Y' corresponding to networks N and N' respectively are related by

$$[Y] = [Y']^T$$

The implementation procedure is described as follows: The first step is to represent a voltage-mode network in terms of nullator and norator model of the active devices and a passive (i.e. reciprocal) network as in Figure 1-2 (a). The second step is to interchange the nullators and norators shown in Figure 1-2(b). The third step is to reverse input port and output port. The resulting system now appears as shown in Figure 1-2 (c). Finally, we synthesize a practical circuit from the resulting nullator and norator network in Figure 1-2(c). The current transfer function is same as the original voltage transfer function, $\frac{I_o}{I_i} = \frac{V_o}{V_i}$.

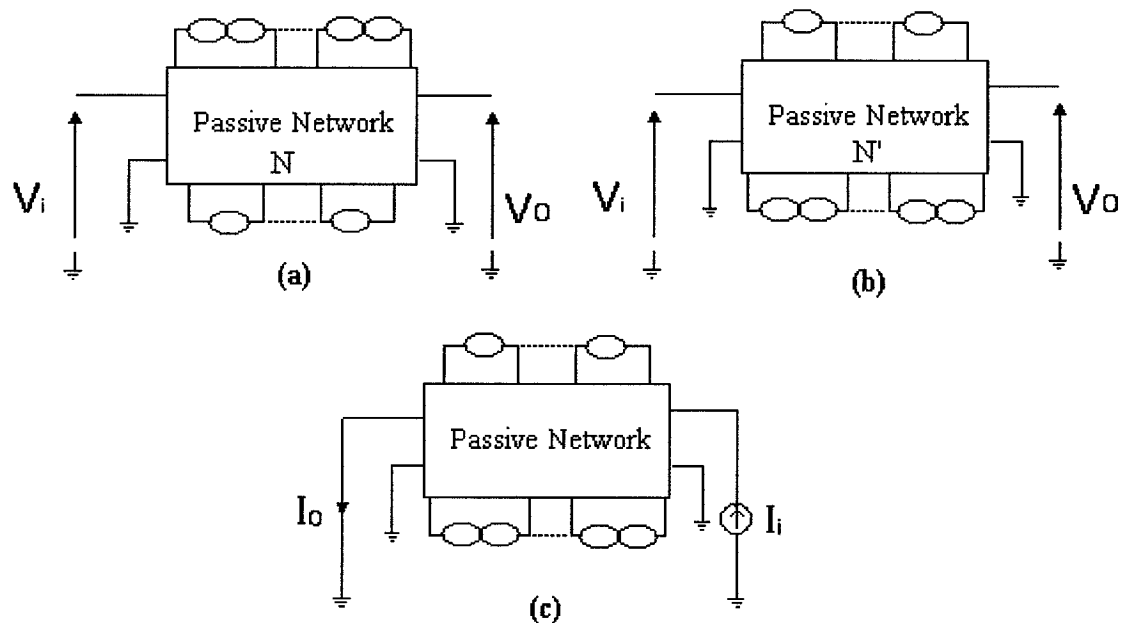


Figure 1-2 Nullator and norator network transform. (a) Nullator and norator network. (b) Exchange of all nullators and norators in (a). (c) CM nullator and norator network transformed from (a).

1.3 Motivation

All the methods of converting a voltage-mode transfer function to a current-mode transfer function described above are based on the works of Swamy et al. It should be

noted that these methods are such that if a voltage-mode filter uses OA as active devices, the corresponding current-mode filter uses current conveyors or current operational amplifiers as active devices. These devices can be modeled as CCCS and hence comply easily with the VM to CM conversion. In the method introduced by A. Carlosena and G. S. Moschytz, a circuit containing controlled sources can be modeled uniquely in terms of nullor-norator circuits, whereas the opposite statement is not always true. The synthesis of an active device from a pair of nullator and norator is not easy. Such procedures require considerable practice and experience and do not lead in all cases to satisfactory solutions [22].

In this thesis, we intend to apply the properties of the nullator and norator and the principle of transposed networks to convert a VM system to a CM system. An extension of the nullor concept presented in [24] to ideal active devices produces a very interesting conclusion. It can be established that a current-mode filter can be obtained from a given voltage-mode filter implemented using an ideal OA considered as a three-terminal VCVS, with any of the four ideal three-terminal controlled sources, i.e., ideal VCVS, CCCS, VCCS, and CCVS. The concept follows from the principle that any ideal controlled source is exactly equivalent to a nullor (nullator-norator pair) [24]. Thus, an ideal three-terminal VCVS based VM filter can be converted to a CM filter using the same ideal VCVS device. Hence, the old active device, OA, can be reused. The modified network will consist of re-using the existing ideal VCVS but with a reversal of the input and output ports. This new method to be introduced in Chapter 2 is also suitable for the four-terminal VCVS configurations. But in the CM network we need an operational floating amplifier (OFA) to replace the VCVS in the VM filter.

To establish the above concept, both single-OA as well as multi-OA filters are considered. The frequency response, effect of non-ideal OA on the pole-frequency and pole-Q characteristics of the CM filter and the associated VM filter, are analyzed and discussed. This is followed by several simulations and lab-bench experimental results. Implementation of the OFA using a modern 0.18 μm CMOS technology and its application are also provided.

1.4 Thesis Organization

In this chapter, we have addressed some historical background regarding the realization of current-mode filters. In Chapter 2, the concept of the nullor and the corresponding network analysis is introduced. Employing these principles, it is proved that a voltage-mode network implemented using a nullor with three-terminal configuration can be converted to a current-mode network using the same nullor with three-terminal configuration. When the nullor is configured as a four-terminal device, the corresponding current-mode network can be implemented using a nullor with four-terminal configuration.

In Chapter 3, we employ the new method introduced in Chapter 2 to convert VM filters to CM filters using single amplifier as well as multiple amplifiers. Theoretical as well as simulation studies are conducted to derive the effect of the finite bandwidth of the OA on the pole-frequency and pole-Q related to the VM and CM filters.

In Chapter 4, we consider the verification of our theoretical work discussed in Chapter 3. We compare the filter responses of the VM and the corresponding CM filters

through simulations as well as laboratory experiments to study the effects of practical components.

In Chapter 5, we consider the realization of CM filters from VM filters that use four-terminal OAs. We show that in order to realize these CM filters, we need the element, operational floating amplifier (OFA), a four-terminal network. Comparison of the filter responses of the VM and the corresponding CM filters is conducted through simulation studies.

Chapter 6 gives details of the implementation of the operational floating amplifier (OFA) using TSMC 0.18 μm CMOS technology. Based on a comparison of different OFA structures, an optimum OFA structure is selected. Then, we discuss each basic building block of the OFA and the corresponding layout considerations. The post-layout simulation for an OFA is presented. We verify the performance of the OFA by converting the Deliyannis-Friend VM filter to the corresponding CM filter using an OFA.

Finally, some conclusions and suggestion for future work are included in Chapter 7.

Chapter 2

The Nullor Principle and Network Analysis

The concept of the nullor is introduced in this chapter. The nullor network as a fundamental sub-network in the classification of RLC-active networks is important to simplify or synthesize RLC-active networks. It is shown that the four basic controlled sources can be realized by means of R-nullor networks. The nodal and loop analysis techniques can be applied to RLC-nullor networks for the analysis of active networks. After the fundamental theory about the RLC-nullor network is established, we explore the realization of the current-mode network from the corresponding voltage-mode network using the principles of transposed networks and nullors. Finally, two important practical realization of the nullor, Operational Amplifier and Operational Floating Amplifier, are introduced.

2.1 Review the Concept of Nullors

2.1.1 Definition of Nullors [24]

A nullor is a two-port network that has the null transmission matrix, that is, it is characterized by the terminal equations:

$$\begin{bmatrix} V_1(s) \\ I_1(s) \end{bmatrix} = \begin{bmatrix} 0 & 0 \\ 0 & 0 \end{bmatrix} \begin{bmatrix} V_2(s) \\ -I_2(s) \end{bmatrix} \quad (2.1)$$

The symbol for the nullor is shown in Figure 2-1(a). From the above definition, the first row can be written as, $V_1 = 0 \cdot V_2 + 0 \cdot (-I_2)$. In physical terms, this implies that the input voltage V_1 is zero, regardless of the output variables V_2, I_2 . The second row can be expressed as, $I_1 = 0 \cdot V_2 + 0 \cdot (-I_2)$. This equation implies that the input current is zero, regardless of the output variables. Therefore, (2.1) simply constrains $V_1(s)$ and $I_1(s)$ to be zero and does not in any way constrain $V_2(s)$ and $I_2(s)$, and insofar as the definition is concerned, $V_2(s)$ and $I_2(s)$ are both arbitrary. This definition also implies that port 1 and port 2 are isolated.

Let us consider the behavior of the nullor at port 1. Port 1 with the property that it maintains zero voltage and zero current flow between its two terminals is called a nullator. A nullator is a one-port network defined by the constraints:

$$V_1(s) = I_1(s) = 0 \quad (2.2)$$

The symbol of a nullator is shown in Figure 2-1(b).

Port 2 with the property that both the voltage and current between its two terminals are arbitrary is called a norator. A norator is a one-port network for which the voltage $V_2(s)$ and the $I_2(s)$ are unconstrained, that is:

$$V_2(s) = \text{arbitrary}, \quad I_2(s) = \text{arbitrary} \quad (2.3)$$

The symbol of a norator is shown in Figure 2-1(c).

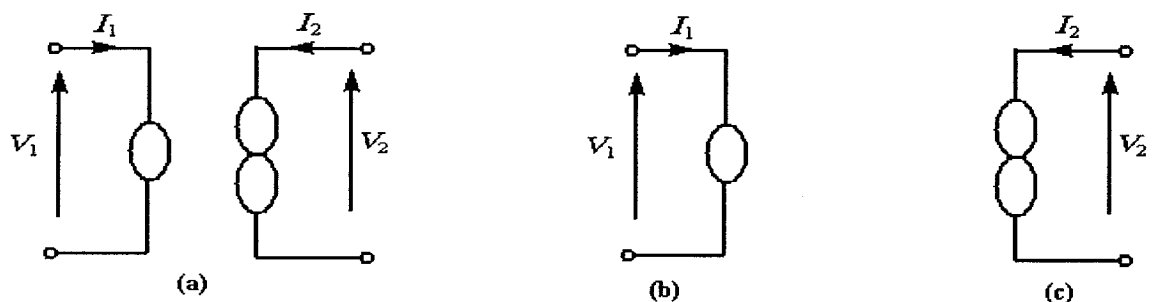


Figure 2-1 (a) Symbol of a nullor (b) Symbol of a nullator. (c) Symbol of a norator

2.1.2 Simplification of Nullor Networks

The V-I constraints of the nullator and norator were addressed in the previous section. The V-I constraints of short-circuit and open-circuit are described as follows:

$$\text{Short-circuit} \quad V(s) = 0 \quad I(s) = \text{arbitrary}$$

$$\text{Open-circuit} \quad V(s) = \text{arbitrary} \quad I(s) = 0$$

These constraints are used to prove the following equivalences for nullor network [24]:

Equivalence 1: A series connection of $\pm R$, $\pm L$, $\pm C$ elements and at least one nullator is equivalent to a nullator, shown in Figure 2-2.

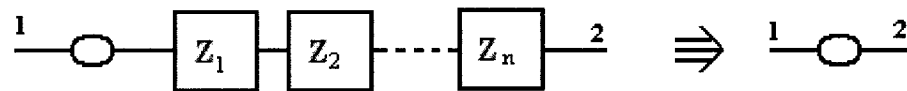


Figure 2-2 Series connection with a nullator

Equivalence 2: A series connection of $\pm R$, $\pm L$, $\pm C$ elements and at least one norator is equivalent to a norator, shown in Figure 2-3.

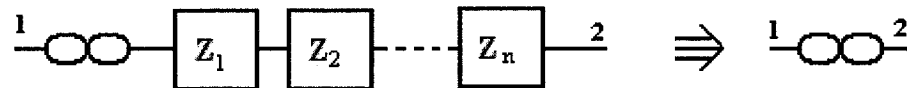


Figure 2-3 Series connection with a norator

Equivalence 3: A parallel connection of $\pm R$, $\pm L$, $\pm C$ elements and at least one nullator is equivalent to a nullator, shown in Figure 2-4.

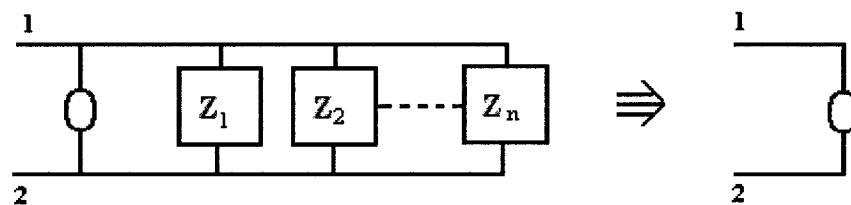


Figure 2-4 Parallel connection with a nullator

Equivalence 4: A parallel connection of $\pm R$, $\pm L$, $\pm C$ elements and at least one norator is equivalent to a norator, shown in Figure 2-5.

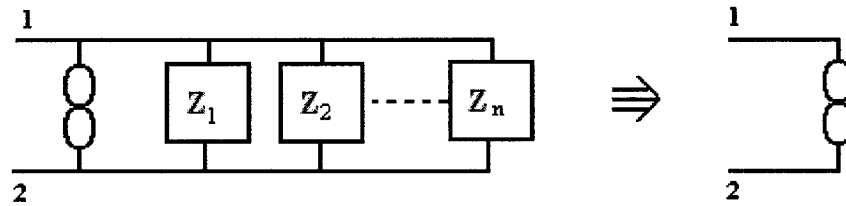


Figure 2-5 Parallel connection with a norator

Equivalence 5: A series connection of $\pm R$, $\pm L$, $\pm C$ elements and at least one nullator and at least one norator is equivalent to an open-circuit, shown in Figure 2-6.

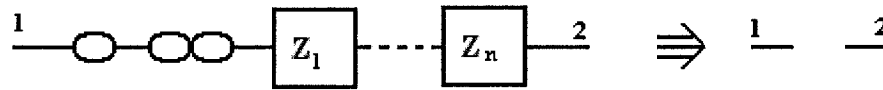


Figure 2-6 Series connection with a nullator and a norator

Equivalence 6: A parallel connection of $\pm R$, $\pm L$, $\pm C$ elements and at least one nullator and at least one norator is equivalent to a short-circuit, shown in Figure 2-7.

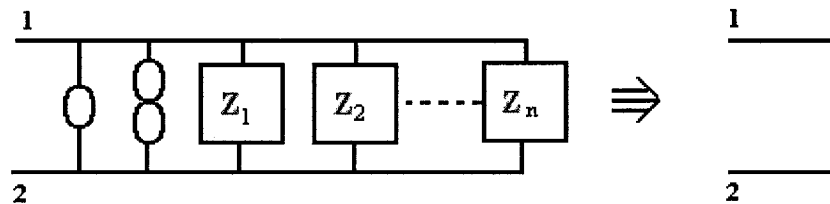


Figure 2-7 Parallel connection with a nullator and a norator

Equivalence 7: The star connection of two three-terminal nullors is equivalent to one four-terminal nullor, shown in Figure 2-8.

The above equivalences are used to simplify active networks and to demonstrate the equivalences between different RC-active circuit configurations.

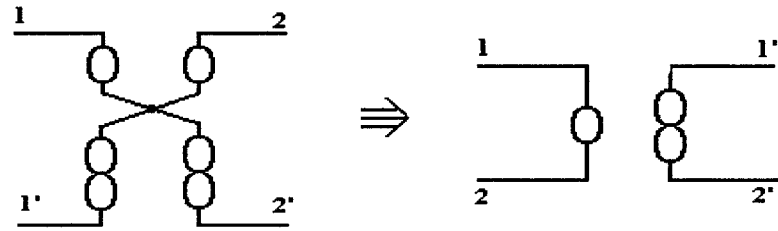


Figure 2-8 Star connection of two three-terminal nullors

2.1.3 The Nullor Models of the Four Controlled Sources

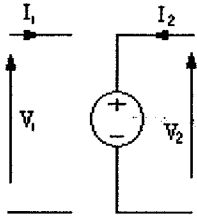
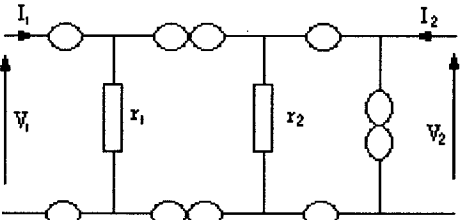
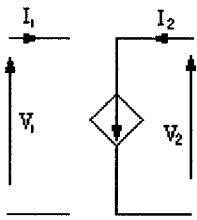
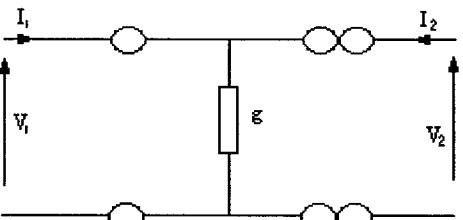
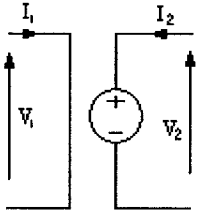
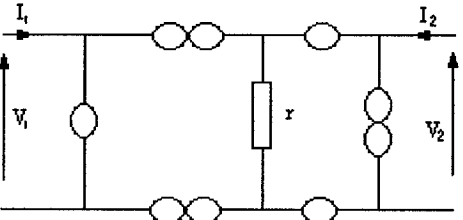
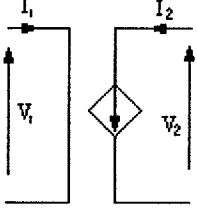
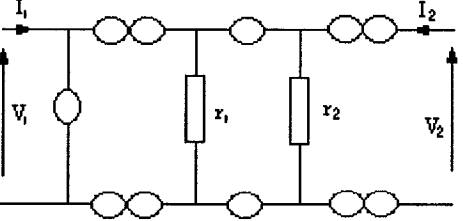
Controlled sources are widely used in the analysis and synthesis of RC-active network. They are voltage control voltage source (VCVS), voltage control current source (VCCS), current control voltage source (CCVS), and current control current source (CCCS). All four controlled sources can be realized using resistor-nullor (R-nullor) networks. The advantages gained from replacing controlled sources by their corresponding R-nullor realizations are (i) ease of circuit analysis, and (ii) possibility of explaining the relationships between apparently unrelated RC-active networks simply replacing the controlled sources by their nullor equivalents.

The nullor-resistor equivalent networks for the four controlled sources are listed in Table 2-1 [24]. The validity of these nullor networks can be checked by applying Kirchoff's voltage law (KVL) and Kirchoff's current law (KCL) in conjunction with the properties of the nullator and the norator which addressed in Section 2.1.2.

A particularly useful result can be resulted from Table 2-1 by applying the principle of the nullor network simplification [24].

An infinite-gain controlled source of any of the four types is exactly equivalent to a nullor.

Table 2-1 Controlled sources and corresponding nullor models [24]

Name	Definition	Symbol	Constraint	Nullor Model
VCVS	$V_2 = uV_1$ $I_1 = 0$ $I_2 = \text{arbitrary}$		$V_2 = \frac{r_1}{r_2} V_1$ $I_1 = 0$ $I_2 = \text{arbitrary}$	
VCCS	$I_2 = gV_1$ $I_1 = 0$ $V_2 = \text{arbitrary}$		$I_2 = gV_1$ $I_1 = 0$ $V_2 = \text{arbitrary}$	
CCVS	$V_2 = rI_1$ $V_1 = 0$ $I_2 = \text{arbitrary}$		$V_2 = rI_1$ $V_1 = 0$ $I_2 = \text{arbitrary}$	
CCCS	$I_2 = \beta I_1$ $V_1 = 0$ $V_2 = \text{arbitrary}$		$I_2 = I_1 \frac{r_1}{r_2}$ $V_1 = 0$ $V_2 = \text{arbitrary}$	

2.2 Network Analysis Methods

2.2.1 Review of the Nodal Analysis of a Passive RLC Network

The nodal analysis of an arbitrarily interconnected network of RLC passive elements and independent current sources are well known. The analysis steps are

Step 1: A datum reference node is selected and labeled node 0. Then, the procedure is to solve the remaining node voltages with respect to the datum reference node.

Step 2: All the other nodes are labeled from 1 to N. Then, the problem is to solve for the corresponding node voltages V_1, V_2, \dots, V_N , where these voltages are with respect to node 0.

Step 3: The nodal equation, $[I] = [Y_N][V]$, contain the current column vector $[I] = \{I_1, I_2, \dots, I_i, \dots, I_N\}$, where the i th component I_i is defined as the sum of the currents flowing into the i th node from the independent current sources. Therefore, each of the I_i term is usually written by inspection and the current vector $[I]$ is thereby obtained.

Step 4: The nodal admittance matrix $[Y_N] = \{y_{ij}\}$ has dimensions $(N \times N)$ and may usually be written by inspection, using

$y_{ij} =$ sum of transform admittances connected to node i .

$-y_{ij} =$ sum of transform admittances connected to nodes i and j .

It follows that $Y_{N \times N}$ is a symmetric matrix: $y_{ij} = y_{ji}$.

Step 5: The N nodal equations of the network are then written in the matrix form.

$$\begin{bmatrix} I_1 \\ \vdots \\ I_i \\ \vdots \\ I_j \\ \vdots \\ I_N \end{bmatrix} = \begin{bmatrix} y_{11} & \cdots & y_{1i} & \cdots & y_{1j} & \cdots & y_{1N} \\ \vdots & & \vdots & & \vdots & & \vdots \\ y_{i1} & \cdots & y_{ii} & \cdots & y_{ij} & \cdots & y_{iN} \\ \vdots & & \vdots & & \vdots & & \vdots \\ y_{j1} & \cdots & y_{ji} & \cdots & y_{jj} & \cdots & y_{jN} \\ \vdots & & \vdots & & \vdots & & \vdots \\ y_{N1} & \cdots & y_{Ni} & \cdots & y_{Nj} & \cdots & y_{NN} \end{bmatrix} \begin{bmatrix} V_1 \\ \vdots \\ V_i \\ \vdots \\ V_j \\ \vdots \\ V_N \end{bmatrix}$$

2.2.2 The Nodal Analysis of a RLC-Nullor Network

A.C. Davis proposed a nodal method for the RLC-nullor networks. This method is quite similar to the nodal analysis method of the passive RLC networks. The details of the proof can be found in [24].

The nodal analysis method for the RLC-nullor networks provides a systematic method to solve the N independent nodal voltages of an $(N+1)$ -node network, where the network contains an arbitrary interconnection of RLC elements, independent current sources and nullors. It is simply an extension of the passive nodal analysis method. Let us consider the case that is involved in obtaining the nodal equations when there are K nullors connected arbitrarily between the nodes of the passive network. The procedure for analyzing RLC-nullor networks is as follows:

Step 1: Remove all the K nullors from the network, leaving a passive $(N+1)$ node network, one node of which is the datum reference node.

Step 2: Write the $(N \times N)$ nodal admittance matrix equations for the remaining $(N+1)$ node passive network. $Y_{N \times N}$ is the passive nodal admittance matrix.

Step 3: For a nullator that was connected between the nodes p and q , for example, add the elements of column q to the elements of column p . Then delete column q . The number of columns of the Y matrix is thereby reduced to $(N-1)$. Repeat this process for every nullator not connected to the datum reference node.

Step 4: For a norator that was connected between the nodes l and m , for example, add the elements of row l to the elements of row m . Then delete row l . The number of rows of the

Y matrix is thereby reduced to $(N-1)$. Repeat this process for every norator not connected to the datum reference node.

Step 5: For a nullator that is connected between node k and the datum reference node, delete the k th column of the admittance matrix. Repeat this process for every nullator connected to the datum reference node.

Step 6: For a norator that is connected between node i and the datum reference node, delete the i th row. Repeat this process for every norator.

Step 7: The preceding six steps result in the reduction of the $(N \times N)$ nodal admittance matrix of the passive network to the $(N-K) \times (N-K)$ nodal admittance matrix of the K -nullor $(N+1)$ node RLC-nullor network. The corresponding $(N-K)$ equations may be solved for the $(N-K)$ independent node voltages.

2.3 RLC-Nullor Network Transformation

If we consider the R-nullor equivalent networks for the four basic controlled sources in Table 2-1, we see that in the procedure mentioned in [22] for converting a VM circuit to a CM circuit, the nullor equivalent of a VCVS naturally gets transformed to the nullor equivalent of a CCCS when we adopt the procedure as mentioned in [22], namely, interchanging the nullator and norator in the R-nullor equivalent circuit of each of the VCVSs in the VM circuit. Thus, interchanging the input and output ports and replacing each VCVS by a CCCS (with input-output ports switched around) appears as a natural and convenient technique for deriving a current-mode system from an associated voltage-mode system, and is consistent with what was proposed in [10]. However, if we consider

ideal controlled source elements (i.e., with infinite gain), the knowledge that any of the four types is exactly equivalent to a nullor [24], leads to the following result.

2.3.1 Three-Terminal Nullor — Three-Terminal OA

Consider a VM circuit N_V implemented using ideal three-terminal VCVS (i.e., with infinite gain). Then, the corresponding CM circuit N_C can be obtained by *replacing each ideal VCVS by any of the four possible controlled sources, namely VCVS, CCCS, VCCS or CCVS, with the input and output ports of the latter switched around relative to that of the VCVS in the given VM network N_V .* Then the reverse short circuit CTF of the resulting network N_C is identical to the forward open circuit VTF of the original VM circuit N_V . As a consequence, it is clear that theoretically the various sensitivities with respect to the corresponding parameters in the two circuits will be identical. It may be mentioned that when N_C uses CCCS to replace the VCVS in N_V , then N_C is nothing but the transpose of N_V as defined in [10].

We thus conclude that as long as the ideal OA is used as a three-terminal device, the same OA can be used to produce identical voltage and current transfer functions, by simply adopting the conversion principles suggested above. We now illustrate the conversion principle by considering the following example.

A voltage-mode circuit implemented using an ideal three-terminal OA (i.e., with infinite gain) is shown in Figure 2-9(a). The voltage gain is $-\frac{R_2}{R_1}$. We now replace the ideal VCVS by its nullor equivalent in Figure 2-9(b), and use the fact that the nullor equivalents of all the four ideal sources are the same. We can replace the ideal VCVS in Figure 2-9(b) by an ideal CCCS to obtain the VM circuit using a CCCS, as shown in

Figure 2-9(c) (where K tends to infinity), whose VTF should be the same as that of the circuit of Figure 2-9(a). If we now take the transpose of the circuit of Figure 2-9(c), we get the circuit shown in Figure 2-9(d), whose reverse CTF according to [10] should be the same as the VTF of that of Figure 2-9(c), which is the same as that of Figure 2-9(a). We get the current gain function $\frac{I_o}{I_i} = -\frac{R_2}{R_1}$. We now replace the nullor version of the VCVS in Figure 2-9(d) by an OA to obtain Figure 2-10, whose CTF is the same as the VTF of the circuit of Figure 2-9(a). It is observed that the CM circuit of Figure 2-10 could have been obtained directly from the VM circuit of Figure 2-9(a) by following the conversion procedure given in the earlier part of this section, by simply turning around the input and output ports of the VCVS in Figure 2-9(a).

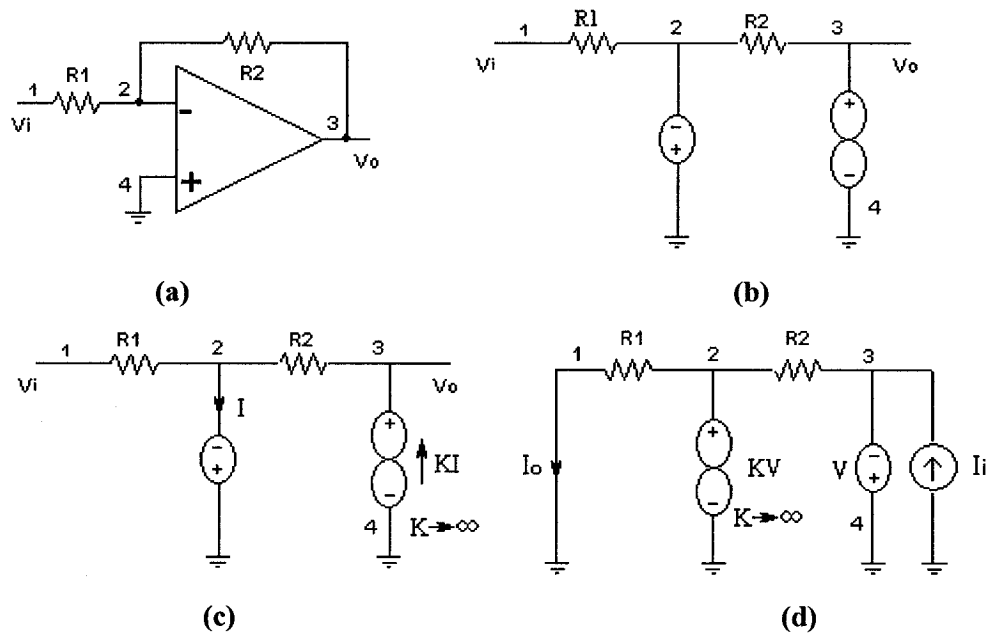


Figure 2-9 (a) VM network. (b) VM network using nullor.(c) VM network using CCCS-nullor. (d) CM network using VCVS-nullor

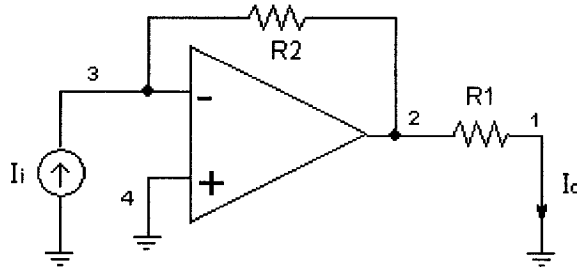


Figure 2-10 The corresponding CM network of Figure 2-9(a)

The above result can be confirmed by a direct analysis of the networks of Figure 2-9(a) and Figure 2-10. Applying KCL, we can get

$$\frac{V_o}{V_i} = \frac{I_o}{I_i} = -\frac{R_2}{R_1} \quad (2.4)$$

Obviously, the CTF of the CM network obtained by using the proposed method is identical to the VTF of the original VM network.

Thus, if we are given a VM network with RC elements and OAs modeled as three-terminal devices, then we can get the corresponding CM network by retaining the RC elements in place and interchanging the input and output terminals of each of the OAs in the VM network. Further, the reverse CTF of the CM network is identical to that of the forward VTF of the original VM network.

2.3.2 Four-Terminal Nullor — Operational Floating Amplifier

Consider a RC-OA network where the OA is modeled as a four-terminal device. Since the four-terminal device can be modeled as a four-terminal nullor, and *any of the four infinite-gain controlled sources is exactly equivalent to a nullor*, we can replace this nullor by a four-terminal CCCS. We now take the transpose of this resulting network

which replaces each four-terminal CCCS by a four-terminal VCVS with its ports reversed (see Chapter 1). Each of these four-terminal VCVS can now be replaced by an OFA.

Thus, if we are given a VM network with RC elements and OAs modeled as four-terminal devices, then we can get the corresponding CM network by retaining the RC elements in place and replacing each of the OAs in the VM network by OFAs with their input and output ports reversed. Further, the reverse CTF of the CM network is identical to the forward VTF of the original VM network. This is illustrated by the following example.

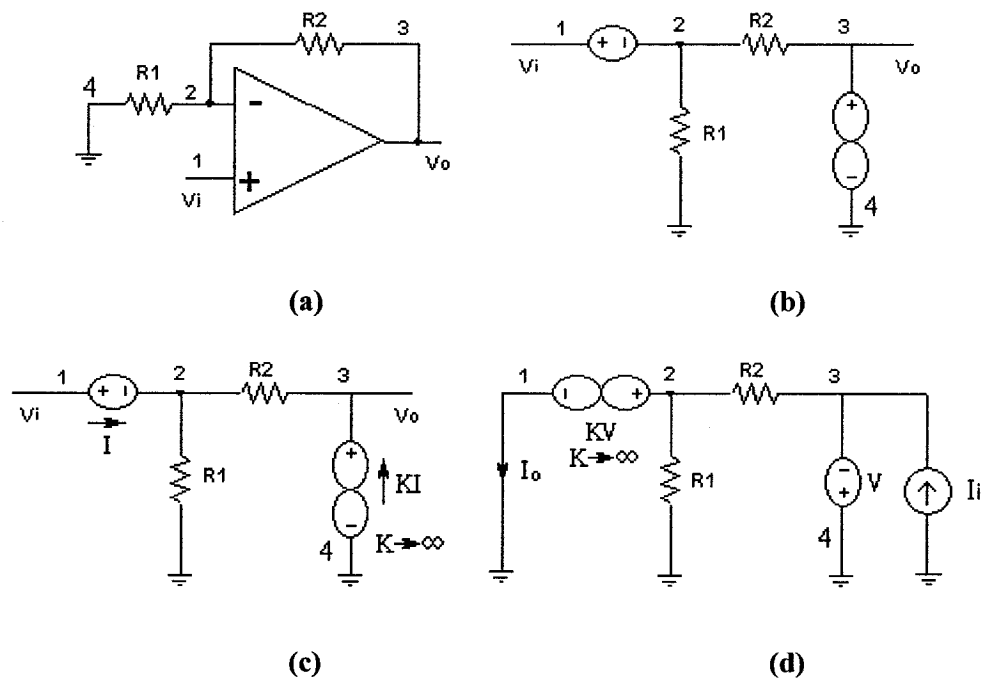


Figure 2-11 (a) VM network. (b) VM network using nullor. (c) VM network using CCCS-nullor. (d) CM network using VCVS-nullor

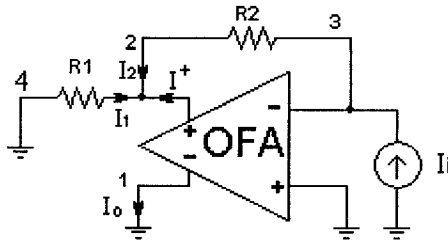


Figure 2-12 The corresponding CM network of Figure 2-11(a)

A voltage-mode circuit implemented using an ideal OA of infinite gain is shown in Figure 2-11(a). We now replace the ideal VCVS by its nullor equivalents shown in Figure 2-11(b). Using the fact that the nullor equivalents of all the four ideal sources are the same, we can replace the ideal VCVS in Figure 2-11(b) by an ideal CCCS to obtain the VM circuit using a CCCS, as shown in Figure 2-11(c) (where K tends to infinity), whose VTF should be the same as that of the circuit of Figure 2-11(a). If we now take the transpose of the circuit of Figure 2-11(c), we get the circuit shown in Figure 2-11(d), whose reverse CTF according to [10] should be the same as the VTF of that of Figure 2-11(c), which is the same as that of Figure 2-11(a). We now replace the nullor version of the VCVS in Figure 2-11(d) by an OFA to obtain Figure 2-12, whose CFT is the same as the VTF of the circuit of Figure 2-11(a). It is seen that the CM circuit of Figure 2-12 could have been obtained directly from the VM circuit of Figure 2-11(a) by following the conversion procedure given in the earlier part of this section, by simply turning around the input and output ports of the VCVS in Figure 2-11(a).

For Figure 2-11(a), applying KCL, it is easy to get

$$\frac{V_o}{V_i} = 1 + \frac{R_2}{R_1} \quad (2.5)$$

For Figure 2-12, KCL at node 2 gives,

$$I_1 + I_2 + I^+ = 0 \quad (2.6)$$

where $V_2 = -I_1R_1 = -I_2R_2$, $I_i = I_2$, and $I^+ = -I_o$, substituting for I_1 and I_2 into (2.6), we get

$$\frac{I_o}{I_i} = 1 + \frac{R_2}{R_1} \quad (2.7)$$

Again, the CTF of the CM network obtained by using the proposed method is identical to the VTF of the original VM network when the OA is configured as a four-terminal device.

2.4 Summary

In this chapter, the concept of nullors has been reviewed. The knowledge that any of the infinite-gain controlled sources is equivalent to a nullor, along with the concept of transposed networks [10], has made it possible to derive current-mode networks from voltage-mode networks. It has been shown that if the ideal OA is configured as a three-terminal device, the same OA can be used to produce the CM network from the VM network having the same transfer function as the latter. Further, if the ideal OA is configured as a four-terminal device, a new device, namely, the OFA described in Chapter 5, needs to be used to produce the CM transfer function which is identical to the VM transfer function.

Chapter 3

Three-Terminal OA-Based VM and CM Filters

The OA acts is a very important active device in the realization of voltage-mode filters. In Chapter 2, we introduced a new method to realize a CM network from a VM network with the same OA being used in both the networks, using the principles of transposed networks and nullors. In this chapter, we consider the conversion of single-amplifier as well as multi-amplifier biquadratic VM filters to CM filters using the same OA, when the OA is configured as a three-terminal network. Since the OA is a finite gain and finite bandwidth device, it may affect the practical performance of the filters. Thus, it is important to study the effect of the OA gain bandwidth on the CM and VM filters. We choose the Akerberg-Mossberg (A & M) biquadratic filter with multi-OA to compare the performance of the CM filter with that of the corresponding VM filter. Both the theoretical and the analog wave bench (AWB) simulation studies are conducted to make a comparison of the pole-Q and pole frequency for the CM and VM filters. Furthermore, the effects of the input impedance and load impedance are also considered in the AWB simulations.

3.1 Fundamentals of Active VM Filters

3.1.1 Operational Amplifiers

Figure 3-1 shows the circuit symbol and the small signal equivalent circuit for an OA with the input terminals numbered 1 and 2 and the output terminal numbered 3. The differential gain is denoted by A , where $V_{out} = A(V^+ - V^-)$. Ideally, the gain, the common-mode rejection ratio, and the input impedances (both differential and common mode) are infinite. The output impedance is zero. In practice, the performance of the filter depends on the nature of the gain A , which produces remarkable effects on the response of the filter built with an OA.

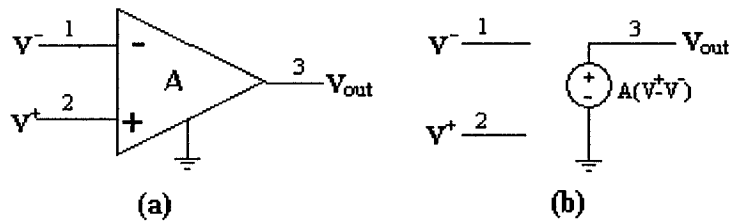


Figure 3-1 (a) Circuit symbol and (b) small signal equivalent circuit of an OA

Apart from the small signal ac characteristics, an OA has several deviations related to the ideal DC operation. Since the IC OA are DC coupled, there are associated DC problems, such as the input offset voltage, the input bias current and the input offset current. The offset will cause the amplifier to operate in a region where the gain might not be at its maximum. Because of DC offset, the dynamic range will likely be impaired. Special attention should be paid to DC problems, especially in the design of active low-pass filters.

Regarding the finite frequency-dependent gain A , Figure 3-2 shows a typical one-pole model frequency response of an OA. Note that gain A has a uniform 6dB/octave roll-off with 3-dB frequency f_b and a unity-gain bandwidth f_t . Such a uniform 6-dB/octave roll-off is required to ensure stable operation of the OA and is achieved by including frequency compensating networks either internally or externally.

The gain A of an OA which has a frequency response as shown in Figure 3-2 is given by

$$A = \frac{A_o}{1 + \frac{s}{\omega_b}} \quad (3.1)$$

where A_o is the DC gain and $\omega_b = 2\pi f_b$.

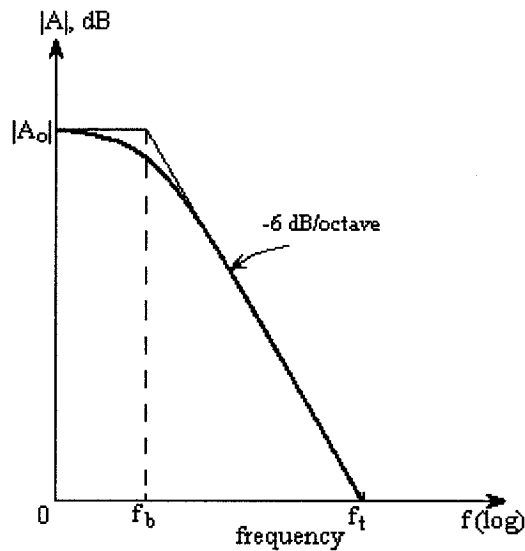


Figure 3-2 One-pole model frequency response of an OA

3.1.2 Mathematical Model of General Filters

Figure 3-3 illustrates a general linear filter, characterized in the time domain by its impulse response $h(t)$, which is the output signal $y(t)$ produced as the response to an unit

impulse $\delta(t)$, applied at the input. For an arbitrary input signal $x(t)$, the output signal $y(t)$ is given by the convolution integral

$$y(t) = \int_{-\infty}^{+\infty} h(t - \tau)x(\tau)d\tau \quad (3.2)$$

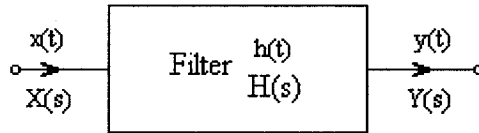


Figure 3-3 A filter on the system level

Under Laplace transformation, (3.2) can be written as

$$Y(s) = H(s) X(s) \quad (3.3)$$

In general, $H(s)$ is written as

$$\begin{aligned} H(s) &= \frac{Y(s)}{X(s)} \\ &= \frac{a_m s^m + a_{m-1} s^{m-1} + \dots + a_0}{b_n s^n + b_{n-1} s^{n-1} + \dots + b_0} = \frac{N(s)}{D(s)} \end{aligned} \quad (3.4)$$

where $m \leq n$ for any realizable physical network, the denominator polynomial $D(s)$ is known as the characteristic polynomial, and the degree of $D(s)$, that is n , is the order of the filter.

According to the categories of the transfer functions of the filters, the four most common types of filters are classified as low-pass (LP), high-pass (HP), band-pass (BP), band-stop (BS) filters. In some applications, a filter exhibits phase delay and constant magnitude without any attenuation over whole frequency band. Such a filter is called an all-pass (AP) filter.

3.1.3 Mathematical Model of Second-Order (Biquadratic) Filters

The transfer function, (3.4), can be factored into products of biquadratic and possibly one bilinear transfer functions [25]. Hence, the biquadratic filters play an important role in the design of higher order filters. A practical second-order transfer function is written as

$$H(s) = \frac{p_2s^2 + p_1s + p_0}{s^2 + \frac{\omega_o}{Q_o}s + \omega_o^2} = \frac{N(s)}{D(s)} \quad (3.5)$$

The denominator polynomial is expressed in terms of ω_o and Q_o , referred to as the pole- ω and pole- Q . The numerator coefficients determine the gain and the type of the filter. Table 3-1 lists some special cases of interest.

Table 3-1 Some Special Cases of Second-order Transfer Functions

Types of filter	$N(s)$
Low-Pass (LP)	$H_o\omega_o^2$
High-Pass (HP)	H_os^2
Band-Pass (BP)	$H_o(\omega_o/Q_o)s$
Band-Stop (BS)	$H_o(s^2 + \omega_o^2)$
Low-Pass Notch (LPN)	$H_o(s^2 + \omega_n^2)$ when $\omega_n > \omega_o$
High-Pass Notch (HPN)	$H_o(s^2 + \omega_n^2)$ when $\omega_n < \omega_o$
All-Pass (AP)	$H_o(s^2 - (\omega_o/Q_o)s + \omega_o^2)$

3.1.4 Realization of the Second-Order Filters

A second-order filter is also named as a biquadratic filter since the transfer function is a ratio of second-order polynomials. A frequency selective transfer function is achieved only when the poles of the transfer function are complex and lie in the left-hand

side of the complex s-plane. A passive network containing only positive resistances and capacitances cannot produce complex poles or zeros. Introducing active devices, such as voltage amplifiers, makes it possible to realize a transfer function with complex poles and zeros.

In general, the realization of a biquadratic filter consists of one or more voltage amplifiers. Minimizing the number of amplifiers has the advantage of lower cost and power dissipation. Single-amplifier filters can achieve a wide useful operating frequency range. Multiple-amplifier filters lend to additional desirable features, such as achieving high Q-factor, enabling easy tuning, and reducing sensitivity to components. In the following sections, we will discuss the single-amplifier filter as well as multi-amplifier filters to realize CM filters from the corresponding VM filters.

3.2 Realizing CM Filter with Three-Terminal Operational Amplifier

In this section, we apply the principle introduced in Chapter 2 to obtain CM filters from VM filters.

3.2.1 Single Amplifier Biquadratic Filter Using Ideal VCVS

Consider the VM single amplifier biquadratic (SAB) filter using an ideal OA (an ideal VCVS), as shown in Figure 3-4. The voltage transfer function of this network is given by

$$\frac{V_o}{V_i} = -\frac{Y_3 Y_4}{Y_1 Y_2 + Y_2 Y_3 + Y_1 Y_3 + Y_1 Y_4} \quad (3.6)$$

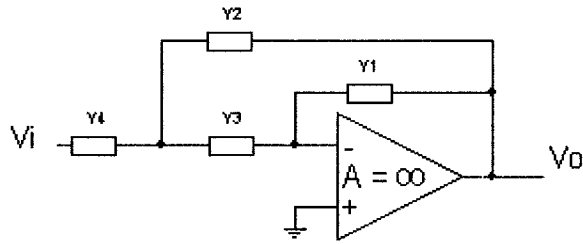


Figure 3-4 Voltage-mode SAB filter

If we now replace the ideal VCVS by its nullor equivalent, and use the fact that the nullor equivalents of all the four ideal sources are the same, we can replace the ideal VCVS in Figure 3-4 by an ideal CCCS to obtain the VM circuit using a CCCS, as shown in Figure 3-5 (where k tends to infinity), whose VTF should be the same as that of the circuit in Figure 3-4. In fact, it can easily be verified that this is true.

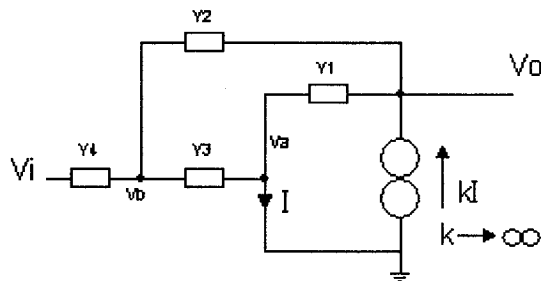


Figure 3-5 Voltage-mode SAB filter using a CCCS

If we now take the transpose of the circuit of Figure 3-5, we get the circuit shown in Figure 3-6, whose reverse CTF according to [10] should be the same as the VTF of that of Figure 3-5, that is, the same as that of Figure 3-4. It can indeed be verified that the reverse CTF I_o/I_i of the CM filter of Figure 3-6 is given by

$$\frac{I_o}{I_i} = -\frac{Y_3 Y_4}{Y_1 Y_2 + Y_2 Y_3 + Y_1 Y_3 + Y_1 Y_4} \quad (3.7)$$

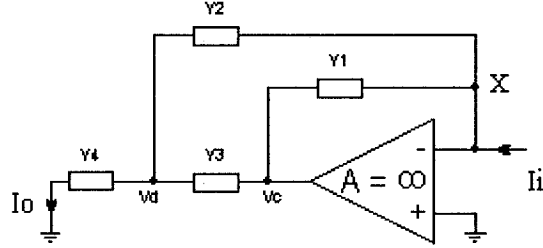


Figure 3-6 Current-mode SAB filter

It is observed that the CM circuit of Figure 3-6 could have been obtained directly from the VM circuit of Figure 3-4 by following the conversion procedure given in the earlier part of this section, by simply turning around the input and output ports of the VCVS in Figure 3-4.

3.2.2 Multiple Amplifier Biquadratic Filter Using Ideal VCVS

Tow-Thomas biquadratic filter

The Tow-Thomas VM filter N_V employing three OAs is shown in Figure 3-7. Its voltage transfer function is given by

$$\frac{V_o}{V_i} = -\frac{\frac{C_1}{C}s^2 + \frac{1}{RC}\left(\frac{R}{R_1} - \frac{r}{R_3}\right)s + \frac{1}{C^2 RR_2}}{s^2 + \frac{1}{CR_4}s + \frac{1}{C^2 R^2}} \quad (3.8)$$

The corresponding CM network N_C can be obtained directly by reversing the input/out ports of each of the VCVS elements in Figure 3-7, and is shown in Figure 3-8.

It can be verified that the reverse CTF of this circuit is given

$$\frac{I_o}{I_i} = - \frac{[\frac{C_1}{C}s^2 + \frac{1}{CR}(\frac{R}{R_1} - \frac{r}{R_3})s + \frac{1}{C^2RR_2}]}{s^2 + \frac{1}{CR_4}s + \frac{1}{C^2R^2}} \quad (3.9)$$

which is the same as the VTF of the VM filter of Figure 3-7.

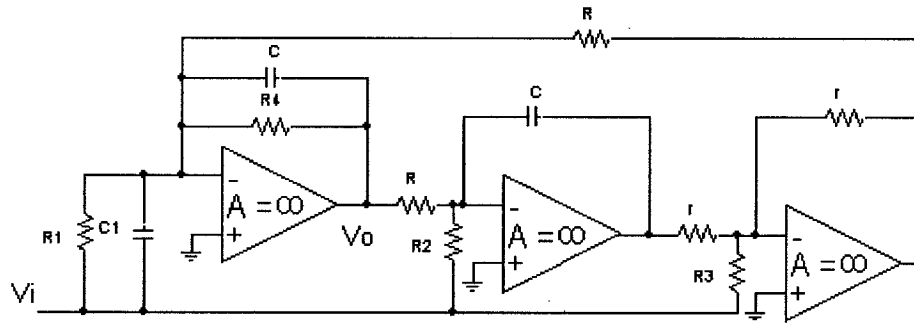


Figure 3-7 Voltage-mode Tow-Thomas biquadratic filter

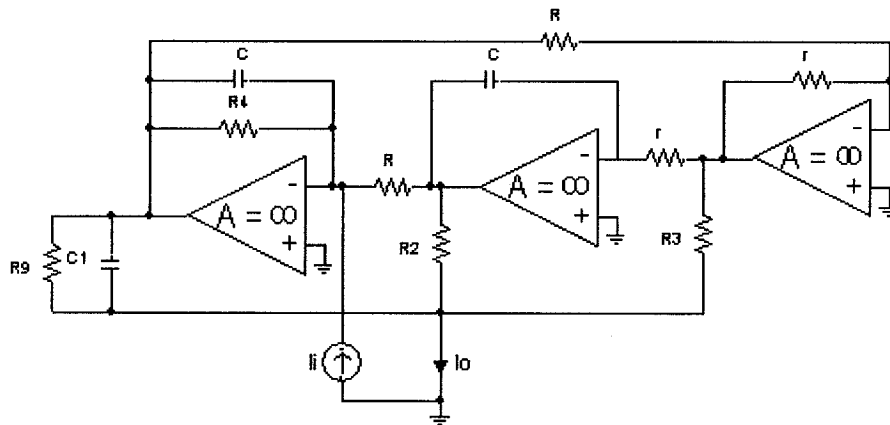


Figure 3-8 Current-mode Tow-Thomas biquadratic filter

Akerberg and Mossberg (A & M) biquadratic filters

The A & M filter which can produce both low-pass and band-pass filter responses depending upon the choice of the output signal node is shown in Figure 3-9. The two voltage transfer functions of the A & M filter are

$$\frac{V_{o1}}{V_i} = -\frac{s/RC_1}{s^2 + s\frac{1}{R_1C_1} + \frac{r_1}{C_1C_2R_2rr_2}} \quad (3.10)$$

and

$$\frac{V_{o2}}{V_i} = -\frac{\frac{r_1}{C_1C_2Rrr_2}}{s^2 + s\frac{1}{R_1C_1} + \frac{r_1}{C_1C_2R_2rr_2}} \quad (3.11)$$

Figure 3-10 shows the corresponding CM network N_C obtained directly from the VM filter by reversing the input/out ports of each of the VCVS elements in Figure 3-9. It can easily be shown that the two current transfer functions are given by

$$\frac{I_o}{I_{i2}} = -\frac{\frac{r_1}{C_1C_2Rrr_2}}{s^2 + \frac{1}{R_1C_1}s + \frac{r_1}{C_1C_2rr_2R_2}} \quad \text{with } I_{i1}=0 \quad (3.12)$$

and

$$\frac{I_o}{I_{i1}} = -\frac{\frac{1}{RC_1}s}{s^2 + \frac{1}{R_1C_1}s + \frac{r_1}{C_1C_2rr_2R_2}} \quad \text{with } I_{i2}=0 \quad (3.13)$$

which are, respectively, the same as the VTFs (V_{o1}/V_i) and (V_{o2}/V_i) of the VM filter of Figure 3-9.

Thus, we can obtain a CM filter from a VM filter that employs three-terminal ideal VCVSs by simply reversing the input/output terminals of each of the VCVSs in the latter. Similarly, we can conclude that if the VM filter consists of only three-terminal CCCS elements, then we can obtain the corresponding CM filter by simply reversing the input/output terminals of the CCCSs in the former.

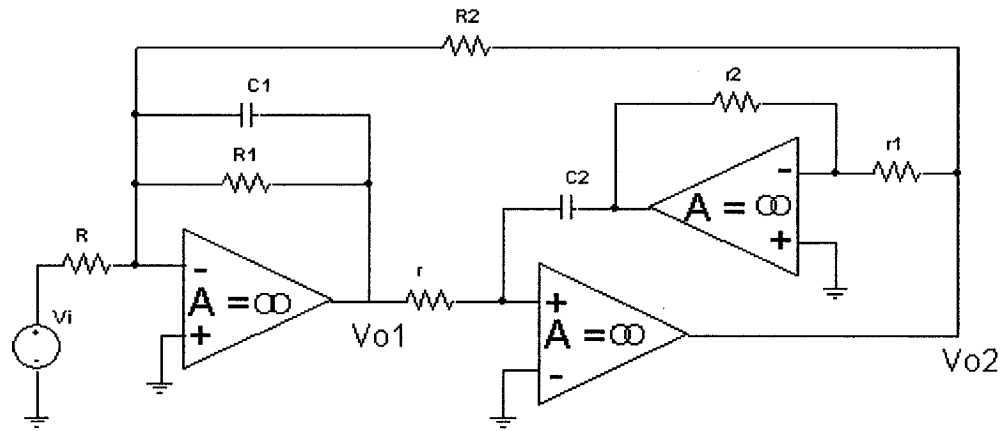


Figure 3-9 Voltage-mode A & M biquadratic filter

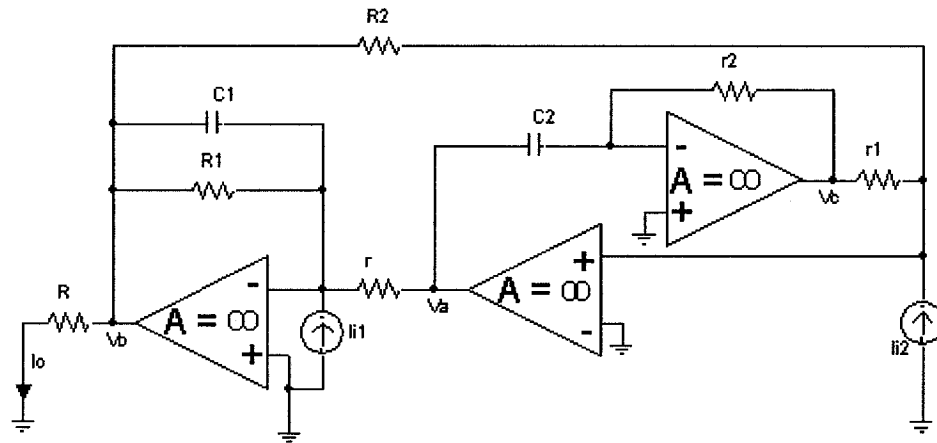


Figure 3-10 Current-mode A & M biquadratic filter

3.3 Effect of Gain Bandwidth of OA on the Pole Frequency and Pole Q

The above analysis has been made under the assumption of ideal passive components and ideal active devices (i.e., ideal OAs). However, it is important to study the effect of the non-ideal characteristics of the active device. Since the active device used is the OA, one important deviation from its ideal characteristic arises due to the

limited amplifier bandwidth. We now analyze the effect of finite gain bandwidth on the pole-frequency and pole-Q factor of the CM filter and compare them with those of the corresponding VM filter.

The analytical procedure is demonstrated for a multi-OA filter, namely, the Akerberg-Mossberg (A & M) three-OA biquad.

3.3.1 The Voltage-Mode A & M Filter

For the VM A & M filter shown in Figure 3-9, let us assume that each OA has a gain A . Then, the LP and BP voltage transfer functions are given by:

$$\frac{V_{o2}}{V_i} = \frac{1/rR}{\frac{1}{R_2 r} + \left(\frac{\frac{1}{R} + \frac{1}{R_2}}{A} + \left(1 + \frac{1}{A} \right) \left(\frac{1}{R_1} + SC_1 \right) \right) \left(\frac{\frac{1}{r} + SC_2}{A} + \frac{\frac{SC_2}{r_1}}{\frac{1}{r_2} + \frac{1/r_2 + 1/r_1}{A}} \right)} \quad (3.14)$$

$$\frac{V_{o1}}{V_i} = \frac{\frac{1}{R} \left(\frac{\frac{1}{r} + SC_2}{A} + \frac{\frac{SC_2}{r_1}}{\frac{1}{r_2} + \frac{1/r_2 + 1/r_1}{A}} \right)}{\frac{1}{R_2 r} + \left(\frac{\frac{1}{R} + \frac{1}{R_2}}{A} + \left(1 + \frac{1}{A} \right) \left(\frac{1}{R_1} + SC_1 \right) \right) \left(\frac{\frac{1}{r} + SC_2}{A} + \frac{\frac{SC_2}{r_1}}{\frac{1}{r_2} + \frac{1/r_2 + 1/r_1}{A}} \right)} \quad (3.15)$$

To evaluate the performance of the VM filters, we use the one-pole model of the OA,

$$A = A(s) = \frac{A_o}{1 + \frac{s}{\omega_b}}$$

where ω_b is the pole frequency. For frequencies $\omega \gg \omega_b$, we may assume

$$A = A(s) \approx \frac{A_o \omega_b}{s} \approx \frac{\omega_t}{s}$$

where $\omega_t \approx A_o \omega_b$ is the unity gain bandwidth of the OA. We further assume that

$$R = R_2 = r = r_1 = r_2, \quad C_1 = C_2 = C, \quad R_1 = Q_o R$$

and $\omega_o \ll \omega_t$,

where ω_o and Q_o are the pole frequency and pole-Q of the filter. With the above assumptions, we get the overall denominator $D_V(s)$ to be

$$\begin{aligned} D_V(s) = & 4 \frac{s^5}{\omega_t^3} + \left[\frac{4\omega_o}{Q_o \omega_t^3} + \frac{8\omega_o}{\omega_t^3} + \frac{3}{\omega_t^2} \right] s^4 + \left[\frac{3\omega_o^3}{Q_o \omega_t^2} - \frac{\omega_o^3}{\omega_t^2} \right] s^3 \\ & + \left[1 + \frac{2\omega_o^2}{\omega_t^2} + \frac{\omega_o^2}{Q_o \omega_t^2} + \frac{3\omega_o}{\omega_t} \right] s^2 + \left[\frac{\omega_o^2}{Q_o \omega_t} + \frac{\omega_o}{Q_o} \right] s + \omega_o^2 \end{aligned} \quad (3.16)$$

Assuming that the actual operating frequency remains close to the pole frequency ω_o , we find the solution following the principle of dominant root search [42]. For this purpose, we use the approximations $s^3 = -\omega_o^2 s$, $s^4 = \omega_o^4$, $s^5 = \omega_o^4 s$ and simplify $D_V(s)$.

This leads to

$$\begin{aligned} D_V(s) \approx & s \frac{4\omega_o^4}{\omega_t^3} + \left[\frac{4\omega_o}{Q_o \omega_t^3} + \frac{8\omega_o}{\omega_t^3} + \frac{3}{\omega_t^2} \right] \omega_o^4 - s \left[\frac{3\omega_o^3}{Q_o \omega_t^2} - \frac{\omega_o^3}{\omega_t^2} \right] \\ & + s^2 \left[1 + \frac{2\omega_o^2}{\omega_t^2} + \frac{\omega_o^2}{Q_o \omega_t^2} + \frac{3\omega_o}{\omega_t} \right] + s \left[\frac{\omega_o^2}{Q_o \omega_t} + \frac{\omega_o}{Q_o} \right] + \omega_o^2 \\ \approx & s^2 \left[1 + \frac{2\omega_o^2}{\omega_t^2} + \frac{\omega_o^2}{Q_o \omega_t^2} + \frac{3\omega_o}{\omega_t} \right] + s \frac{\omega_o}{Q_o} \left[1 + \frac{\omega_o}{\omega_t} + \frac{4Q_o \omega_o^3}{\omega_t^3} - \frac{3\omega_o^2}{\omega_t^2} + \frac{Q_o \omega_o^2}{\omega_t^2} \right] \\ & + \omega_o^2 \left[1 + \frac{4\omega_o^3}{Q_o \omega_t^3} + \frac{8\omega_o^3}{\omega_t^3} + \frac{3\omega_o^2}{\omega_t^2} \right] \\ \approx & \Delta_v \left[s^2 + s \frac{\omega_o(1+\gamma_v)}{Q_o \Delta_v} + \frac{\omega_o^2(1+\delta_v)}{\Delta_v} \right] \\ = & \Delta_v (s^2 + s \frac{\omega_{oa}}{Q_{oa}} + \omega_{oa}^2) \end{aligned}$$

where
$$\Delta_v = 1 + \frac{2\omega_o^2}{\omega_t^2} + \frac{\omega_o^2}{Q_o\omega_t^2} + \frac{3\omega_o}{\omega_t}$$

$$\gamma_v = \frac{\omega_o}{\omega_t} + \frac{4Q_o\omega_o^3}{\omega_t^3} - \frac{3\omega_o^2}{\omega_t^2} + \frac{Q_o\omega_o^2}{\omega_t^2}$$

$$\delta_v = \frac{4\omega_o^3}{Q_o\omega_t^3} + \frac{8\omega_o^3}{\omega_t^3} + \frac{3\omega_o^2}{\omega_t^2}$$

The terms like $(\frac{\omega_o}{\omega_t})^2, (\frac{\omega_o}{\omega_t})^3 \dots$ can be ignored, and $\frac{1}{(1+x)^n} \approx 1-nx$ for first-order

accuracy, $x \ll 1$, where $x = \frac{\omega_o}{\omega_t}$, we get the following expressions for the deviations in the

pole-frequency and pole-Q of the VM filter of Figure 3-9.

$$\sigma_v = \frac{\omega_{oa} - \omega_o}{\omega_o} = \left(\frac{1 + \delta_v}{\Delta_v} \right)^{\frac{1}{2}} - 1 \approx -\frac{3\omega_o}{2\omega_t} \quad (3.17)$$

and

$$\eta_v = \frac{Q_{oa} - Q_o}{Q_o} = \frac{[\Delta_v(1 + \delta_v)]^{\frac{1}{2}}}{(1 + \gamma_v)} - 1 \approx \frac{\omega_o}{2\omega_t} \quad (3.18)$$

where ω_{oa} and Q_{oa} are the realized values.

3.3.2 The Current-Mode A & M Filter

Figure 3-10 shows the CM A & M filter. The LP and BP current transfer functions (CTF) are obtained as

$$\frac{I_o}{I_{i2}} = \frac{1/rR}{\frac{1}{R_2 r} + \left(\frac{1}{Ar} + \left(1 + \frac{1}{A} \right) \left(\frac{1}{R_1} + SC_1 \right) \right) \left(\frac{\frac{1}{R_2} + \frac{1}{r_1} + \frac{SC_2}{r_1}}{A} + \frac{1}{r_2 + \frac{1/r_2 + SC_2}{A}} \right)} \quad (3.19)$$

and

$$\frac{I_o}{I_{i1}} = \frac{\frac{1}{R} \left(\frac{\frac{1}{R_2} + \frac{1}{r_1} + \frac{SC_2}{r_1}}{A} + \frac{1}{r_2 + \frac{1/r_2 + SC_2}{A}} \right)}{\frac{1}{R_2 r} + \left(\frac{1}{Ar} + \left(1 + \frac{1}{A} \right) \left(\frac{1}{R_1} + SC_1 \right) \right) \left(\frac{\frac{1}{R_2} + \frac{1}{r_1} + \frac{SC_2}{r_1}}{A} + \frac{1}{r_2 + \frac{1/r_2 + SC_2}{A}} \right)} \quad (3.20)$$

With the same assumptions as the VM filter in Section 3.3.1, we get denominator $D_I(s)$ to be

$$\begin{aligned} D_I(s) = & 2 \frac{s^5}{\omega_i^3} + \left[\frac{2\omega_o}{Q_o \omega_i^3} + \frac{4\omega_o}{\omega_i^3} + \frac{2}{\omega_i^2} \right] s^4 + \left[\frac{2\omega_o^4}{Q_o \omega_i^3} + \frac{2\omega_o^4}{\omega_i^3} + \frac{2\omega_o^3}{Q_o \omega_i^2} + \frac{4\omega_o^3}{\omega_i^2} + \frac{\omega_o^2}{\omega_i} \right] s^3 \\ & + \left[1 + \frac{\omega_o}{Q_o \omega_i} + \frac{2\omega_o^2}{\omega_i^2} + \frac{4\omega_o^2}{Q_o \omega_i^2} + \frac{4\omega_o}{\omega_i} \right] s^2 + \left[\frac{\omega_o}{Q_o} + \frac{\omega_o^2}{\omega_i} + \frac{2\omega_o^2}{Q_o \omega_i} \right] s + \omega_o^2 \end{aligned} \quad (3.21)$$

We approximate $s^3 = -\omega_o^2 s$, $s^4 = \omega_o^4$, $s^5 = \omega_o^4 s$ and simplify $D_I(s)$. This leads to

$$\begin{aligned} D_V(s) \approx & s \frac{4\omega_o^4}{\omega_i^3} + \left[\frac{4\omega_o}{Q_o \omega_i^3} + \frac{8\omega_o}{\omega_i^3} + \frac{3}{\omega_i^2} \right] \omega_o^4 - s \left[\frac{3\omega_o^3}{Q_o \omega_i^2} - \frac{\omega_o^3}{\omega_i^2} \right] \\ & + s^2 \left[1 + \frac{2\omega_o^2}{\omega_i^2} + \frac{\omega_o^2}{Q_o \omega_i^2} + \frac{3\omega_o}{\omega_i} \right] + s \left[\frac{\omega_o^2}{Q_o \omega_i} + \frac{\omega_o}{Q_o} \right] + \omega_o^2 \\ \approx & s^2 \left[1 + \frac{2\omega_o^2}{\omega_i^2} + \frac{\omega_o^2}{Q_o \omega_i^2} + \frac{3\omega_o}{\omega_i} \right] + s \frac{\omega_o}{Q_o} \left[1 + \frac{\omega_o}{\omega_i} + \frac{4Q_o \omega_o^3}{\omega_i^3} - \frac{3\omega_o^2}{\omega_i^2} + \frac{Q_o \omega_o^2}{\omega_i^2} \right] \\ & + \omega_o^2 \left[1 + \frac{4\omega_o^3}{Q_o \omega_i^3} + \frac{8\omega_o^3}{\omega_i^3} + \frac{3\omega_o^2}{\omega_i^2} \right] \end{aligned}$$

$$\begin{aligned} &\approx \Delta_I \left[s^2 + s \frac{\omega_o(1+\gamma_I)}{Q_o\Delta_I} + \frac{\omega_o^2(1+\delta_I)}{\Delta_I} \right] \\ &= \Delta_I (s^2 + s \frac{\omega_{oa}}{Q_{oa}} + \omega_{oa}^2) \end{aligned}$$

where
$$\Delta_I = 1 + \frac{\omega_o}{Q_o\omega_t} + \frac{2\omega_o^2}{\omega_t^2} + \frac{4\omega_o^2}{Q_o\omega_t^2} + \frac{4\omega_o}{\omega_t}$$

$$\gamma_I = \frac{2\omega_o}{\omega_t} - \frac{2\omega_o^3}{\omega_t^3} - \frac{2\omega_o^2}{\omega_t^2} - \frac{4Q_o\omega_o^2}{\omega_t^2}$$

$$\delta_I = \frac{2\omega_o^3}{Q_o\omega_t^3} + \frac{4\omega_o^3}{\omega_t^3} + \frac{2\omega_o^2}{\omega_t^2}$$

Again, Using the assumption that terms like $(\frac{\omega_o}{\omega_t})^2, (\frac{\omega_o}{\omega_t})^3 \dots$ can be ignored, and that

$\frac{1}{(1+x)^n} \approx 1-nx, x \ll 1$, where $x = \frac{\omega_o}{\omega_t}$, we get the following expressions for the

deviations in the pole-frequency and pole-Q of the CM filter of Figure 3-10.

$$\sigma_I = \frac{\omega_{oa} - \omega_o}{\omega_o} = \left(\frac{1 + \delta_I}{\Delta_I} \right)^{\frac{1}{2}} - 1 \approx -\left(\frac{2\omega_o}{\omega_t} + \frac{\omega_o}{2Q_o\omega_t} \right) \quad (3.22)$$

and

$$\eta_I = \frac{Q_{oa} - Q_o}{Q_o} = \frac{[\Delta_I(1 + \delta_I)]^{\frac{1}{2}}}{(1 + \gamma_I)} - 1 \approx \frac{\omega_o}{2Q_o\omega_t} \quad (3.23)$$

where ω_{oa} and Q_{oa} are the realized values.

3.3.3 Simulation Results for Pole- ω and Pole-Q

Tables 3-2 to 3-7 give the simulation and calculation results for the deviations of the pole-frequency and the pole-Q. The CAD tool used is the Analog Workbench (AWB)

with hSpice simulator. In all the cases, the OA gain-bandwidth is 1 MHz.

Band-pass A & M Filter with Ideal Source and Load

Tables 3-2 and 3-3 give the variation of the pole- ω and pole-Q for the second-order VM and CM band-pass A &M filters with different ω_o and Q_o values.

Table 3-2 Voltage-mode band-pass A & M filters

ω_o (rad/s) (desired)	Q_o (desired)	% error in ω_o		% error in Q_o		ω_o/ω_t	$\omega_o/Q_o\omega_t$
		simulation	σ_V	simulation	η_V		
10^2	1.0	0.00	0.00	0.0	0.00	1.59×10^{-5}	1.59×10^{-5}
	5.0			0.0	0.00		3.18×10^{-6}
	10.0			0.0	0.00		1.59×10^{-6}
	20.0			0.0	0.00		7.95×10^{-7}
10^3	1.0	0.00	-0.02	0.0	0.01	1.59×10^{-4}	1.59×10^{-4}
	5.0			0.0	0.01		3.18×10^{-5}
	10.0			0.0	0.01		1.59×10^{-5}
	20.0			0.0	0.01		7.95×10^{-6}
10^4	1.0	-0.30	-0.24	0.3	0.08	1.59×10^{-3}	1.59×10^{-3}
	5.0			0.4	0.08		3.18×10^{-4}
	10.0			0.5	0.08		1.59×10^{-4}
	20.0			0.7	0.08		7.95×10^{-5}
10^5	1.0	-2.49	-2.39	1.0	0.80	1.59×10^{-2}	1.59×10^{-2}
	5.0			2.2	0.80		3.18×10^{-3}
	10.0			3.4	0.80		1.59×10^{-3}
	20.0			5.8	0.80		7.95×10^{-4}

Table 3-3 Current-mode band-pass A & M filters

ω_o (rad/s) (desired)	Q_o (desired)	% error in ω_o		% error in Q_o		ω_o/ω_t	$\omega_o/Q_o\omega_t$
		simulation	σ_I	simulation	η_I		
10^2	1.0	0.00	0.00	0.0	0.00	1.59×10^{-5}	1.59×10^{-5}
	5.0		0.00	0.0	0.00		3.18×10^{-6}
	10.0		0.00	0.0	0.00		1.59×10^{-6}
	20.0		0.00	0.0	0.00		7.95×10^{-7}
10^3	1.0	0.00	-0.04	0.0	0.01	1.59×10^{-4}	1.59×10^{-4}
	5.0		-0.03	0.0	0.00		3.18×10^{-5}
	10.0		-0.03	0.0	0.00		1.59×10^{-5}
	20.0		-0.03	0.0	0.00		7.95×10^{-6}
10^4	1.0	-0.38	-0.40	0.4	0.08	1.59×10^{-3}	1.59×10^{-3}
	5.0		-0.34	0.4	0.02		3.18×10^{-4}
	10.0		-0.33	0.4	0.01		1.59×10^{-4}
	20.0		-0.32	0.4	0.00		7.95×10^{-5}
10^5	1.0	-3.22	-3.98	0.8	0.80	1.59×10^{-2}	1.59×10^{-2}
	5.0		-3.34	1.6	0.16		3.18×10^{-3}
	10.0		-3.26	2.9	0.08		1.59×10^{-3}
	20.0		-3.22	5.6	0.04		7.95×10^{-4}

From Tables 3-2 and 3-3, we see that when $\omega_o = 10^2$ rad/s, all the errors are zero. As the frequency increases, the errors increase. When $\omega_o = 10^5$ rad/s, the simulation errors for ω_o for the VM and CM filters are respectively -2.49% and -3.22%, which are close to the calculated values. The simulation errors for Q_o are around 1.0~5.8% for the VM filter and 0.8~5.6% for the CM filter, which means that the CM filter has an error value less than that of the VM filter. The Q_{oa} of the VM filter is enhanced more than that of the CM filter if Q_o is high. Hence, the simulation results and calculations show that the performances of the CM and VM filters match very well, especially when the pole frequency of the filter is far smaller than that of the OA unity gain bandwidth.

Low-pass A & M Filter with Ideal Source and Load

Tables 3-4 and 3-5 show the variation of the pole- ω and pole- Q of the second-order VM and CM low-pass A & M filters with different ω_o and Q_o values.

Table 3-4 Voltage-mode low-pass A & M filters

ω_o (rad/s) (desired)	Q_o (desired)	% error in ω_o		% error in Q_o		ω_o/ω_t	$\omega_o/Q_o\omega_t$
		simulation	σ_V	simulation	η_V		
10^2	1.0	0.00	0.00	0.0	0.00	1.59×10^{-5}	1.59×10^{-5}
	5.0			0.0	0.00		3.18×10^{-6}
	10.0			0.0	0.00		1.59×10^{-6}
	20.0			0.0	0.00		7.95×10^{-7}
10^3	1.0	0.00	-0.02	0.0	0.01	1.59×10^{-4}	1.59×10^{-4}
	5.0			0.0	0.01		3.18×10^{-5}
	10.0			0.0	0.01		1.59×10^{-5}
	20.0			0.0	0.01		7.95×10^{-6}
10^4	1.0	-0.30	-0.24	0.0	0.08	1.59×10^{-3}	1.59×10^{-3}
	5.0			0.4	0.08		3.18×10^{-4}
	10.0			0.6	0.08		1.59×10^{-4}
	20.0			0.9	0.08		7.95×10^{-5}
10^5	1.0	-2.49	-2.39	1.0	0.80	1.59×10^{-2}	1.59×10^{-2}
	5.0			1.0	0.80		3.18×10^{-3}
	10.0			3.9	0.80		1.59×10^{-3}
	20.0			5.8	0.80		7.95×10^{-4}

From Tables 3-4 and 3-5, we see that when $\omega_o = 10^2$ rad/s, all the errors are zero. As the frequency increases, the errors increase. When $\omega_o = 10^5$ rad/s, the simulation errors for ω_o for the VM and CM filters are respectively -2.49% and -3.22%, which are close to the calculated values. The simulation errors for Q_o are around 1.0~5.8% for the VM filter and -1.0~4.0% for the CM filter, which means that the CM filter has an error value less

than that of the VM filter. The Q_{oa} of the VM filter is enhanced more than that of the CM filter if Q_o is high. Hence, the simulation results and calculations show that the performances of the CM and VM filters match very well, especially when the pole frequency of the filter is far smaller than that of the OA unity gain bandwidth.

Table 3-5 Current-mode low-pass A & M filters

ω_o (rad/s) (desired)	Q_o (desired)	% error in ω_o		% error in Q_o		ω_o/ω_t	$\omega_o/Q_o\omega_t$
		simulation	σ_I	simulation	η_I		
10^2	1.0	0.00	0.00	0.0	0.00	1.59×10^{-5}	1.59×10^{-5}
	5.0			0.0	0.00		3.18×10^{-6}
	10.0			0.0	0.00		1.59×10^{-6}
	20.0			0.0	0.00		7.95×10^{-7}
10^3	1.0	0.00	-0.03	0.0	0.01	1.59×10^{-4}	1.59×10^{-4}
	5.0			0.0	0.00		3.18×10^{-5}
	10.0			0.0	0.00		1.59×10^{-5}
	20.0			0.0	0.00		7.95×10^{-6}
10^4	1.0	-0.38	-0.32	0.0	0.08	1.59×10^{-3}	1.59×10^{-3}
	5.0			0.2	0.02		3.18×10^{-4}
	10.0			0.2	0.01		1.59×10^{-4}
	20.0			0.4	0.00		7.95×10^{-5}
10^5	1.0	-3.22	-3.19	-1.0	0.80	1.59×10^{-2}	1.59×10^{-2}
	5.0			0.0	0.16		3.18×10^{-3}
	10.0			1.3	0.08		1.59×10^{-3}
	20.0			4.0	0.04		7.95×10^{-4}

Non-ideal Input Source and Output Load

Tables 3-6 and 3-7 show the effect of the input impedance and the load impedance on the pole- ω and pole- Q of the band-pass and the low-pass CM filters. R_s is

the input impedance. R_L is the load impedance. We choose the values of the R_s are 100k Ω and 1M Ω and that of the R_L are 10, 100, and 1000 Ω .

Table 3-6 Current-mode band-pass filters with non-ideal input and output

$Q_o = 10$							
ω_o (desired)	$R_L (\Omega)$	$R_s = 100 \text{ k}$		$R_s = 1 \text{ M}$		ω_o/ω_i	$\omega_o/Q_o\omega_i$
		% error in ω_o	% error in Q_o	% error in ω_o	% error in Q_o		
10^3	10	-0.06	0.0	-0.06	0.0	1.59×10^{-4}	1.59×10^{-5}
	100		0.0		0.0		
	1000		0.0		0.0		
10^4	10	-0.38	0.4	-0.38	0.4	1.59×10^{-3}	1.59×10^{-4}
	100		0.4		0.4		
	1000		0.4		0.4		
10^5	10	-3.30	2.9	-3.22	2.9	1.59×10^{-2}	1.59×10^{-3}
	100		2.9		2.9		
	1000		2.9		2.9		

$Q_o = 20$							
ω_o (desired)	$R_L (\Omega)$	$R_s = 100 \text{ k}$		$R_s = 1 \text{ M}$		ω_o/ω_i	$\omega_o/Q_o\omega_i$
		% error in ω_o	% error in Q_o	% error in ω_o	% error in Q_o		
10^3	10	-0.06	0.0	-0.06	0.0	1.59×10^{-4}	7.95×10^{-6}
	100		0.0		0.0		
	1000		0.0		0.0		
10^4	10	-0.38	0.4	-0.38	0.4	1.59×10^{-3}	7.95×10^{-5}
	100		0.4		0.4		
	1000		0.4		0.4		
10^5	10	-3.30	5.6	-3.22	5.5	1.59×10^{-2}	7.95×10^{-4}
	100		5.6		5.5		
	1000		5.6		5.5		

Table 3-7 Current-mode low-pass filters with non-ideal input and output

$Q_o = 10$							
ω_o (desired)	$R_L (\Omega)$	$R_S = 100 \text{ k}$		$R_S = 1 \text{ M}$		ω_o/ω_t	$\omega_o/Q_o\omega_t$
		% error in ω_o	% error in Q_o	% error in ω_o	% error in Q_o		
10^3	10	-0.06	0.0	-0.06	0.0	1.59×10^{-4}	1.59×10^{-5}
	100		0.0		0.0		
	1000		0.0		0.0		
10^4	10	-0.38	0.2	-0.38	0.2	1.59×10^{-3}	1.59×10^{-4}
	100		0.2		0.2		
	1000		0.2		0.2		
10^5	10	-3.30	1.3	-3.22	1.3	1.59×10^{-2}	1.59×10^{-3}
	100		1.3		1.3		
	1000		1.3		1.3		

$Q_o = 20$							
ω_o (desired)	$R_L (\Omega)$	$R_S = 100 \text{ k}$		$R_S = 1 \text{ M}$		ω_o/ω_t	$\omega_o/Q_o\omega_t$
		% error in ω_o	% error in Q_o	% error in ω_o	% error in Q_o		
10^3	10	-0.06	0.0	-0.06	0.0	1.59×10^{-4}	7.95×10^{-6}
	100		0.0		0.0		
	1000		0.0		0.0		
10^4	10	-0.38	0.4	-0.38	0.4	1.59×10^{-3}	7.95×10^{-5}
	100		0.4		0.4		
	1000		0.4		0.4		
10^5	10	-3.30	4.0	-3.22	4.0	1.59×10^{-2}	7.95×10^{-4}
	100		4.0		4.0		
	1000		3.9		4.0		

From Tables 3-6 and 3-7, we see that there is negligible difference in the performances of the filters between the ideal and non-ideal input and output conditions. In other words, there is little effect of the non-ideal input and output conditions on the performance of the CM filters.

In this section, we compared the deviations of the ω_o and Q_o between the VM and CM filters. We also examined the effects of non-ideal input source and output load. All the simulation and calculation results about the pole-frequency and Q-factor show the CM and VM filters match very well, especially when the pole frequency of the filter is far smaller than the OA gain bandwidth.

3.4 Summary

The principles of transposed networks and nullors have been used in this chapter to realize CM filters from the corresponding VM filters using the same operational amplifier, when the operational amplifier is configured as a three-terminal device. Single-amplifier as well as multi-amplifier biquadratic VM filters have been considered for transforming them to the corresponding CM filters. Simulation and theoretical analysis have been conducted to study the effects of the gain bandwidth of the OA on the pole-frequency and the pole-Q of the VM and CM filters. These studies show that the performances of the CM filters match closely with that of the corresponding VM filters. Finally, the simulation results of the non-ideal input impedance and non-ideal load impedance have shown that there is negligible effect on the performance of the VM and CM filters. Thus, the new method introduced in Chapter 2 is really an easy way to realize CM filters from VM filters using the operational amplifier as the active device.

Chapter 4

Experiment and Simulation Results

In Chapter 3, the principles of transposed networks and nullors have been applied to convert CM filters from the corresponding VM filters when the OA is configured as a three-terminal device. We have shown through theoretical analysis that the transfer function of the CM filter agrees with that of the associated VM filter. To validate the theoretical analysis, suitable simulations and experimental work are necessary. In this chapter, we use the Analog Wave Bench (AWB) and the pSpice simulations to make a comparison of the frequency responses of the CM and the corresponding VM filters using the ideal version of the VCVS as well as the commercial version of the OA, which is available in the AWB linear device library.

To confirm the theoretical work, we use available commercial discrete components to validate our results experimentally.

4.1 Simulation of the Current-Mode and the Voltage-Mode Filters

4.1.1 Single-OA Biquadratic Filter

In Figure 4-1 shows a voltage-mode low-pass biquadratic filter using an infinite-gain VCVS. The filter specifications are: $f_o = 100$ Hz, $Q_o = 0.707$ and $|H_o| = 1$. The component values are (as in [36]): $R_1 = R_2 = 199.7$ k Ω , $R_3 = 12.68$ k Ω , $C_1 = 0.1$ μ F, and $C_2 = 0.01$ μ F. In Figure 4-2, we show the corresponding current-mode version of the same

filter using the infinite-gain VCVS, as per the method described earlier. In the pSpice simulations, a value of 10^5 is used for the gain of the VCVS. Figure 4-3 shows that the response of the CM filter is the same as that of the VM filter.

In order to study the performance of the two circuits using a non-ideal OA, we use the practical OA device, μ A741. Figure 4-4 shows the low-pass filter of Figure 4-1 using this device, available in the pSpice linear device library. Figure 4-5 shows the current-mode version of the same filter using the same OA. The simulated voltage and current responses are shown in Figure 4-6. As can be seen, the two responses are indistinguishable.

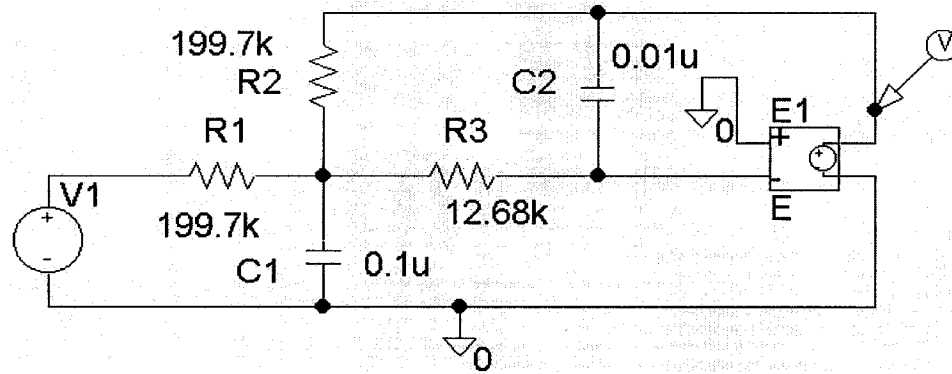


Figure 4-1 Voltage-mode low-pass SAB filter using an ideal VCVS

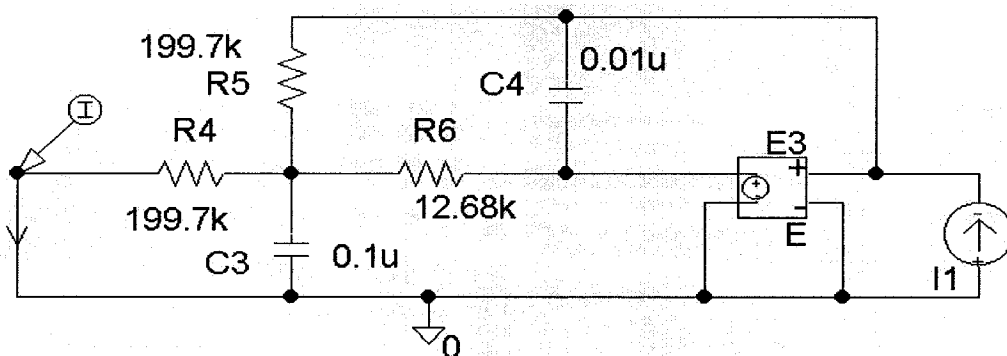


Figure 4-2 Current-mode low-pass filter SAB using an ideal VCVS

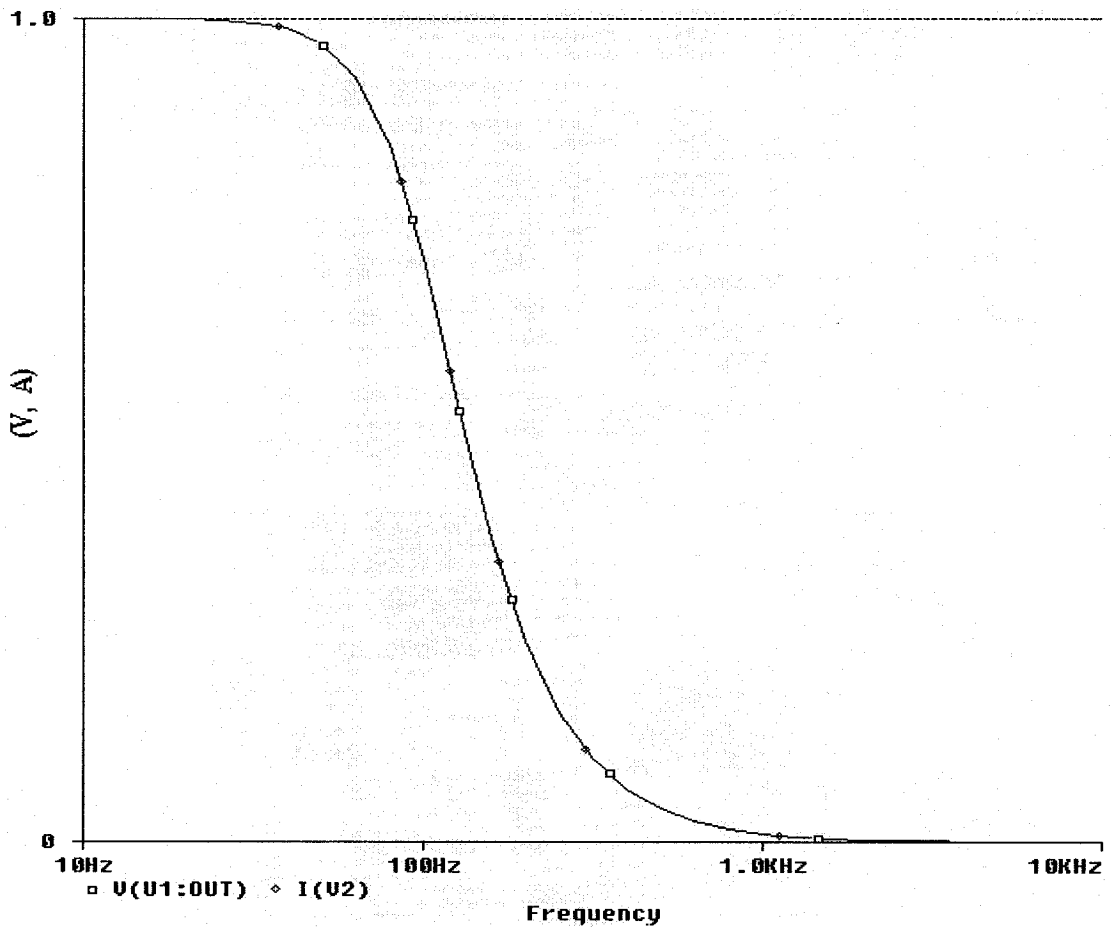


Figure 4-3 Frequency responses of the VM and the CM low-pass SAB filters using an ideal VCVS

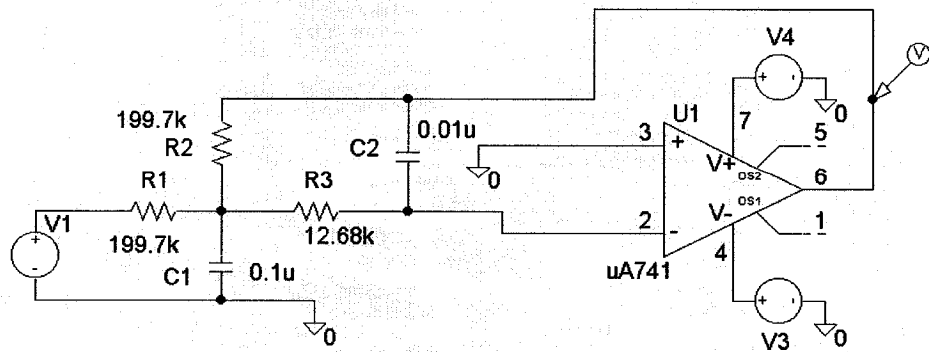


Figure 4-4 Voltage-mode low-pass SAB filter using a non-ideal OA

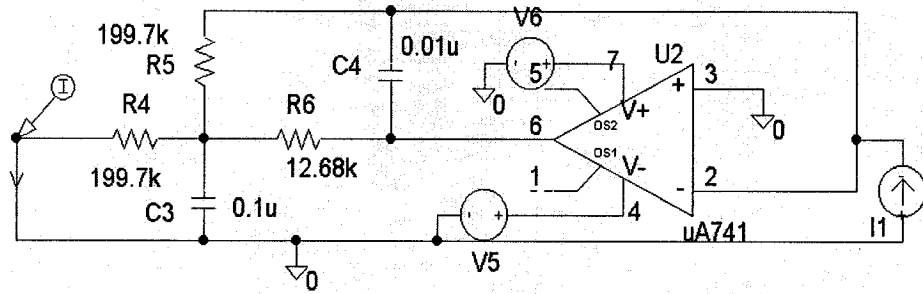


Figure 4-5 Voltage-mode low-pass SAB filter using a non-ideal OA

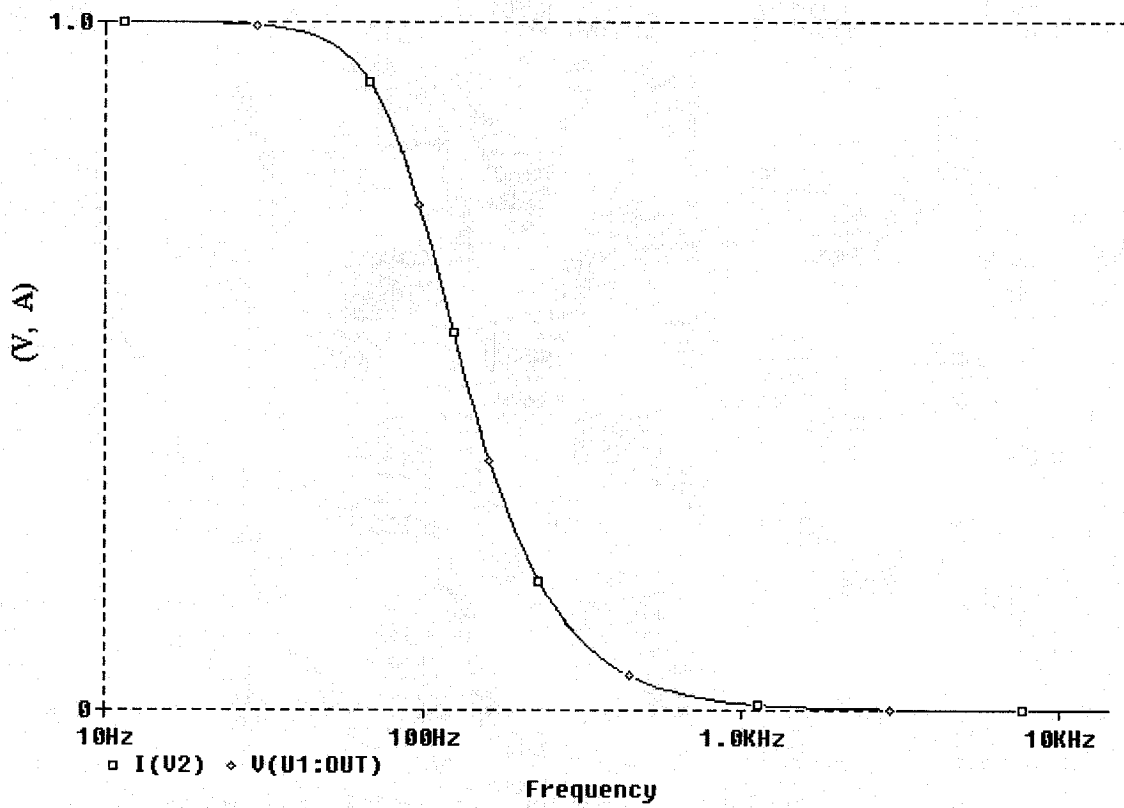


Figure 4-6 Frequency responses of the VM and the CM low-pass SAB filters using a non-ideal OA

4.1.2 Multi-OA Biquadratic Filter

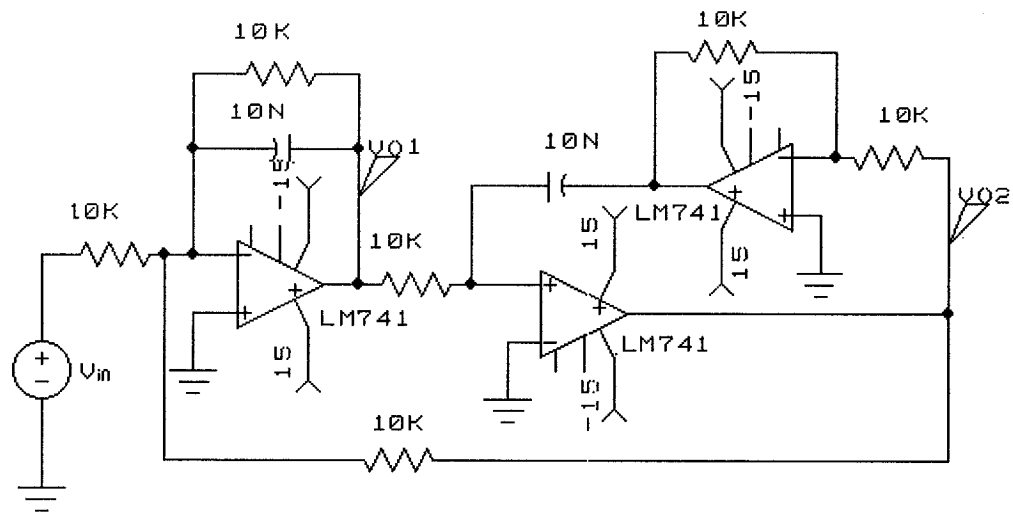


Figure 4-7 Voltage-mode A & M filter using non-ideal OAs

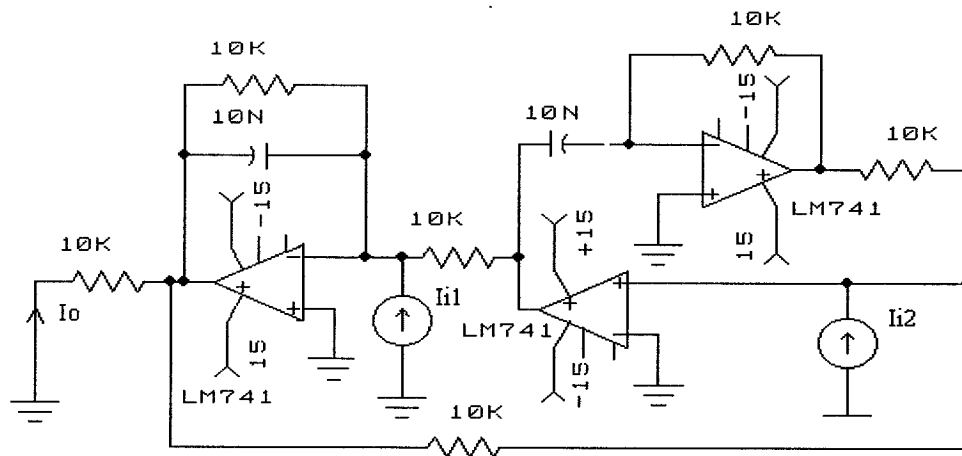


Figure 4-8 Current-mode A & M filter using non-ideal OAs

We also verified the results using non-ideal model active devices for the multi-OA biquadratic filter. Figure 4-7 shows the Akerberg-Mossberg VM structure realizing both the low-pass V_{o1}/V_{in} and the band-pass filters V_{o2}/V_{in} using practical OA devices,

i.e., LM 741. The filter specifications are: $f_o = 1.59 \text{ kHz}$, $Q_o = 1$ and $|H_o| = 1$. The component values are shown in the figure. Figure 4-8 shows the current-mode version of the same filter using the same OAs. The simulated voltage and current responses of band pass filter are shown in Figure 4-9. The simulated voltage and current responses of low pass filter are shown in Figure 4-10. These responses are obtained by using the AWB hSpice simulator and are indistinguishable too.

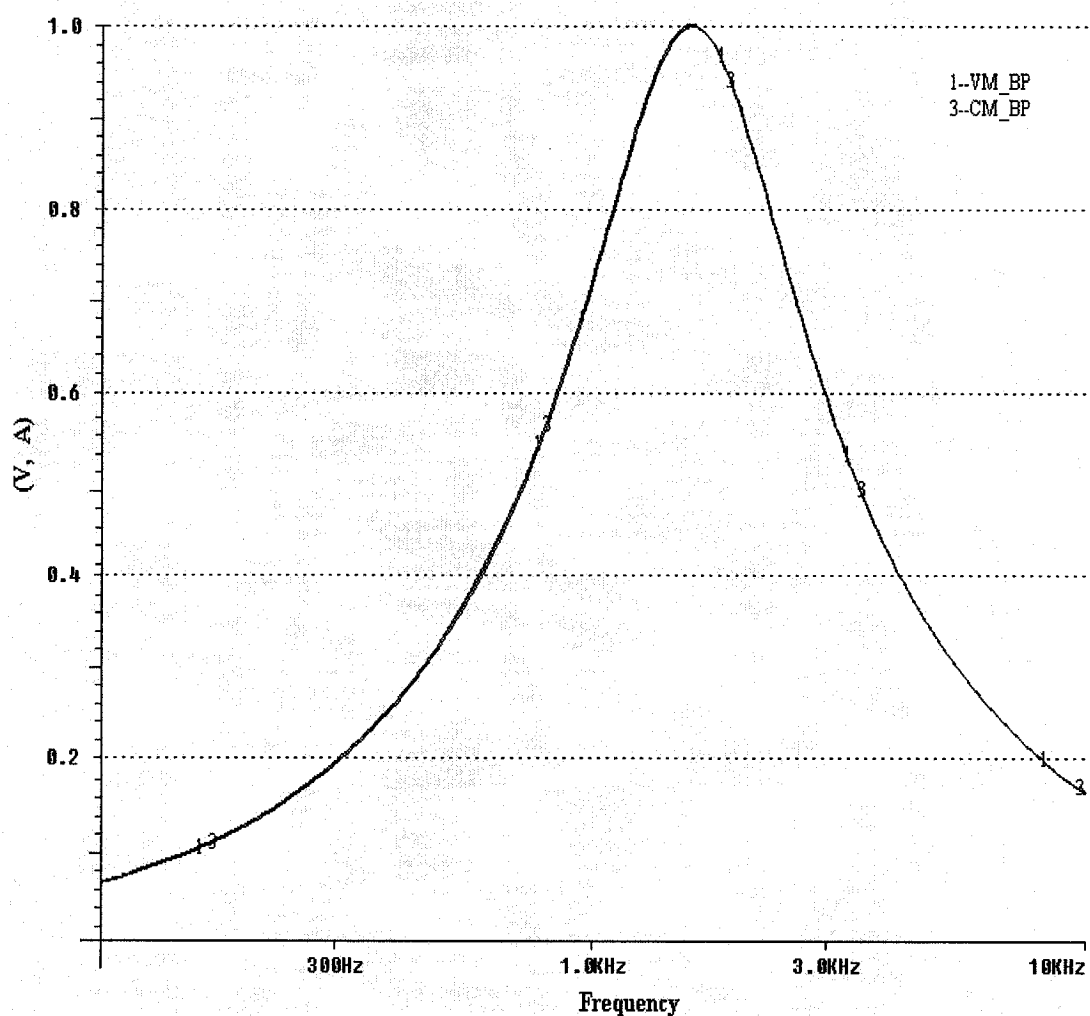


Figure 4-9 Frequency responses of the VM and the CM band-pass A & M filters using non-ideal OAs

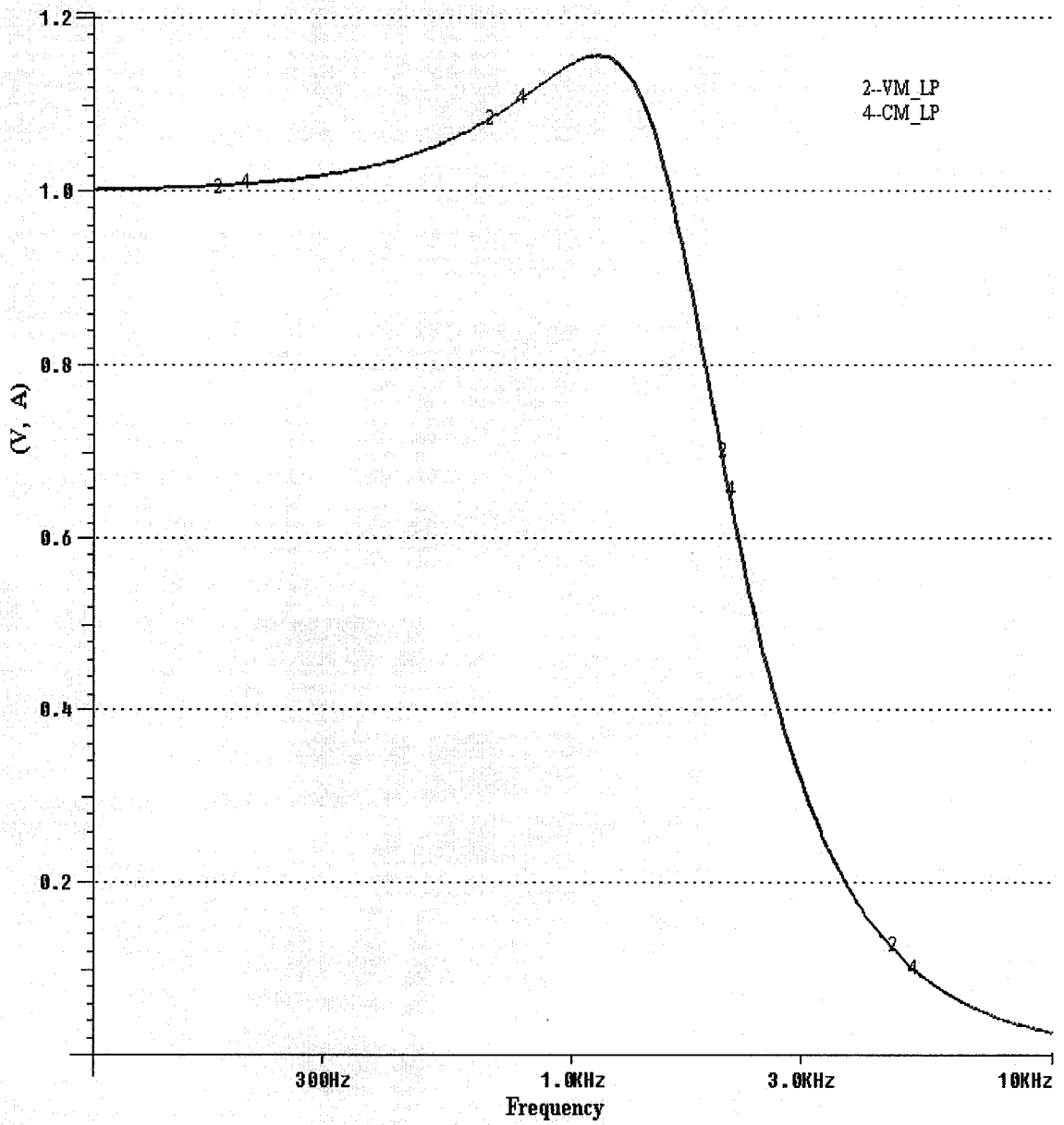


Figure 4-10 Frequency responses of the VM and the CM low-pass A & M filters using non-ideal OAs

4.2 Lab-Bench Experiment

The simulation results presented above provide a validation of the theoretical analysis discussed in Chapter 3. However, a more convincing proof lies in actually building circuits with available discrete components and devices and testing the same. We choose the A & M filter to demonstrate the experimental verification of the concepts presented earlier in this thesis. We use existing commercial device, such as LM741, discrete resistors and capacitors, and set up the CM filter and the corresponding VM filter circuits and compare their performances. In what follows, the characteristics of some commercially available components and the lab-bench test set up are presented. Finally, the test data are used to generate the CM and VM frequency responses.

4.2.1 Characteristics of the Discrete Components

The OA (LM741)

LM741 is one of the mature products of National Semiconductors and is used as an active device (OA) in the lab experiment. The main characteristics of this device are as follows:

Supply Voltage:	-18 / +18 V
Input Voltage range:	-18 — +18 V
Input Offset Voltage:	1 mV
Slew Rate:	0.5 V/us
Gain Bandwidth product:	1 MHz
Large Signal Voltage Gain:	15 V/mV
Phase Margin:	60 degrees

The LM741 package order diagram is shown in Figure 4-11.

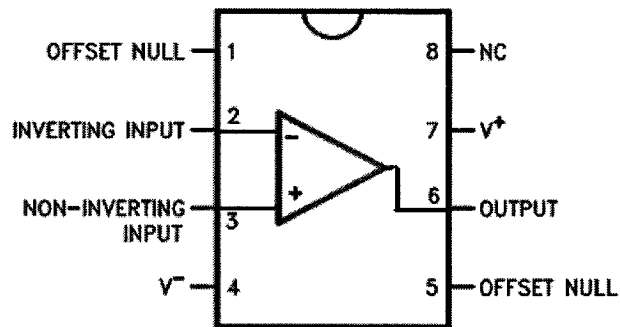


Figure 4-11 LM741 package order diagram.

Voltage to Current Converter

LM13700 is selected as a voltage-current converter device. LM13700 is again one of the mature products of National Semiconductors. The main characteristics of this device are as follows:

Supply Voltage:	-18 / +18 V
Input Voltage:	-18 — +18 V
Input Offset Voltage:	0.4 mV
Transconductance (g_m):	9600 $\mu\text{A/V}$
Slew Rate:	50 V/ μs
Open Loop Bandwidth:	2 MHz

The LM13700 package order diagram is shown in Figure 4-12.

Resistors and Capacitors

The resistors and capacitors are used as the passive devices. The tolerance of resistors and capacitors used is 10 %.

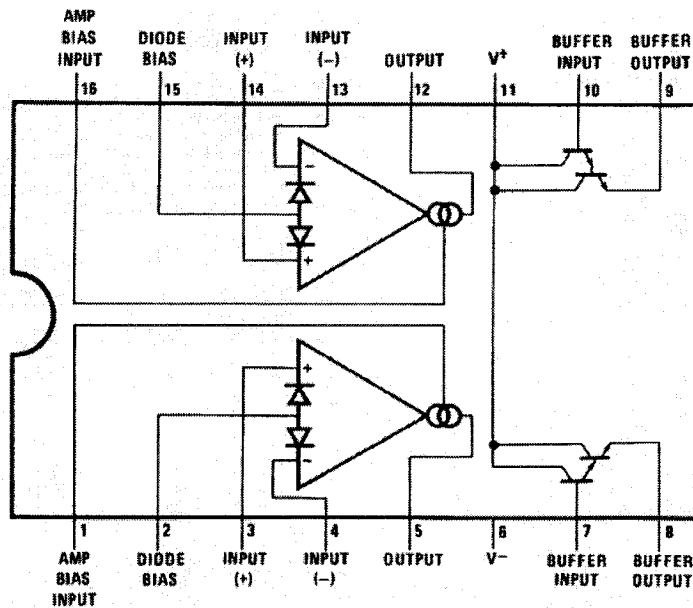


Figure 4-12 LM13700 package order diagram

4.2.2 Experimental Test Set Up

Figure 4-13 shows the system level diagram of the experimental arrangement adopted to verify the responses of the VM and CM filters.

The signal generator generates the voltage signal as an input signal. The T-connector distributes the input signal to two branches, the VM filter and the CM filter branches. The transconductance device LM13700 converts the voltage signal to a current signal.

For a single pole OA model with a gain-bandwidth (GBW) ω_t , the useful frequency range is below $\omega_t/30$ [41]. Considering the gain-bandwidth of 1MHz, the pole-frequency of the filter should be restricted to be less than 33 KHz. Based on the above discrete component values, the A & M filter is designed for

Pole Frequency: 1.59 KHz. Q-Factor: 1.

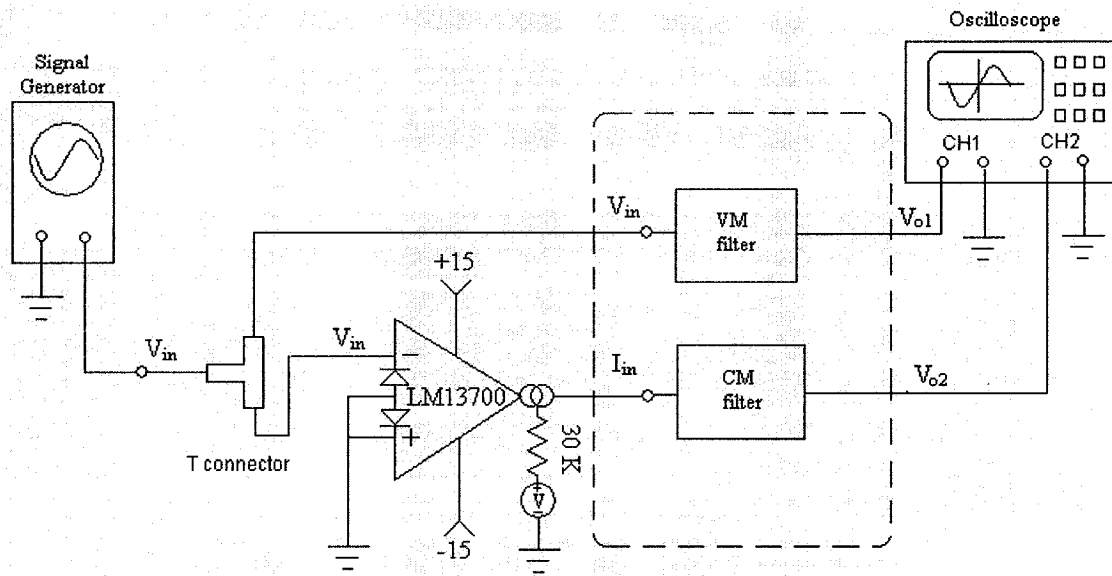


Figure 4-13 Lab-bench experiment set up

4.2.3 Experimental Results

Testing the VM filter is more direct. We connect the node V_{in} to the input signal and node V_{o1} to the detector of the oscilloscope, see Figure 4-14.

$$VTF = V_{o1}/V_{in}$$

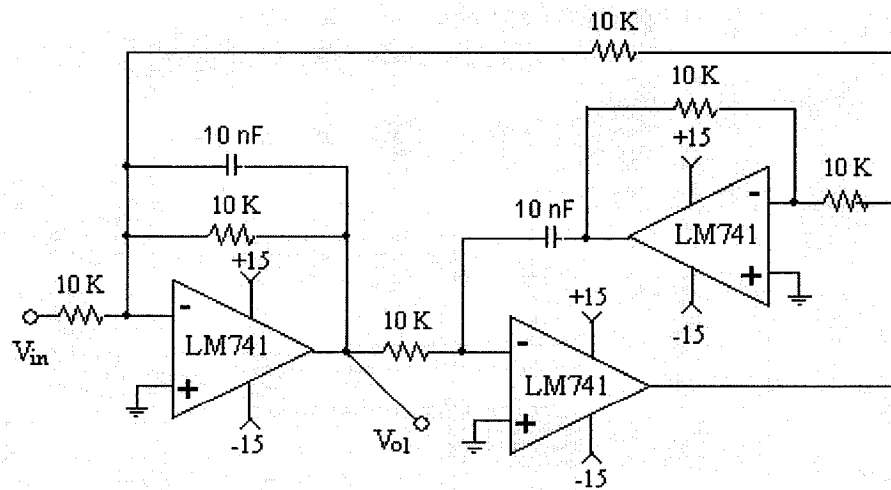


Figure 4-14 Voltage-mode A & M filter for the lab-bench experiment

To test the CM filter, we have some restrictions. In order to keep LM13700 working in the linear range, the peak-peak value of the input signal should be lower than 500 mV (practical value is 82.4 mV). The actual transconductance $g_m = 10000 \mu\text{mho}$ even though the typical $g_m = 9600 \mu\text{mho}$. Now

$$I_{in} = g_m V_{in}$$

$$V_{o2} = R_o I_o$$

$$CTF = \frac{I_o}{I_{in}} = \frac{V_{o2}}{R_o V_{in} g_m} = \frac{1}{100} \times \frac{V_{o2}}{V_{in}}$$

The above equation indicates that we can test the voltage-mode transfer function instead of the current-mode transfer function. The test nodes are shown in Figure 4-15. Node I_{in} is connected with the output of the LM13700. Node V_{o2} is connected with the detector of the oscilloscope.

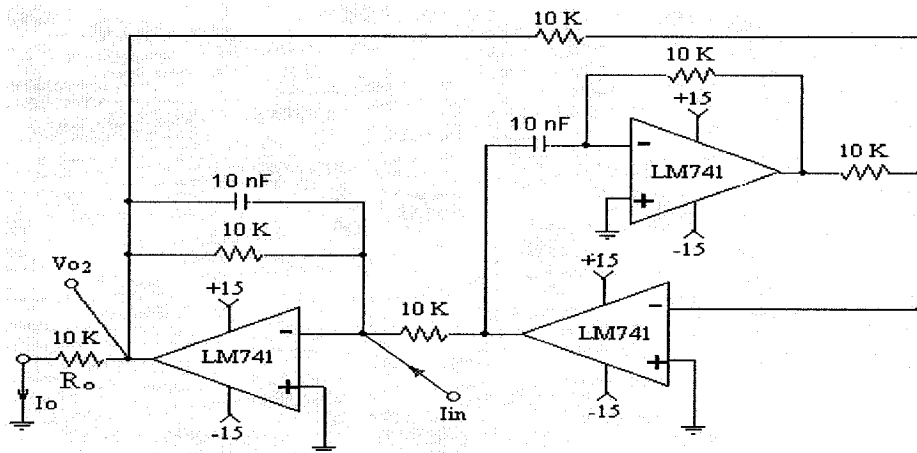


Figure 4-15 Current-mode A & M filter for the lab-bench experiment

Figures 4-16, 17, and 18 show the responses at different frequencies, namely 742Hz, 1559Hz, and 3238Hz. The CH1 and CH2 in these figures indicate the peak-peak voltages of the outputs of the VM and CM filters respectively. Comparing the waveforms

of the VM and CM outputs in each of these figures, we observe that they match very well. The frequency responses of the CM and VM filters from 100Hz to 20kHz obtained using Matlab, are shown in Figure 4-19. It is seen that the responses of the VM and the CM A & M filters are almost identical.

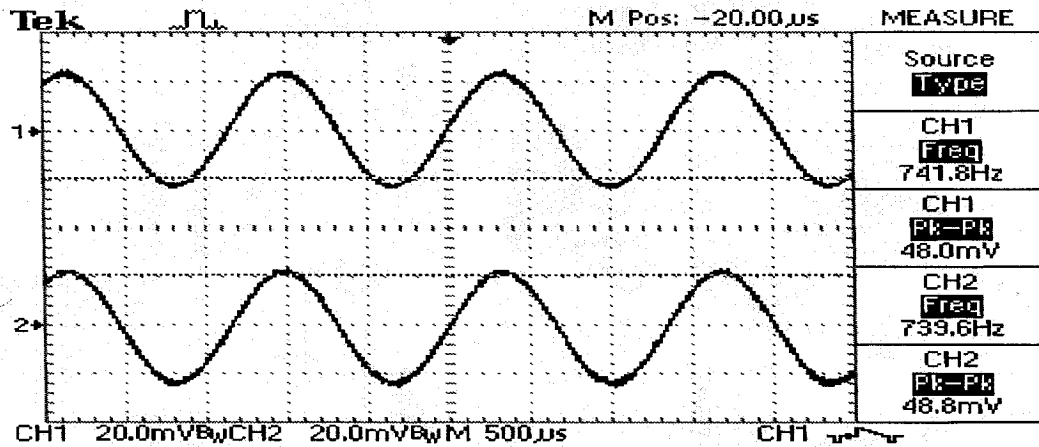


Figure 4-16 The output signals of the VM and CM filters at frequency 724Hz

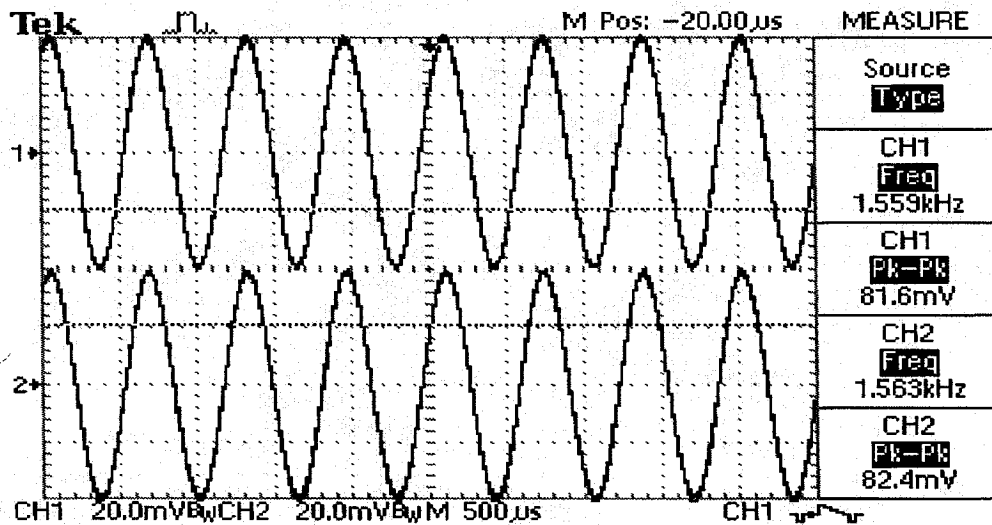


Figure 4-17 The output signals of the VM and CM filters at frequency 1559Hz

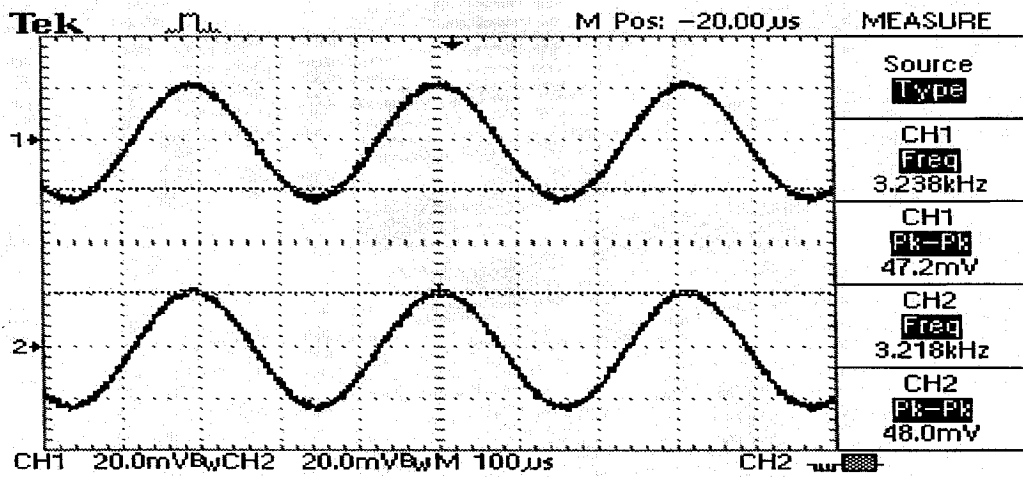


Figure 4-18 The output signals of the VM and CM filters at frequency 7238Hz

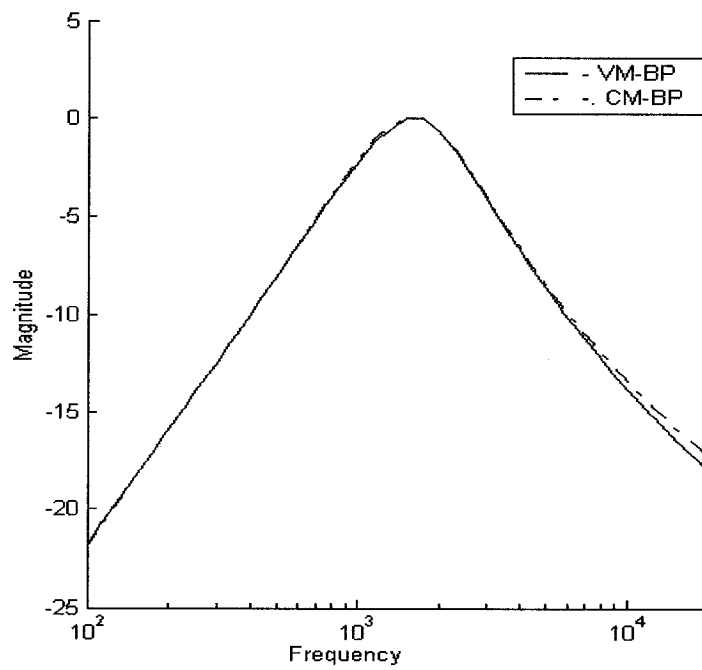


Figure 4-19 Magnitude-frequency responses of the VM and CM band-pass A & M filters

4.3 Summary

In this chapter, we have conducted a thorough theoretical analysis on the effect of finite gain bandwidth on the CM filters and the corresponding VM filters from which the CM filters have been derived using the principles of network transposition and nullors. Simulations have also been conducted on the same filters using AWB and pSpice. These results have shown that the performance of the CM filter is identical to that of the VM filter.

The band-pass A & M filter was implemented by using discrete components, such as resistors, capacitors, and LM741 OAs. A comparison of the frequency responses of the CM filter and its associated VM filter have shown that the performance of the CM filter matches that of the VM filter very well excepting at very high frequencies.

Chapter 5

Four-Terminal OA-Based VM Filters and OFA-Based CM Filters

In this chapter, we consider the realization of CM filters from VM filters that use four-terminal OA. In Chapter 2, it has been shown that a new device, operational floating amplifier (OFA) is needed to realize the CM networks, when an operational amplifier is configured as a four-terminal network for the corresponding VM network. We first discuss the characteristics of the OFA and then apply the new method introduced in Chapter 2 to convert single-amplifier as well as multi-amplifier biquadratic VM filters to CM filters with the OFA as the active device. The theoretical analysis is then validated with suitable simulation work. We use the analog wave bench (AWB) simulations to compare the frequency responses of the CM filter with that of the VM filter using commercial version of OA or OFA.

5.1 Operational Floating Amplifier (OFA)

Generally, an operational floating amplifier (OFA) is a high-gain transconductance amplifier with two floating input and two floating output terminals, and which can realize a four-terminal nullor. The name OFA has also been referred to as a four-terminal floating nullor (FTFN) [27],[28],[30],[32],and [37]. An OFA consists of a nullator ($V_1 = 0, I_1 = 0$) at one port and a norator at the other port with arbitrary (V_2 and

I_2) as shown in Figure 5-1(a). The corresponding symbol is shown in Figure 5-1(b). According to the definition of the nullor, the terminals of the OFA possess these characteristics:

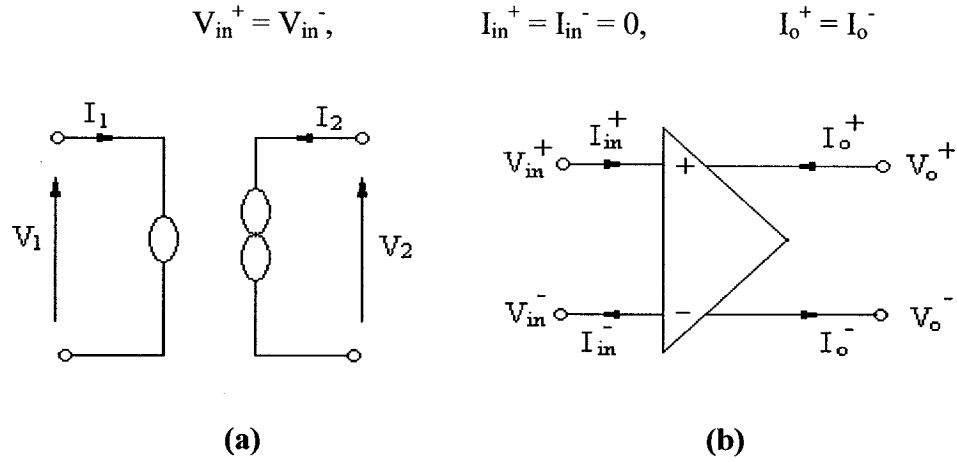


Figure 5-1 (a) Nullor model and (b) Symbol of an OFA

A simulation model of the OFA can be realized by using the non-ideal model of active devices, LM741 and bipolar transistors (*pnp* 2N2905 and *npn* 2N2222), as shown in Figure 5-2 [37].

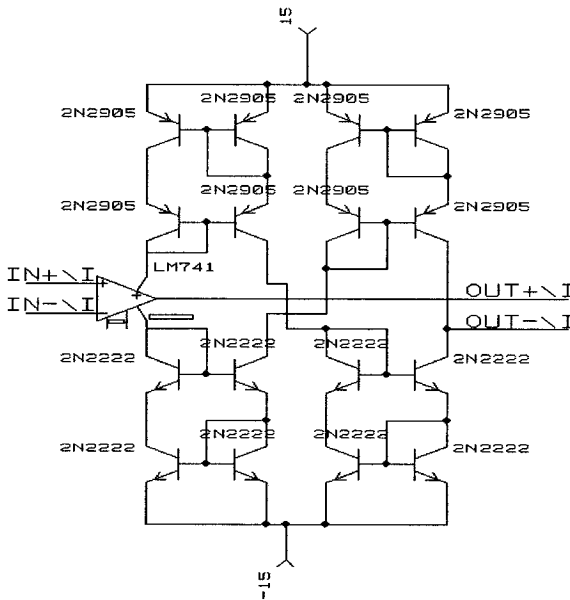


Figure 5-2 Implementation circuit of an OFA adapted from [37]

The LM741 with current mirrors that replicate its power supply currents to a new terminal, i.e., the fourth terminal, can implement an OFA. These devices are chosen from the AWB component library.

5.2 Realizing CM Filter Using OFA

In Chapters 3 and 4, the case of the voltage amplifier with three-terminal structure was discussed. We now discuss the case of the voltage amplifier with a four-terminal structure and realize CM filters using OFAs from the corresponding VM filters using four-terminal OAs by applying the principles of transposed networks and nullors.

5.2.1 Single-OA Biquadratic Filter

Figure 5-3 shows the standard configuration of a single amplifier biquadratic (SAB) filter network using a single amplifier with finite gain K . The voltage transfer function of the filter is given by

$$\frac{V_o}{V_i} = -\frac{KY_1Y_3}{(Y_1 + Y_2 + Y_5)(Y_3 + Y_4 + Y_6) + Y_3(Y_4 + Y_6) - K\{Y_6(Y_1 + Y_2 + Y_3 + Y_5) + Y_2Y_3\}} \quad (5.1)$$

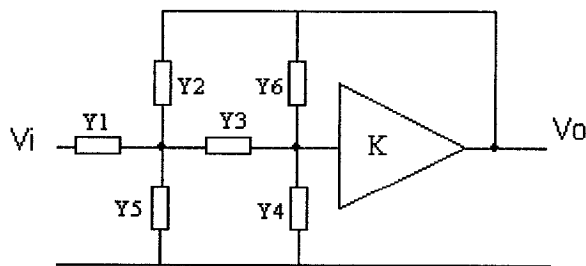


Figure 5-3 VM SAB filter using a finite gain amplifier

By choosing the admittances properly, (5.1) can realize second-order filters with low-pass, band-pass, and high-pass characteristics. The amplifier with positive gain (i.e., K is positive) can be realized in Figure 5-4, which also is known as the filter with no input terminals grounded, and $K = 1 + Y_8/Y_7$.

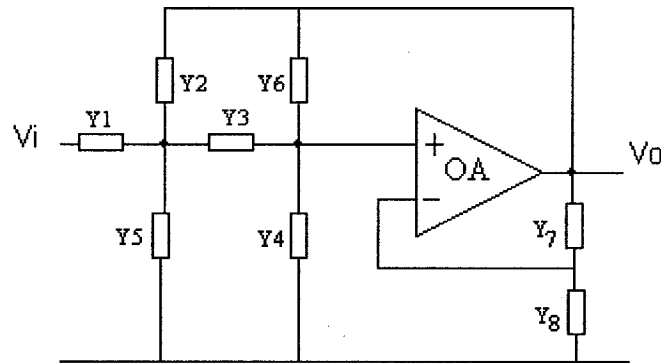


Figure 5-4 VM SAB using an ideal OA with four-terminal configuration

Figure 5-5 shows the OA replaced by OFA and switched around as well as the input and output nodes, relative to Figure 5-4. We now analyze this network for the current transfer function (CTF) I_o/I_i .

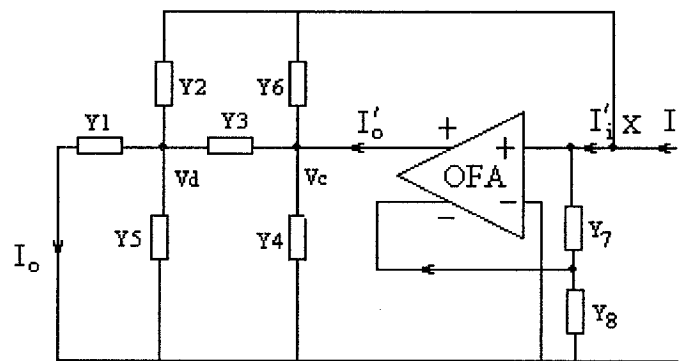


Figure 5-5 CM SAB filter using an ideal OFA

Let us first consider the sub-circuit consisting of the OFA, Y_7 , and Y_8 . Applying KCL, we get

$$K = \frac{I_o'}{I_i} = 1 + \frac{Y_8}{Y_7} \quad (5.2)$$

$$\text{KCL at the node X, gives} \quad V_c Y_6 + V_d Y_2 + I_i - I_i' = 0 \quad (5.3)$$

$$\text{KCL at node } V_d \text{ gives,} \quad -V_d Y_1 - V_d Y_5 - V_d Y_2 + (V_c - V_d) Y_3 = 0 \quad (5.4)$$

$$\text{KCL at node } V_c \text{ gives,} \quad -V_c Y_4 - V_c Y_6 + I_o' + (V_d - V_c) Y_3 = 0 \quad (5.5)$$

Substituting for V_c and I_o' from (5.4), (5.5), and (5.2) into (5.3), can get:

$$KI_i = \frac{(Y_1 + Y_2 + Y_5)(Y_3 + Y_4 + Y_6)V_6}{Y_3} + (Y_3 + Y_4 + Y_6)V_d - Y_3 V_d - \frac{KY_6(Y_1 + Y_2 + Y_5)V_d}{Y_3} - KY_6 Y_3 V_d - KY_2 V_d \quad (5.6)$$

But $V_d Y_1 = I_o$. Substituting for V_d in (5.6), we get finally

$$\frac{I_o}{I_i} = - \frac{KY_1 Y_3}{(Y_1 + Y_2 + Y_5)(Y_3 + Y_4 + Y_6) + Y_3(Y_4 + Y_6) - K\{Y_6(Y_1 + Y_2 + Y_3 + Y_5) + Y_2 Y_3\}} \quad (5.7)$$

which is the same as V_o/V_i in (5.1).

We have considered SAB filter above. We shall now consider a well-known filter that employs more than one OA in the realization of the VM filter and obtain the corresponding CM filter using OFAs.

5.2.2 Multi-OA Biquadratic Filter

Figure 5-6 shows the configuration of a three-OA band pass filter proposed by Mikhael and Bhattacharyya, the M & B filter [26]. Both input terminals of all the three OAs are floating in this case. It is more representative of the four-terminal amplifier filters.

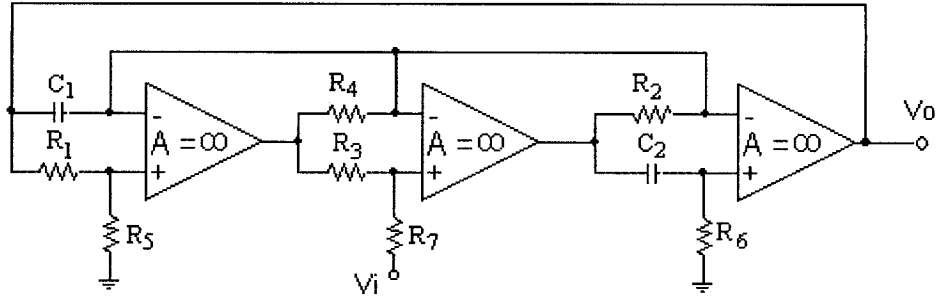


Figure 5-6 VM M & B biquadratic filter using ideal OAs with

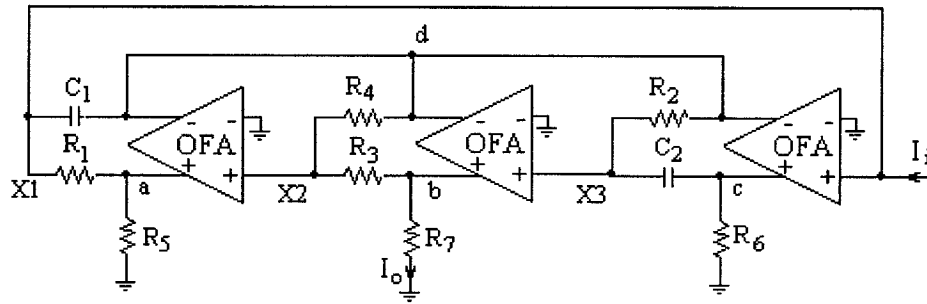


Figure 5-7 CM M & B biquadratic filter using ideal OFAs

The voltage transfer function is given by

$$\frac{V_o}{V_i} = \frac{\frac{G_1 G_4 G_7}{G_3 C_1} \left(1 + \frac{G_5}{G_1}\right) s}{G_5 s^2 + \frac{G_1 G_4 G_7}{G_3 C_1} s + \frac{G_1 G_2 G_6}{C_1 C_2}} \quad (5.8)$$

The configuration of the associated current-mode filter is shown in Figure 5-7 after we apply the principles of transposed networks and nullors. The CTF can be derived as follows:

$$\text{At node X1,} \quad -G_1 V_a - Y_1 V_d = I_i \quad (5.9), \text{ where } Y_1 = SC_1$$

$$\text{At node X2,} \quad -G_3 V_b - G_4 V_d = 0 \quad (5.10)$$

$$\text{At node X3,} \quad -G_2 V_d - Y_2 V_c = 0 \quad (5.11), \text{ where } Y_2 = SC_2$$

The property of the OFA gives:

$$I_o^+ = I_o^-$$

At node b,

$$Y_1V_d + G_4V_d + G_2V_d + (G_1 + G_5)V_a + (G_3 + G_7)V_b + (Y_2 + G_6)V_c = 0 \quad (5.12)$$

Substituting for V_a , V_b and V_c in (5.12), we get

$$-I_iG_3Y_2(G_1+G_5) = (Y_1Y_2G_3G_5 + Y_2G_1G_4G_7 + G_1G_2G_3G_6)V_d \quad (5.13)$$

Then, $V_d = \frac{G_3}{G_4}V_b$ and $V_bG_7 = I_o$.

Substituting for V_d from (5.13), we finally get

$$\frac{I_o}{I_i} = \frac{\frac{G_1G_4G_7}{G_3C_1}(1 + \frac{G_5}{G_1})s}{G_5s^2 + \frac{G_1G_4G_7}{G_3C_1}s + \frac{G_1G_2G_6}{C_1C_2}} \quad (5.14)$$

which is identical with the VTF in (5.8).

5.3 Simulation of the Four-Terminal OA Configuration

5.3.1 Single-OA Biquadratic Filter

Figure 5-8 shows the schematic of a finite gain SAB filter with a band-pass response in the voltage-mode operation. A practical device, LM 741, realizes the OA. The specifications for the band-pass response are: $f_o=159.2$ Hz, $Q_o=1$ and $|H_o|=2$. The passive component values are shown in the figure. Figure 5-9 shows the corresponding current-mode filters using an OFA.

Figure 5-10 shows the responses of the voltage-mode and current-mode filters, obtained by using the AWB hSpice simulator. The simulation results agree well with the theoretical analysis. The two response curves are almost identical.

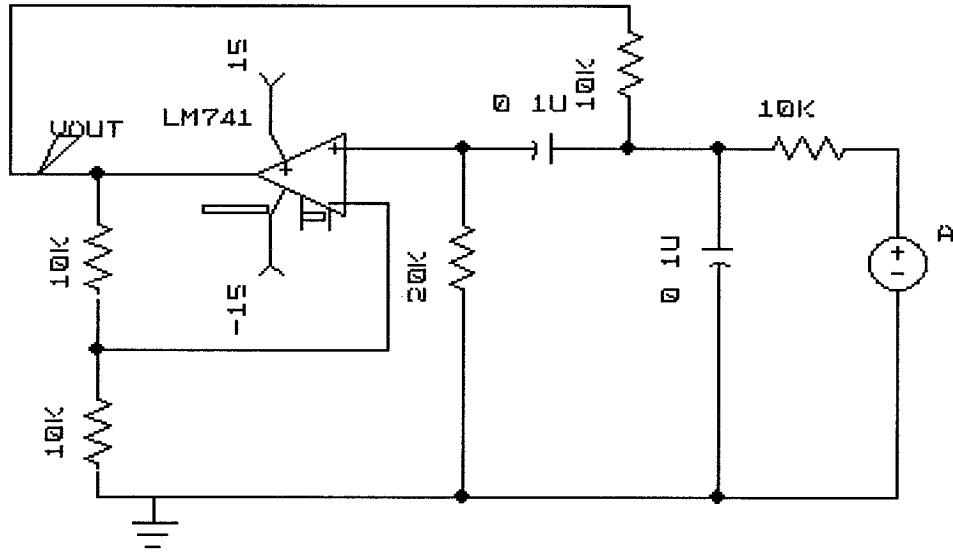


Figure 5-8 VM band-pass SAB filter using a non-ideal OA

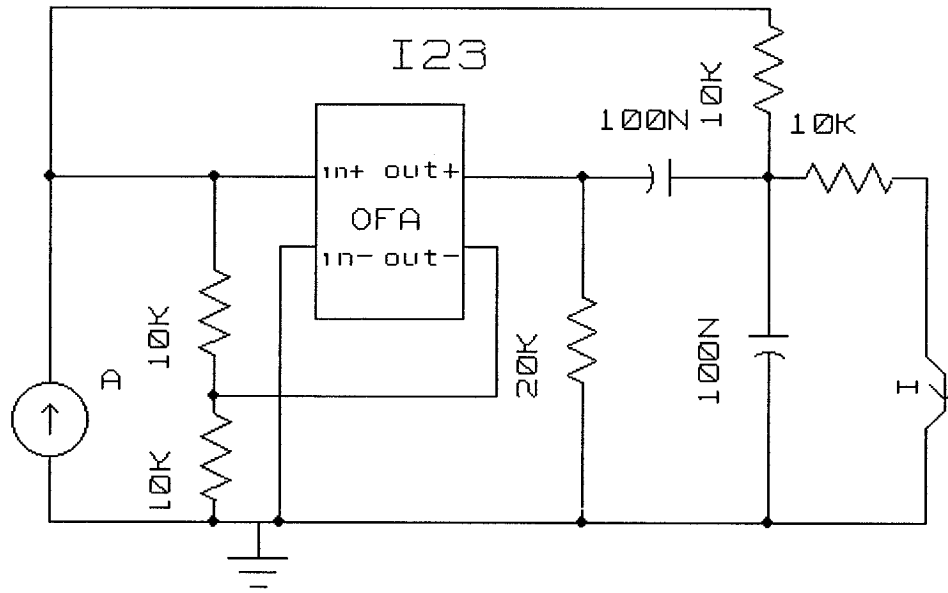


Figure 5-9 CM band-pass SAB filter using a non-ideal OFA

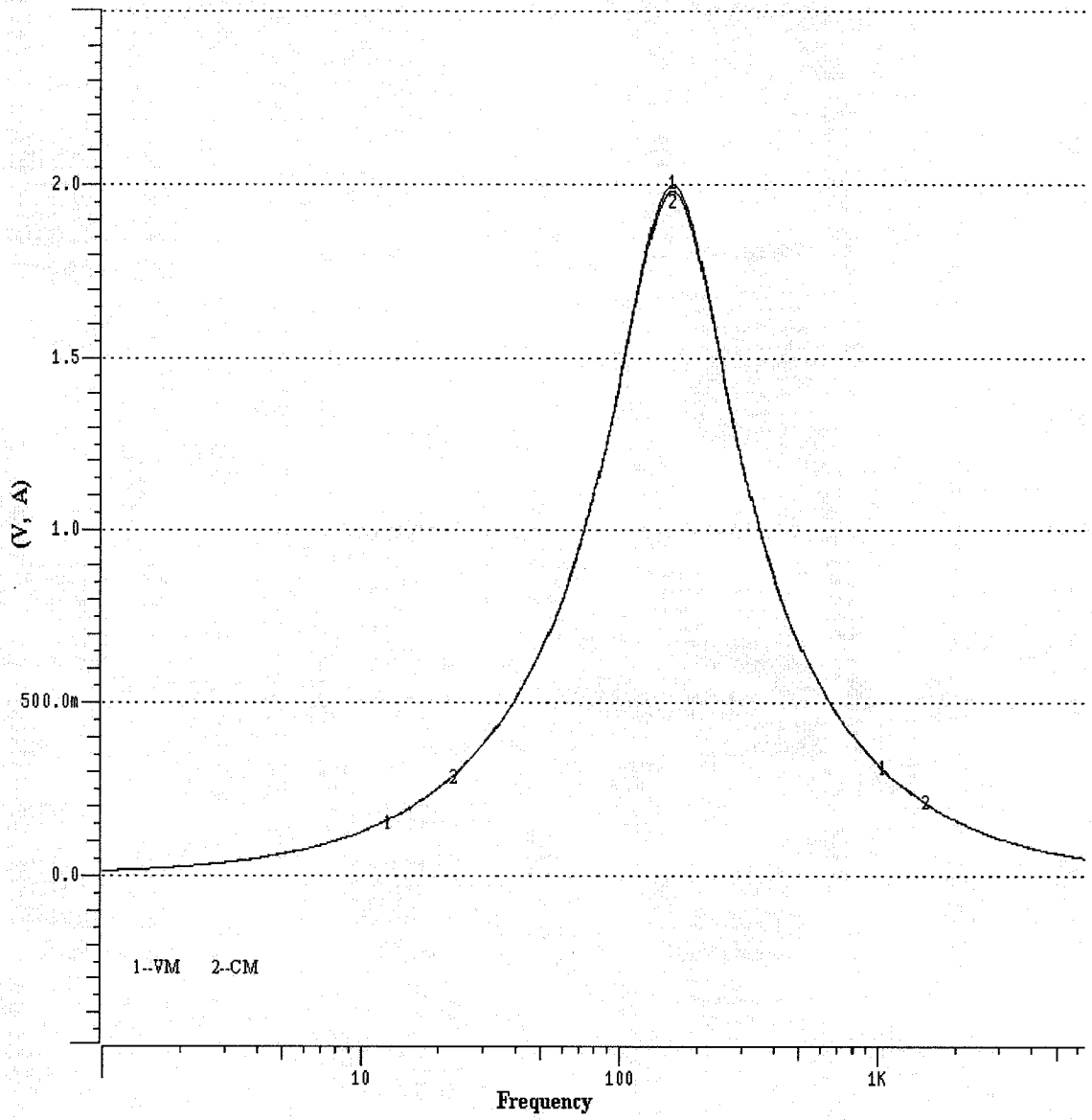


Figure 5-10 Frequency responses of the VM and CM band-pass SAB filter

5.3.2 Multi-OA Biquadratic Filter

Figure 5-11 shows the schematic of the VM band-pass M&B biquadratic filter proposed by Mikhael and Bhattacharyya [26]. A practical device, LM 741, realizes the OA. The specifications for the band-pass response are: $f_o=159.2$ Hz, $Q_o=2$ and $|H_o|=2$. All the values of the components are shown in the figure. Figure 5-12 shows the corresponding current-mode filter.

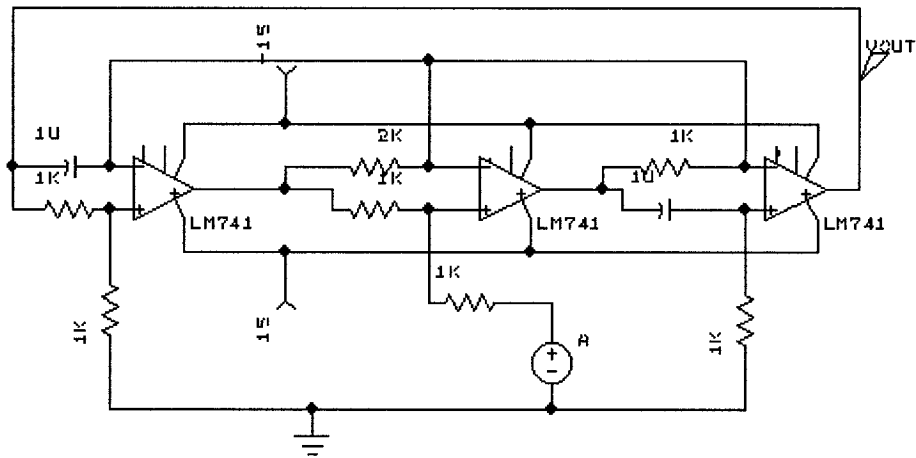


Figure 5-11 VM band-pass M & B filter using non-ideal OAs

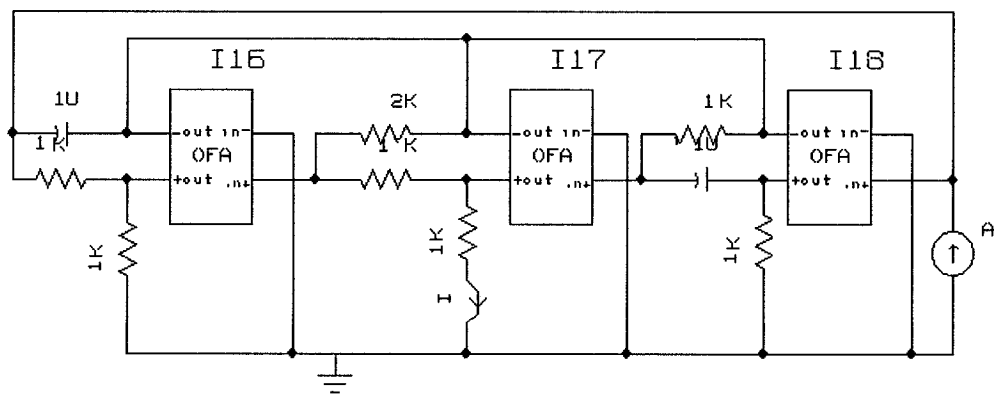


Figure 5-12 CM band-pass M & B filter using non-ideal OFAs

Figure 5-13 shows the responses of the voltage-mode and current-mode filters, obtained by using the AWB hSpice simulator. The simulation results also agree with the theoretical analysis. The response of the CTF is very close to that of the VTF.

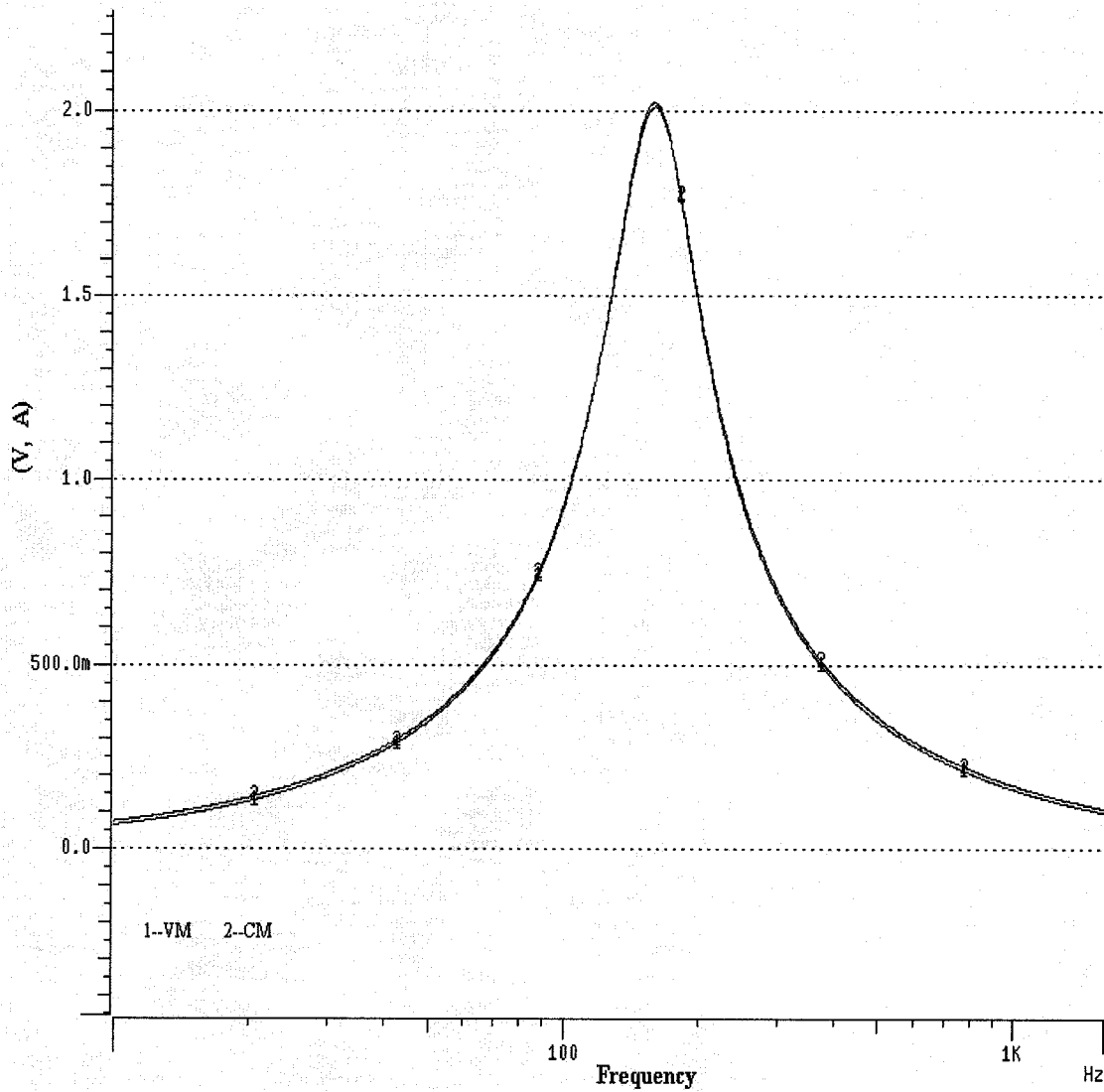


Figure 5-13 Frequency responses of the VM and CM band-pass M & B filter

5.4 Summary

This chapter has introduced the characteristics of a new active device, OFA. The OFA satisfies the definition of the four-terminal nullor and has been implemented by using OA and bipolar transistors. Then we utilized the method proposed in Chapter2, based on transposed networks and nullors, to realize biquadratic CM filters from the associated VM filters using single voltage amplifier as well as multiple voltage amplifiers, when the operational amplifier is configured as a four-terminal device in the VM filter. The voltage amplifier used in the CM filter is the operational floating amplifier, OFA. The AWB simulation was used to validate the theoretical results. Both the theoretical analysis and simulations have shown that the performance of the CM filter matches with that corresponding VM filter very well.

Chapter 6

Realizing Operational Floating Amplifier in CMOS Technology

In the previous chapters, two types of nullor configurations are introduced, the three-terminal nullor and the four-terminal nullor. An OA with one input connected to ground realizes a three-terminal nullor. An operational floating amplifier (OFA) with two floating output terminals can realize the four-terminal nullor. There is no commercial version of the OFA now. In this chapter, the IC version of the operational floating amplifier (OFA) is considered and an integrated version of the OFA using TSMC 0.18 μm CMOS technology is developed. An OFA architecture from several proposed OFA or FTFN architectures which are suitable for the TSMC 0.18 μm CMOS technology is selected. Each sub-circuit of the OFA and the corresponding layout are given. Finally, the layout at the chip level for the whole system is also considered. When the OFA is designed using IC technology (i.e., TSMC 0.18 μm CMOS), the tolerance of the IC components may cause variations in the responses of the CM and VM filters, and the agreement in the performance of the CM and the associated VM filters may become worse. This is investigated by using corner analysis technique to analyze the performance of the OFA introduced in this chapter. Furthermore, the performance of the OFA and the new method introduced in Chapter 2 are studied by utilizing the OFA in the CM filter derived from the VM Deliyannis-Friend band-pass filter [38] using post-layout simulation.

6.1 Realizations of OFAs

The practical realizations of OFAs can be categorized into three groups, the OA-based OFA [27],[30],[31],[33], and [37], the second generation current conveyer or (CCII-based) OFA [32], and some special structures introduced in [28],[29], and [31]. A brief review of these techniques is given next.

6.1.1 OA-Based OFA

An implementation model of the OA-based OFA is shown in Figure 6-1 [27]. The port relations of the OFA can be characterized as

$$V_{in}^+ = V_{in}^-, \quad I_1 = I_2 = 0, \quad I_{o}^+ = I_{o}^-.$$

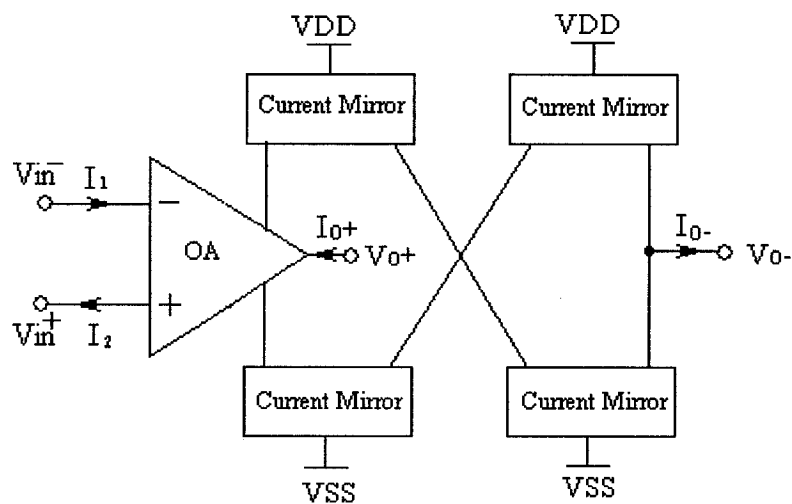


Figure 6-1 Implementation model of an OFA

Since this realization uses a single active element (OA), it generally exhibits a better performance in terms of noise, linearity, and tracking current error over the CCII-based realization. It should be noted that the output impedance at the V_{o}^+ terminal is very low while the impedance at the V_{o}^- terminal is very high. This makes the OFA usable as both

a voltage amplifier (terminal V_o^+) and a transconductance amplifier (terminal V_o^-). Thus, it can be utilized in both the voltage-mode and current-mode applications. Since the current mirrors replicate the whole supply current, the error in the current between the two output terminals may be enlarged due to the unbalance between the upper half and the lower half circuits, device matching, and ripples in VDD and VSS etc.. To reduce this error, a more accurate structure is introduced in Figure 6-2 [30]. This is a bipolar implementation of an OFA.

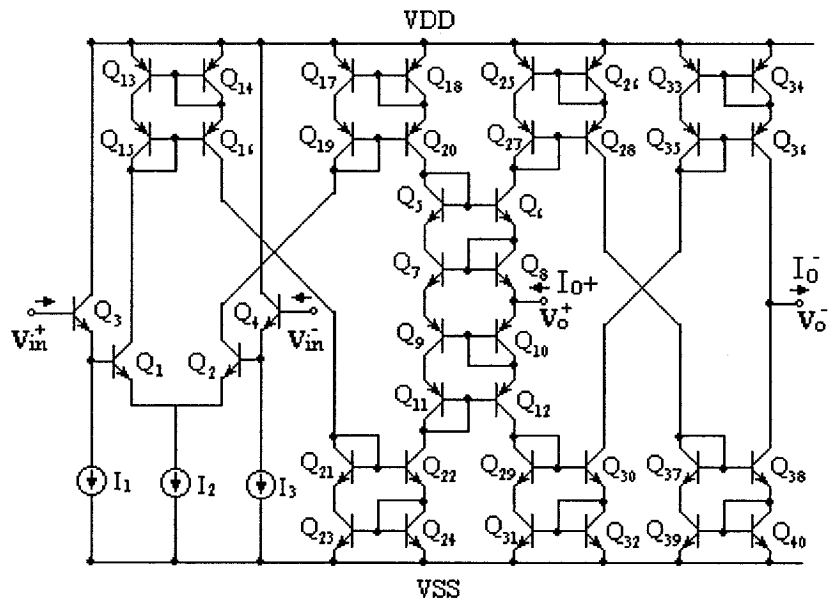


Figure 6-2 OA-Based implementation of an OFA

The operation of Figure 6-2 can be explained as follows: This circuit basically consists of a voltage amplifier and seven standard Wilson current mirrors. Transistors Q_1 to Q_{24} operate as an OA with a very high input impedance and a low output impedance. Transistors Q_{25} to Q_{36} operate as Wilson current mirrors, which provide high output impedance and more accurate tracking of the current between the two terminals. These current mirrors copy the current I_o^+ to the terminal V_o^- with $I_o^+ = I_o^-$.

6.1.2 CCII-Based OFA

The two-CCII realization is shown in Figure 6-3. This structure is a balanced structure at both the input and the output ports [32]. At the input port

$$\begin{aligned} V_x = V_{x2}, & & V_y = V_{x1}, & \rightarrow & V_x = V_y. \\ I_x = I_y = 0 & & & & \end{aligned}$$

The currents at the output port are

$$I_{12} = -I_z, \quad I_{12} = I_w, \quad \rightarrow \quad I_w = -I_z$$

The above equations indicate that this structure satisfies the definition of the nullor. Actually, careful observation shows that the input port of this circuit is not completely isolated from the output port. Due to the current conveyed through the input resistance (R_x) at node p, there will be a voltage tracking error $V_y - V_x$ when one of the input terminals is grounded. This will violate the definition of a nullor at the input.

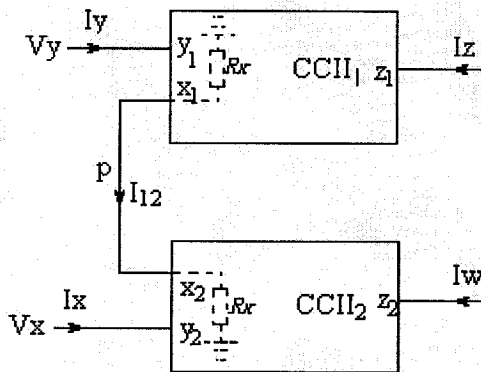


Figure 6-3 CCII-Based implementation of an OFA

Some other special realizations have been reported in [28],[29], and [31]. They employ special characteristics and techniques. They are more complex and are not discussed here.

6.2 System Structure and Basic Building Blocks

Section 6-1 presented some techniques for the realization of an OFA. A novel realization circuit of the OFA is introduced in this section [33]. The OFA using TSMC 0.18 μm CMOS technology is implemented. In this technology, the dc supply voltages are restricted to 1.8 and 3.3 volts. In this design, the latter supply voltage is chosen. The schematic diagram of the OFA is shown in Figure 6-4. It is an OA based structure. The OA should be designed with a high gain as well as a high gain-bandwidth in order to make it close to the ideal OA. The current mirrors copy the current at the terminal V_{o^+} to the terminal V_{o^-} . The special features of this circuit are as follows:

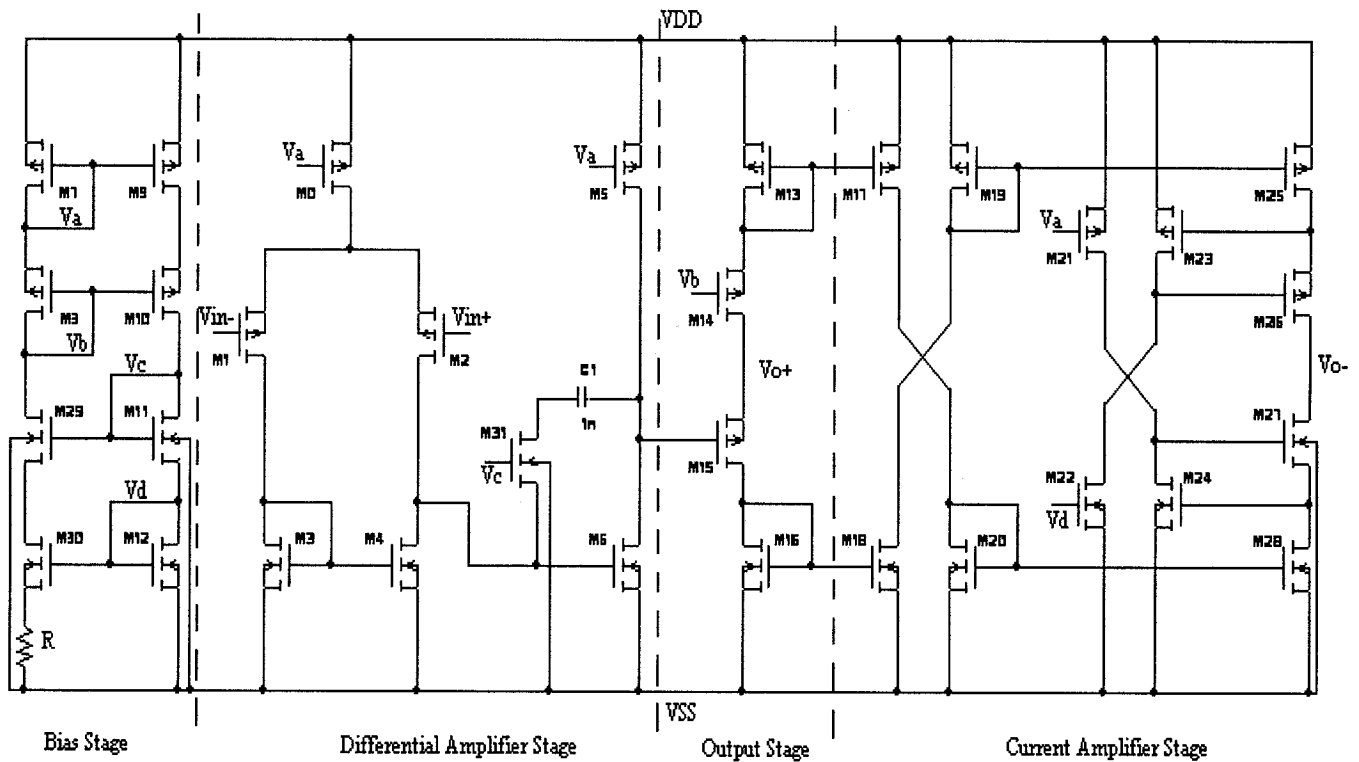


Figure 6-4 The schematic of the OFA

- (a) It is simple, having one OA and four current mirrors.
- (b) It has a high common mode rejection and power supply rejection.
- (c) It has a high gain (over 80 dB) and a high gain bandwidth (around 100 MHz).
- (d) It has a more accurate small-signal current tracking between the two output terminals. Details are discussed in Section 6.2.4.

Each of the sub-circuits of the OFA is now described.

6.2.1 Bias Stage

The OA must maintain a good performance under all kind of environments. The transconductance of the transistors is one of the most important parameters that must be stabilized for a robust design. The bias circuit in Figure 6-4 satisfies such a requirement. This structure is modified from the original one [35] by adding one more p-MOS transistor stack (M_3 and M_{10}), which constructs a cascaded current mirror with transistors M_1 and M_9 . The transistor transconductance of M_{12} is only determined by the geometric ratios, and is independent of the power-supply voltages, process parameters, temperature, or any other parameter with large variability [35]. Specifically, for the case of $(W/L)_{30} = 4(W/L)_{12}$, the transconductance is

$$g_{m12} = \frac{2 \left[1 - \sqrt{\frac{(W/L)_{12}}{(W/L)_{30}}} \right]}{R} = 1/R \quad (6.1)$$

where $(W/L)_{30}$ is the ratio of the width to the length of M_{30} and $(W/L)_{12}$ that of M_{12} .

Since all the transistor currents are derived from the same biasing network and the ratios of the currents are mainly dependent on the geometry, the transconductances of the other transistors are also stabilized.

For all the NMOS transistors

$$g_{mi} = g_{m12} \times \sqrt{\frac{(W/L)_i I_i}{(W/L)_{12} I_{12}}} \quad (6.2)$$

and all PMOS transistors

$$g_{mi} = g_{m12} \times \sqrt{\frac{\mu_p (W/L)_i I_i}{\mu_n (W/L)_{12} I_{12}}} \quad (6.3)$$

6.2.2 Differential Amplifier Stage

The objective of the differential amplifier stage is to amplify only the difference between two different potentials regardless of the common-mode value. A two-stage CMOS differential amplifier is shown in Figure 6-4. The first gain stage is a differential-input single-ended output stage, and consists of transistors M_0 to M_4 . The second gain stage is a common-source gain stage with an active load, and consists of M_5 and M_6 . The small-signal analysis of this differential amplifier gives the voltage gain as [35]

$$A_v = -\frac{g_{m1} g_{m6}}{(g_{ds2} + g_{ds4})(g_{ds5} + g_{ds6})} \quad (6.4)$$

The gain of the differential amplifier is proportional to the transconductances of the transistors M_1 and M_6 and the output impedances of the transistors M_2 , M_4 , M_5 , and M_6 .

The compensation of the two-stage differential amplifier consists of the capacitor C_1 and the transistor M_{31} . The capacitor, C_1 , realizes what is called the dominant-pole

compensation. It controls the dominant first pole and thereby the frequency. Transistor M_{31} has V_{DS} equal to zero. Thus, M_{31} operates as a resistor with a resistance R_C in the triode region. This transistor is included in order to realize a left-half-plane zero at frequencies around or above the unity-gain frequency. The addition of such an extra left-half-plane zeros called lead-compensation. Without M_{31} , there is a right-half-plane zero, which makes compensation as well as stability very difficult. The zero is given by the relationship [35],

$$\omega_z = \frac{-1}{C_c(1/g_{m6} - R_c)} \quad (6.5)$$

If R_C equal to $1/g_{m6}$, the right-half-plane zero can be eliminated. Figure 6-4 gives a solution for the lead-compensation that is independent of the process, supply voltage, and temperature variations. The product $R_c g_{m6}$ is given by

$$R_c g_{m6} = \frac{(W/L)_6}{(W/L)_{31}} \sqrt{\frac{(W/L)_{11}}{(W/L)_{12}}} \quad (6.6)$$

6.2.3 Output Stage

The function of the output stage is to work as a current transformer. Most of the output stages have a high current gain and a low voltage gain. The characteristics of the output stage are: (1) to provide sufficient output power in the form of voltage and current, (2) to avoid signal distortion, and (3) to provide isolation from the current amplifier stage.

The output stage is as shown in Figure 6-4. Transistor M_{15} works as a source follower amplifier with an active load M_{14} . Two current mirrors, one consisting of

transistors M_{13} and M_{17} and the other consisting of transistors M_{16} and M_{18} , copy the currents to the next stage.

6.2.4 Current Amplifier Stage

The function of the current amplifier stage is to replicate the current on the load to another output terminal of the OFA. The gain of the current amplifier is unity. Figure 6-4 shows this current amplifier, which consists of four current mirrors.

In Section 6.1, it was noted that the OFA has two output terminals, one with a low output impedance and the other with a high output impedance. The two terminals with different impedances appearing in the same circuit require the difference between them to be as large as possible. In order to realize the ideal condition, the impedance of one output terminal should be 100 times smaller than the load impedance, and the impedance of the other should be 100 times larger than the load impedance. That is, if the impedance of one output terminal is $1\text{k}\Omega$, the impedance of the other output terminal should be at least $10\text{M}\Omega$ and the impedance of the load should be around $100\text{k}\Omega$. Under this condition, the error of tracking the small-signal currents between the two output terminals can be kept under 1%. It is impossible to implement this device by using a common cascade configuration.

Negative feedback technique can be used to increase the output impedance. Figure 6-5 shows an enhanced output-impedance current mirror consisting of M_{19} , M_{23} , M_{25} , and M_{26} . The basic idea is to use a feedback amplifier, the transistor M_{23} , to keep the drain-source voltage across M_{26} as stable as possible, irrespective of the output voltage. The addition of the amplifier increases the output impedance by a factor equal to one plus

the loop gain that would occur for a classical cascade current mirror. The output impedance is given by [35]

$$r_o \approx (1+A)r_{ds26}g_{m26}r_{ds25} \quad (6.7)$$

where A is the gain of the amplifier.

If the values of r_{ds} , A , and g_m are properly chosen, then r_o could be very large. A similar analysis could be applied to the current mirror consisting of the NMOS transistors, M_{20} , M_{24} , M_{27} and M_{28} as shown in Figure 6-4.

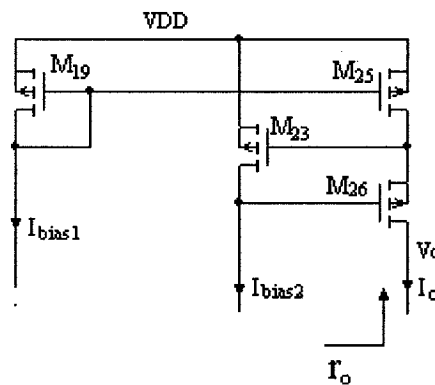


Figure 6-5 Enhanced output-impedance current mirror

6.2.5 The Performance of the OFA

The performance of the OFA with $I_{bias} = 100\mu A$, $R_L = 100K$, and $C_L = 10$ pf is summarized in Table 6-1. This design specification is based on the requirement of the filter, where the OFA will be used as an active device.

Table 6-1 Specification of the OFA

Parameters	Value
Voltage gain	80 dB
Gain bandwidth	10 MHz
Phase margin	65 degree
Low output resistance	1 k Ω
High output resistance	10 M Ω
Input offset	1 mV
Max output current	100 μ A

6.3 Basic Building Blocks Implemented by Layout

6.3.1 Transistor

The OFA circuit contains some critical and large-size transistors. This large transistor can be formed by using several smaller transistors connected in parallel, resembling a finger structure. This structure has two advantages: reducing the parasitic junction capacitance and optimizing the resistance of the gate poly along the width of the transistor [34]. This is important in high frequency applications. Figure 6-6(a) shows the layout of a transistor, which is composed of four smaller transistors. The equivalent schematic symbol is shown in Figure 6-6(b).

Precision matching between transistors is critical in the design of the differential transistor pair as well as current mirrors of the OFA. The approach of common-centroid layout helps to minimize the matching errors caused by the gradient effects across a microcircuit, such as due to temperature or a change in the gate-oxide thickness across

the microcircuit [34]. A simplified common-centroid layout of two identical matched transistors, M1 and M2, is shown in Figure 6-7(a). The symbol is shown in Figure 6-7(b).

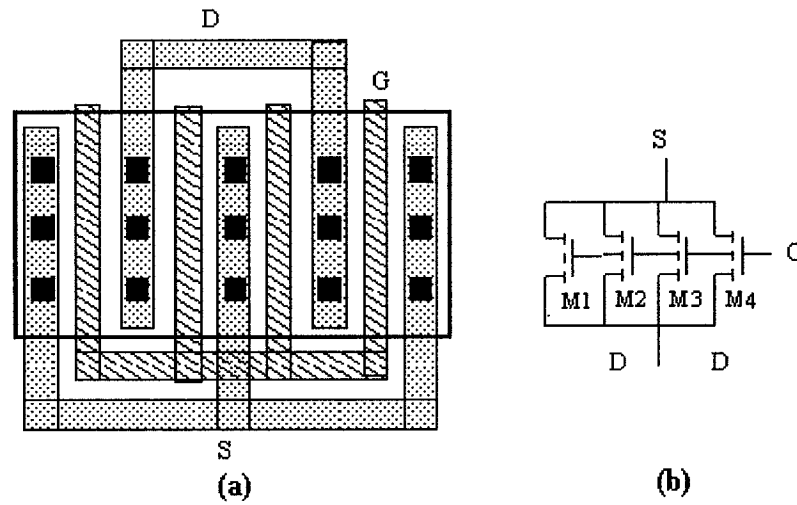


Figure 6-6 Fingered structure to reduce parasitic drain capacitances.

(a) Layout. (b) Equivalent symbol of (a).

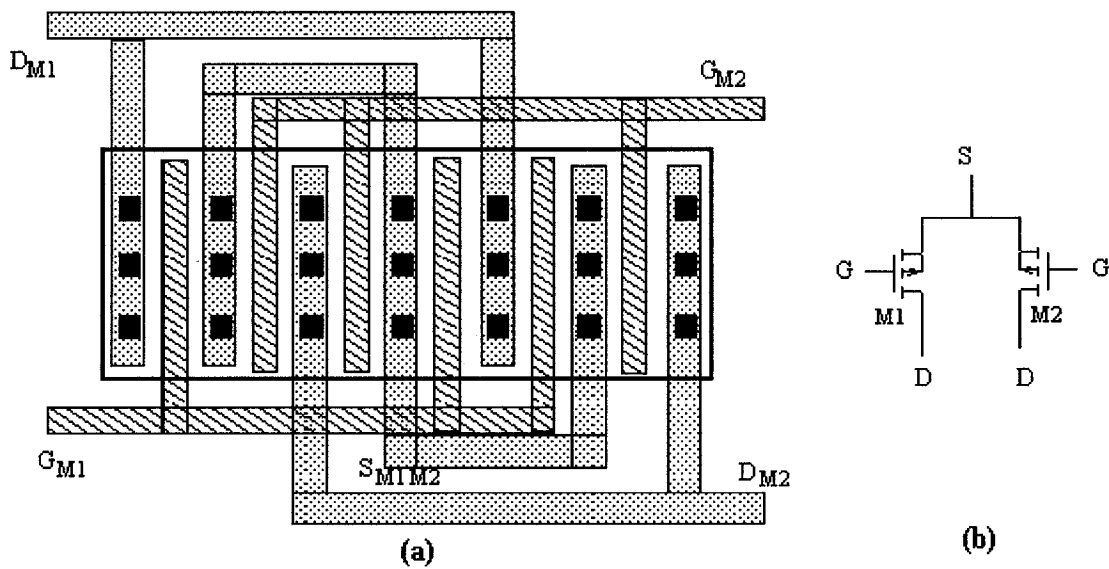


Figure 6-7 Common-centroid structure to minimize the matching errors.

(a) Layout. (b) Equivalent symbol of (a).

6.3.2 MIM Capacitor

The capacitors are realized using MiM capacitor in the TSMC 0.18 μm CMOS technology. MiM capacitor is formed by the CTM (capacitor top metal, also known as metal 5 prime) as the top layer with metal-5 as the bottom layer. The capacitor is sandwiched physically between the bottom plate metal and the next metal layer above, with a thin dielectric between the bottom plate and the upper plate. Figure 6-8 shows the cross-section of a MiM capacitor. Figure 6-9 shows the layout diagram. The grounded guard ring shields the noise to get into or out of the capacitor.

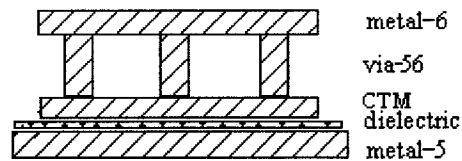


Figure 6-8 The cross-section of MiM capacitor

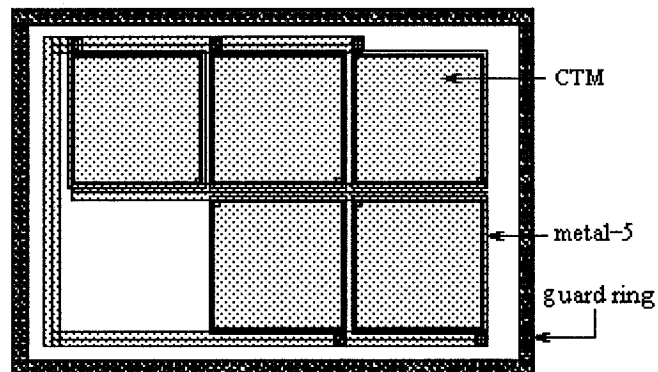


Figure 6-9 Capacitor layout diagram

6.3.3 Resistor

Integrated resistors can be realized using passive and active components. Based on the material used, the passive resistors compatible with the CMOS technology can be categorized into four groups, metal resistors, polysilicon resistors, diffusion resistors and well resistors. Another type of resistors is the active resistor, which is implemented by a CMOS transistor. This technique works with a much less area than that required for passive resistors. The MOS transistor can work in both saturation and linear regions. In our design, the transistor works in the triode region. The value of a resistor in such a configuration is:

$$r_{ds} = \frac{1}{\mu_n C_{ox} \left(\frac{W}{L}\right) (V_{gs} - V_T)} \quad (6.8)$$

Figure 6-10 shows this configuration. The layout of the resistor is the same as the transistor layout.

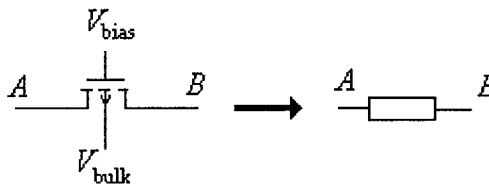
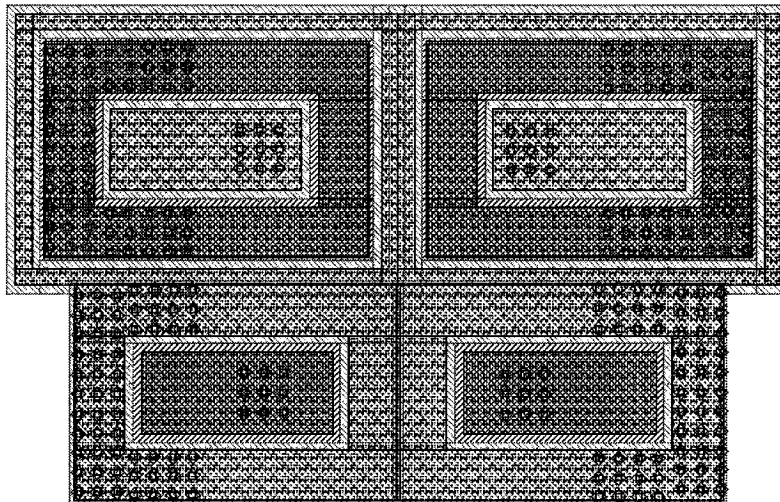


Figure 6-10 Transistor version of resistor

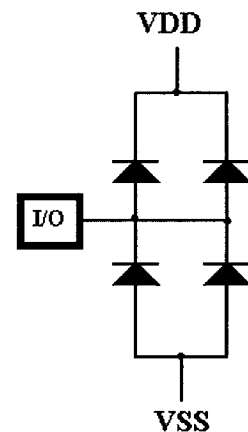
6.3.4 ESD Protection Structure

A chip has an input and output (I/O) interface to the outside world. This interface may cause accumulation of large voltage due to the leakage current flowing into the parasitic capacitance at the input electrode (i.e., gate) of a transistor. The large voltage

may physically damage the transistors. The electrostatic discharge (ESD) protection device can redirect unwanted charge away from the sensitive internal circuitry. Canadian microelectronics corporation (CMC) provides one type of ESD protection layout for the TSMC 0.18 μ m technology. The ESD layout and the corresponding schematic symbol are shown in Figure 6-11(a) and (b). The series connection of two diodes discharges the positive or negative charge into the ground to protect the input or output terminals from being destroyed by high voltage. The EDS protection devices are added on all the I/O pads in the OFA layout design.



(a) Layout of the diodes



(b) Symbol of (a)

Figure 6-11 ESD protection layout

6.4 System Layout

In previous sections, the layout of the various basic building blocks has been described. The function of each block determines as to how to handle the layout issues,

such as isolation, matching, placement, device splitting, and many other techniques. Finally, the complete system (OFA) is obtained by interconnecting the function blocks properly.

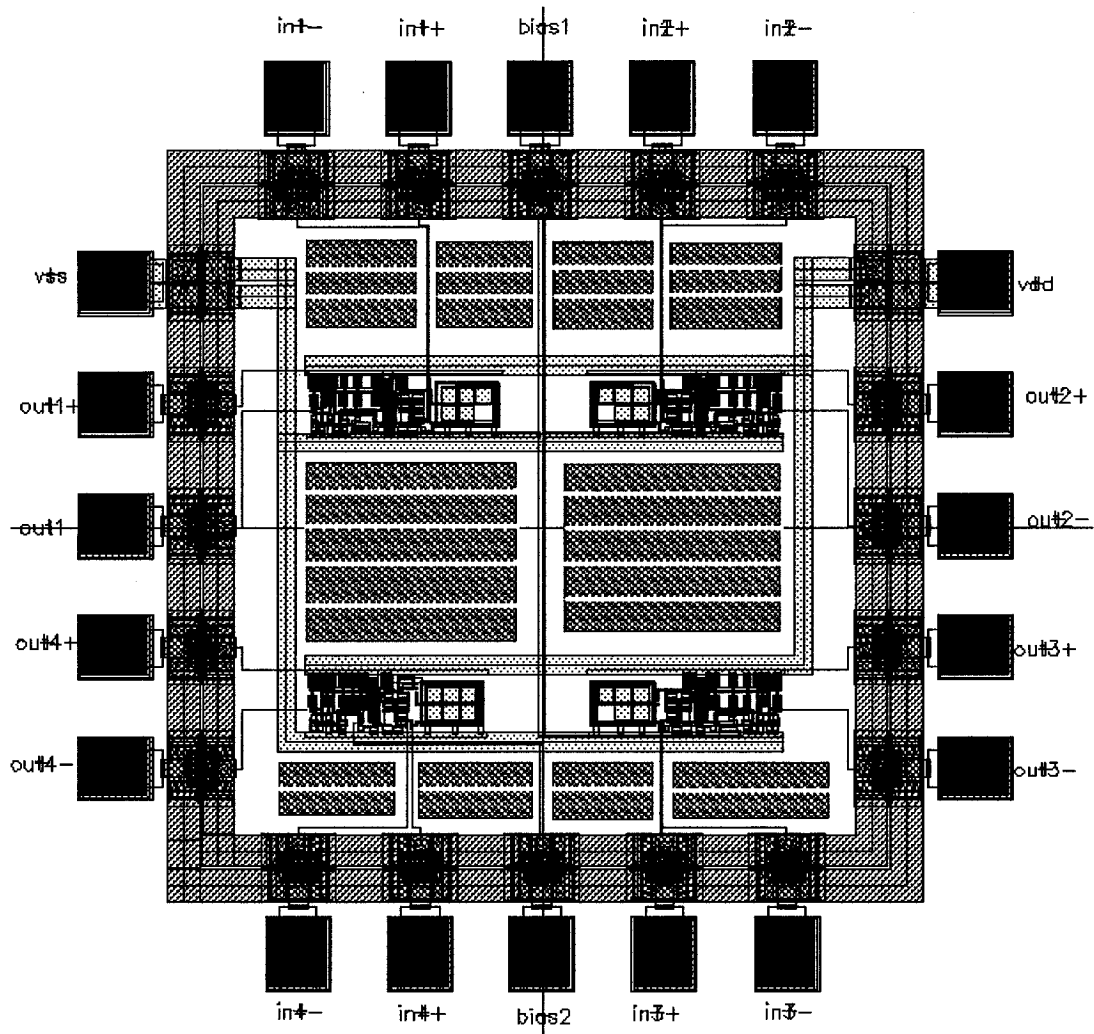


Figure 6-12 The OFA system layout (Area: 1000 x 1000 μm^2)

After completing the layout of the OFA, the layout at the chip level is considered. The chip level includes consideration of the core system, bonding pads, and package. The whole die area is 1000 x 1000 μm^2 inclusive of the pad frame. Four OFAs are placed on

one chip and supplied by one power supply. Because of the limitation of the die area, only two bias pads can be placed on the chip. Each bias pad provides bias voltage for two OFAs. The input pads are placed far from the output pads to avoid interference [34]. As a rule of thumb, the current density is $1\text{mA}/\mu\text{m}$. The width of all the interconnection wires is computed according to this value. To protect the damage from the ESD, the ESD protection devices are added on all the I/O pads. The completed circuit layout is shown in Figure 6-12.

6.5 The Performance of the OFA

Table 6-2 The specification of the OFA after layout

Parameters	Values
Voltage gain	89 dB
Gain bandwidth	85 MHz
Phase margin	65 degree
CMR	-1.0 ~ +1.1 V
Output Swing	-0.68 ~ +1.45 V
Slew rate +	4.64 V/ μs
Slew rate -	4.82 V/ μs
CMRR@100KHz	96 dB
PSRR	92 dB
Noise	$3.2 \mu\text{V}/\sqrt{\text{Hz}}$
THD	0.68%
Low output resistance	620 Ω
High output resistance	>50 M Ω
Input offset	-18 μV
Max output current	105 μA
Power dissipation	3.6 mW

The system layout has been described in Section 6.4. Table 6-2 shows the post-layout simulation results of the characteristics of the OFA under the condition of temperature of 27°C and the TSMC 0.18 μm process using Cadence Spectre simulator.

6.5.1 Corner Analysis of the OFA

The IC fabrication is a complex process of chemical reactions and physical variations that causes the deviations of the electronic device performances. These variations are described by using physically based process and geometry level statistical modeling [39]. The MOSFET devices are typically based on the process and the geometry parameters, such as gate oxide thickness (T_{ox}), threshold voltage (V_{th}), length L and width W . Numerical analysis known as *corner analysis* can perform the simulation to ensure the best and the worst cases of the circuit at the end of the manufacturing process, so that all the sets of the parameters produce acceptable results.

Corner analysis provides a convenient way to measure a circuit performance while simulating the circuit with the sets of the parameters that represent the most extreme variations in the manufacturing process. These simulation results can determine whether the circuit performance is met, even when the random process variations combine in their most unfavorable patterns. A CMOS transistor is a temperature dependent device. Both the carrier mobility (μ) and the threshold voltage (V_{th}) are inversely proportional to the temperature [35] [40]. Industrially, the range of temperature is from -40°C to 85°C. The worst cases of the corner analysis for the OFA can be considered as follows.

Fast NMOS, Fast PMOS at temperature of 85°C.

Slow NMOS, Slow PMOS at temperature of -40°C.

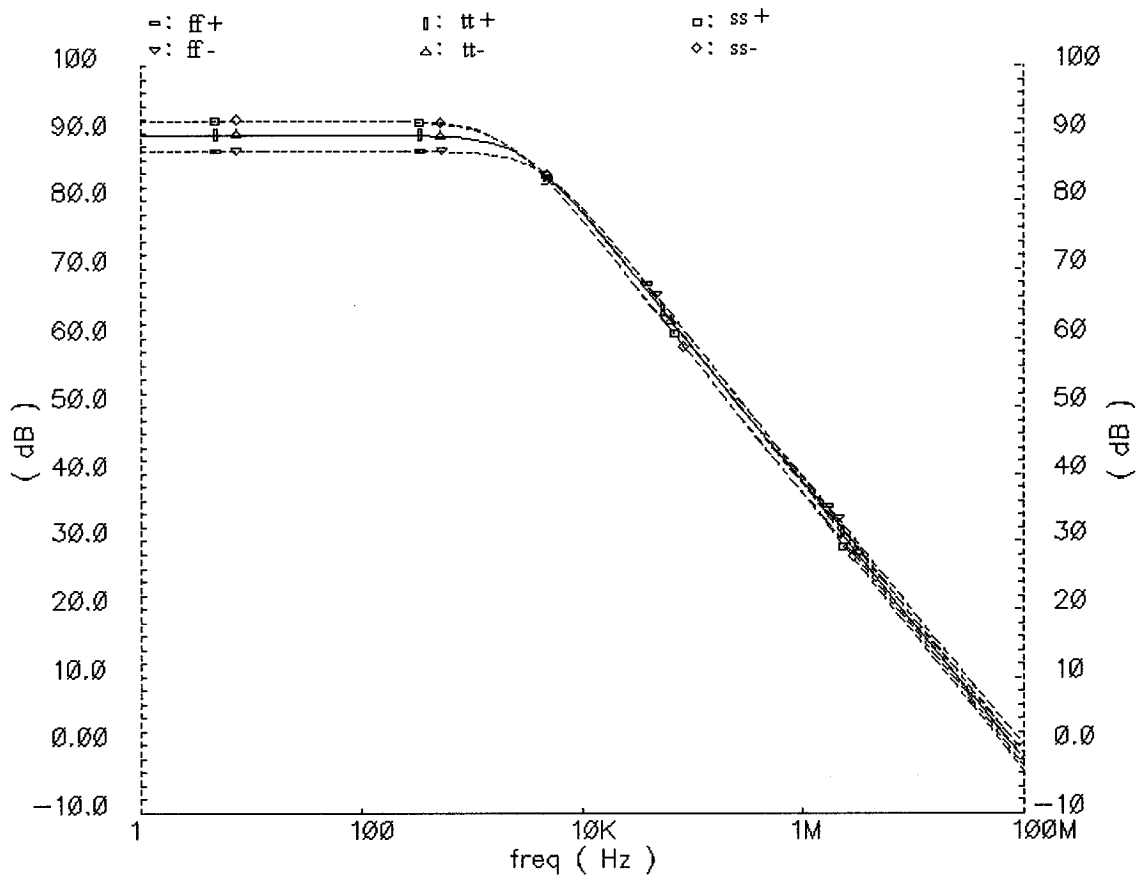


Figure 6-13 Corner analysis for the gain of the OFA

Figure 6-13 shows the simulation results of the open loop gain of the OFA under the different conditions, fast-fast, slow-slow, and general models. The AC magnitude response varies with the change in the temperature and MOSFET model parameters. The fast-fast curve gives a DC-gain of 87dB and a gain-bandwidth of 98 MHz. The slow-slow curve gives a DC-gain of 91.8dB and a gain-bandwidth of 68 MHz. Comparing with the typical case at a temperature of 27°C, which gives a DC-gain of 89.6dB and a gain-bandwidth of 78 MHz, the derivations of the DC-gain and the gain-bandwidth are around 2dB and 10MHz respectively. The fast-fast corner produces the lowest gain and the slow-

slow corner produces the highest gain. It could be determined whether these possible outcomes are acceptable in our applications.

6.5.2 Deliyannis-Friend Biquadratic Filter

Deliyannis-Friend biquadratic filter [38] is selected to verify the performance of the OFA implemented using TSMC 0.18 μ m CMOS technology by the post-layout simulation. Figure 6-14 shows the schematic of a Deliyannis-Friend biquadratic band-pass filter proposed by Friend [38]. The specifications of the band-pass filter are: $f_o=1.59$ kHz, $Q_o=10$, and $|H_o|=50$. The values of the components are shown in the figure. Figure 6-15 shows the corresponding current-mode filter realized by the same OFA. Figure 6-16 shows the response of the voltage- mode and the current-mode filters using Cadence Spectre simulator. The simulation results also agree with the theory analysis. The response of the CTF is same as that of the VTF.

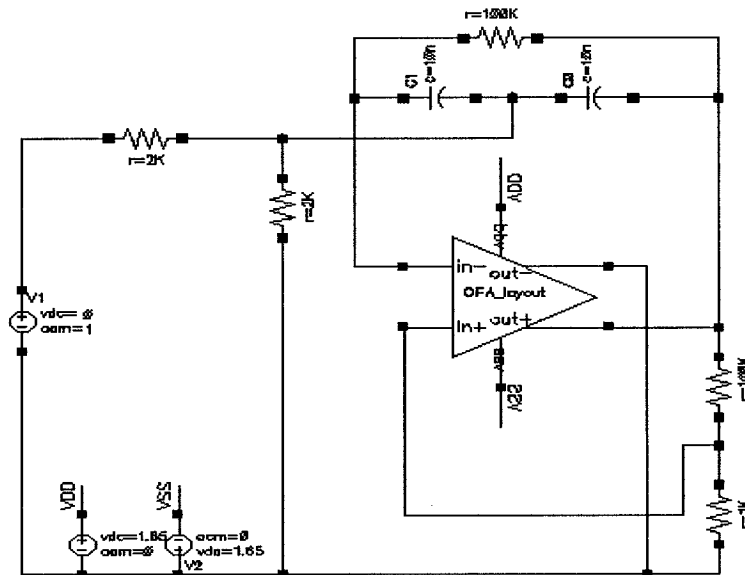


Figure 6-14 Voltage-mode band-pass Deliyannis-Friend biquadratic filter

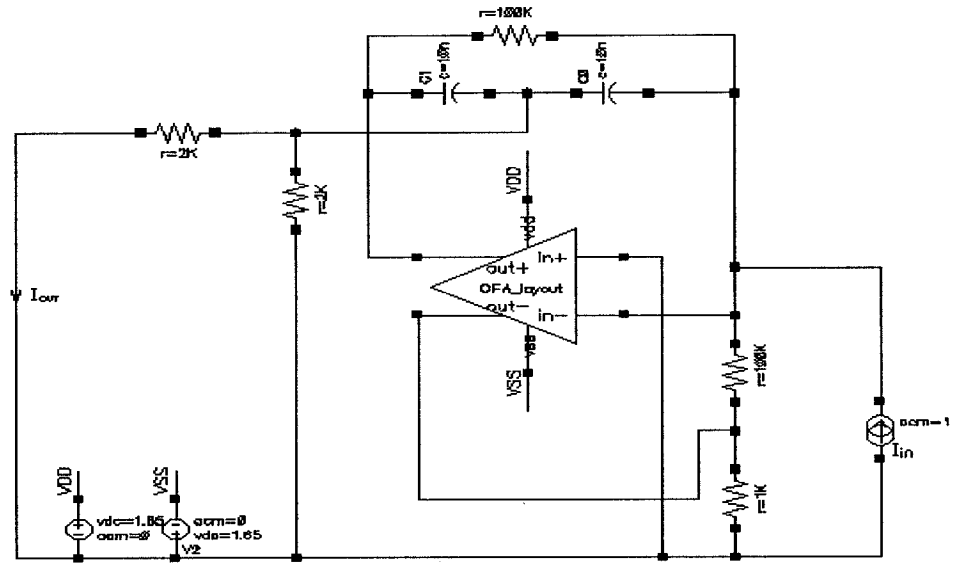


Figure 6-15 Current-mode band-pass Deliyannis-Friend biquadratic filter

6.6 Summary

This chapter has reviewed the two general methods of implementing an OFA or FTFN, one based on the OA and the other on CCII. The OA-based OFA structure [33] has been chosen and implemented in this thesis. The basic building blocks, such as the bias circuit, differential input stage, output stage, current amplifier, and compensation circuit, have been discussed. These various building blocks has been assembled to realize a high-gain OFA at the circuit level. The implementations of the transistor, resistor, capacitor, and ESD protection at the layout level have been introduced. The layout of the whole system using TSMC 0.18 μm CMOS technology has been done and the performance of the OFA verified using Cadence Spectre simulation. The simulation results have shown that the frequency response of the OFA meets the desired specifications. Finally, comparison of the responses of the VM and the CM band-pass Deliyannis-Friend biquadratic filter has been made, validating our theoretical work.

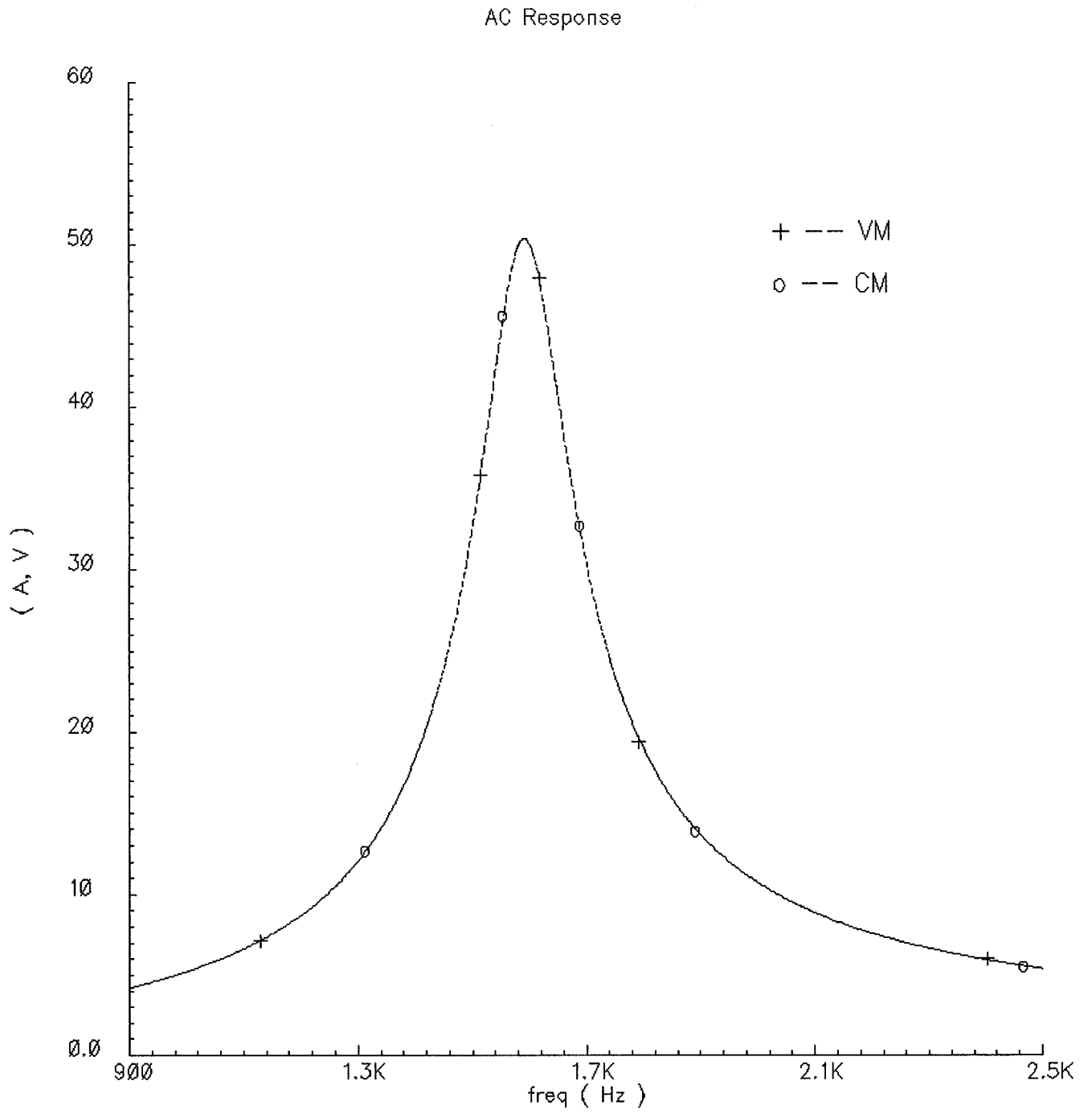


Figure 6-16 Frequency responses of the VM and the CM Deliyannis-Friend biquadratic band-pass filter

Chapter 7

Conclusion

This chapter summarizes the key contributions regarding the new methodology introduced in this thesis to realize current-mode filters from operational amplifier-based voltage-mode filters using the principles of transposed networks and nullors, and highlights some possible future research directions.

7.1 Conclusion

This thesis has been concerned with the investigation of design techniques for realizing current-mode (CM) filters using existing voltage-mode (VM) filter structures. The existing techniques and the concept of nullors have been reviewed. It has shown that CM networks can be realized from VM networks that use operational amplifiers (OAs) by combining the principle of transposed networks and the concept of nullors. The resulting CM networks either use the same OAs or operational floating amplifier (OFAs)

It has been shown that the same OA used in the VM filter can be reused in the design of the CM filter, when the OA is configured as a three-terminal device in the VM filter. An OFA is needed in the CM filter when the OA is used as a four-terminal device in the VM filter. Detailed analysis has been conducted regarding the effect of the finite gain bandwidth of the OA on the pole-frequency and pole-Q of the filters. The analysis

has shown that the performance variations of the CM filter and its associated VM filter are of the same order of magnitude.

Since theoretical analysis is not enough to prove the feasibility for practical applications, some well known second-order filters with single as well as multiple OAs have been selected for the AWB and pSpice simulations to verify the proposed technique of converting VM filters to CM filters. Further, a VM Akerberg-Mossberg (A&M) biquadratic filter and the corresponding CM filter have been built with discrete components, such as resistors, capacitors, and LM741 (OA) devices. The simulation results and the lab-bench experimental results have shown that the performance of the CM filter matches very well with that of the corresponding VM filters.

Due to the unavailability of commercial OFA, an IC chip version of the OFA is selected from several existing structures and then implemented using TSMC 0.18 μ m CMOS technology. The OFA has been used to build and simulate a CM as well as its corresponding VM second-order filter. The agreements of the filter responses have been very satisfactory.

In summary, this research is expected to bring a new methodology in the practical realization of CM filters from their VM counterparts. The good old operational amplifier can be reused to implement the associated CM filters as their counterparts. This method can also be extended to four-terminal OA configurations with wide applications in the design of CM filters.

7.2 Future Work

It is necessary to conduct detailed theoretical analysis of the effect of finite gain bandwidth in the case of CM filters obtained using OFAs. It is also necessary to study the effects of non-ideal impedance situations both at the input and output. The tracking current error between the two output terminals of the OFA may cause a difference in the performance of the CM and the corresponding VM filters. It is necessary to reduce the sensitivity of the current transfer function of the CM filter to the tracking current error of the OFA. This will help in the design of more robust OFAs to be used in the design of CM filters from well-known VM filters that use OAs.

It has been mentioned that an infinite gain controlled source of any of the four types is exactly equivalent to a nullor. Hence, it is worthwhile studying in detail the filters obtained from OA-based VM filters using VCCS or CCCS.

References

1. P.V.Ananda Mohan, "Current-Mode VLSI Analog Filters: Design and Applications", Boston, MA, Birkhauzer, 2003, ISBN 0-817-64277-3.
2. T. Deliyannis, Y. Sun and J.K. Fidler, "Continuous-time Active Filter Design", Florida, CRC Press, 1999, ISBN 0-849-32573-0.
3. S.S. Lee, R.H. Zele, D.J. Allstot and G. Liang, "CMOS Continuous-time Current-mode Filters for High-frequency Applications," IEEE J. Solid-State Circuits, vol. 28, pp. 323-329, March 1993
4. J.T. Nabicht, E. Sanchez-Sinencio and J. Ramirez-Angulo, "A Programmable 1.8–18 MHz High Q Fully-differential Continuous-time Filter With 1.5–2 V Power Supply," IEEE ISCAS, vol. 5, pp. 653-656, June 1994
5. S.L. Smith and E. Sanchez-Sinencio, "Low Voltage Integrators for High-Frequency CMOS Filters Using Current-Mode Techniques," IEEE Trans. On Circuits Syst. II, vol. 43, pp. 39-48, Jan. 1996.
6. A. Fabre and M. Alami, "Insensitive Current-Mode Bandpass Implementations-Based Nonideal Gyration," IEEE Trans. On Circuits Syst.-I, vol. 39, pp. 152-155, Feb. 1992.
7. T.S. Fiez and D.J. Allstot, "CMOS Switched-Current Ladder Filters," IEEE J. Solid-State Circuits, vol. 25, pp. 1360-1367, Dec. 1990

8. J. Ramirez-Angulo, M. Robinson, and E. Sanchez-Sinencio, "Current-Mode Continuous-Time Filters: Two Design Approaches," IEEE Trans. On Circuits Syst.-II, vol. 39, pp. 337-341, June 1992
9. D.R. Frey, "Log Domain Filtering: An Approach to Current Mode Filtering," IEE Proc. Pt. G, vol. 140, pp. 406-416, Dec. 1993
10. B.B.Bhattacharyya, and M.N.S. Swamy, "Network Transposition and Its Application in Synthesis", IEEE Trans. On Circuit Theory, vol. 18, pp. 394-397, May 1971.
11. M.N.S. Swamy, C. Bhusan and B.B.Bhattacharyya, "Generalized Duals, Generalized Inverses and Their Applications", Journal of the Institution of Electronic and Radio Engineers, vol. 44, pp. 95-99, Feb.1974.
12. M.N.S. Swamy, C. Bhusan and B.B.Bhattacharyya, "Generalized Dual Transposition and Its Applications", Journal Franklin Inst., vol.301, pp.465-476, May 1976.
13. M.N.S. Swamy and K. Thulasiraman, "Graphs, Networks, and Algorithms", John Wiley and Sons Ltd., ©1981, ISBN 0-47-103503-3.
14. M.N.S. Swamy and R.Raut: "Realization of (gm-c) Current-mode Filters From Associated(gm-c) Voltage-mode Filters", IEEE MWSCAS, vol. 2, pp. 625–628, August 2002.
15. M.N.S. Swamy, R. Raut and Z. Tang, "Generation of new OTA-C Oscillator Structures Using Network Transposition", IEEE MWSCAS, vol. 1, pp. 73–76, July 2004.

16. S.W. Director and R.A. Rohrer, "The Generalized Adjoint Network and Network Sensitivities," *Trans. on Circuit Theory*, vol. 16, pp. 318-323, August 1969.
17. G.W. Roberts, and A.S. Sedra, "All current mode selective circuits", *Electronic Letters*, vol. 25, pp. 759-761, June 1989.
18. G.W. Roberts, and A.S. Sedra, "Adjoint Networks Revisited", *Proc. ISCAS, IEEE*, pp.540-544, 1990.
19. G.W. Roberts, and A.S. Sedra, "A general class of current amplifier-based biquadratic filter circuits", *IEEE Trans. on CAS-I*, vol. 39, pp. 257-263, April 1992.
20. G. H. Wang, K. Watanabe and Y. Fukui, "An Extended Dual Transformation Approach to Current-mode Circuit Synthesis", *IEEE ISCAS*, vol. 3, pp.2294-2295, May 1990.
21. G. H. Wang, Y. Fukui, K. Kubota, K. Watanabe, "Voltage-mode to Current-mode Conversion by an Extended Dual Transformation", *IEEE ISCAS*, vol.3, pp.1833 – 1836, June 1991.
22. A. Carlosena and G.S. Moschytz, "Nullators and Norators in Voltage to Current Mode Transformations", *Int. J. of Circuit Theory and Applications*, vol.21, pp. 421-424, 1993.
23. G.S.Moschytz and A. Carlosena, "A Classification of Current-Mode Single Amplifier Biquads Based on a Voltage-to-Current Transformation", *IEEE Trans. on CAS-II*, vol. 41, pp.151-156, February 1994.
24. L.T. Bruton, "RC-Active Circuits Theory and Design", Prentice-Hall Inc., ©1980, ISBN 0-13-753467-1.

25. M.S.Ghausi and K.R.Laker, "Modern Filter Design", Prentice-Hall Inc., ©1981, ISBN 0-13-594663-8.
26. W. B. Mikhael and B.B.Bhattacharyya, "A Practical Design for Insensitive RC-Active Filters," IEEE Trans. On CAS., vol. 22, pp. 407-415, May 1975.
27. R. Senani, "A Novel Application of Four-Terminal Floating Nullors", IEEE Proc., vol. 75, pp. 1544-1546, Nov. 1987.
28. U. Cam, A. Toker and H. Kuntman, "CMOS FTFN Realization Based On Translinear Cells", Electronics Letter, vol. 36, pp.1255-1256, July 2000.
29. R. Senani, "On Equivalent Form of Single OA Sinusoidal RC Oscillators", IEEE. Trans. On CAS-I, vol. 41, pp. 617-624, Oct. 1994.
30. A. Jiraseri-amornkum, B. Chipipop, and W. Surakamponorn, "Novel Translinear-Based Multi-Output FTFN", IEEE ISCAS, vol. 1, pp.180 – 183, May 2001.
31. J.H. Huijsing, "Operational Floating Amplifier," IEE Proc. Circuits, Devices and Systems, vol. 137, pp. 131–136, April 1990.
32. M.T. Abuelma'atti, "Universal Current-mode Filter Using Single Four-terminal Floating Nullor", Microelectronics Journal, vol. 31, pp. 123–127, 2000.
33. U.C. Am and H. Kuntman, "CMOS Four Terminal Floating Nullor Design Using a Simple Approach", Microelectronics Journal, vol. 30, pp. 1187–1194, 1999.
34. D. Clein, "CMOS IC Layout Concepts, Methodologies, and Tools", Butterworth-Heinemann, ©2000, ISBN 0-75-067194-7.
35. D. Johns and K. Martin, "Analog Integrated Circuit Design", John Wiley & Son Inc., ©1997, ISBN 0-47-114448-7.

36. L.P.Huelsman, "Active and Passive Analog Filter Design", McGraw-Hall Inc., ©1993, ISBN 0-07-030860-8.
37. B.Chipipop and W.Suracamponorn, "Realization of Current Mode FTFN-based inverse Filter", Electronics letters, vol.3 5, pp. 690-620, April 1999.
38. J.J. Friend, "A Single Operational Amplifier Biquadratic Filter Section", IEEE Int. Sym. Circuit Theory, pp. 189, Dec. 1970.
39. R. Ricardo and J.A.G. Jess, "Design of System on a Chip", Kluwer Academic Publishers, ©2004, ISBN 1-40-207928-1.
40. "BSIM3v3.2.2 MOSFET Model User Manual", University of California, Berkeley, ©1999.
41. J. Silva-Martinez, M. Steyaert and W. Sansen, "High-Performance CMOS Continuous-Time Filters", KLUWER Academic Publishers, ©1993, ISBN 0-79-239339-2.
42. D. Akerberg and K. Mossberg, "A Versatile Active RC Building Block with Inherent Compensation for the Finite Bandwidth of the Amplifier", IEEE Trans on CAS-21, pp.75-78, 1974.